AN INTEGRATED EARTHQUAKE IMPACT ASSESSMENT SYSTEM

Report No. 11-02

Sheng-Lin Lin
Amr S. Elnashai
Billie F. Spencer, Jr.
Youssef M. A. Hashash
Larry A. Fahnestock

May 2011

ABSTRACT

This report presents a methodology for the refined, reliable, integrated and versatile assessment of the impact of earthquakes on civil infrastructure systems by using free-field and structural instrumentation as well as hybrid simulation. The methodology is presented through a seamlessly-integrated, transparent, transferable and extensible software platform, referred to as NEES Integrated Seismic Risk Assessment Framework (NISRAF). The software tool combines all necessary components in order to obtain the most reliable earthquake impact assessment results possible. The components are (i) hybrid simulation, (ii) free-field and (iii) structural sensor measurements, (iv) hazard characterization, (v) system identification-based model updating, (vi) hybrid fragility analysis and (vii) impact assessment software.

NISRAF has been built and demonstrated via applications to an actual test bed in the Los Angeles area. Based on an instrumented six-story steel moment resisting frame building and free-field station records, site response analysis was performed, and hazard characterization and surface ground motion records were generated for further use during the hybrid simulations and fragility analyses. Meanwhile, the finite element model was built, and the natural frequencies and mode shapes were identified using suitable algorithms. The numerical model was updated through a sensitivity-based model updating technique. Next, hybrid simulations—with the most critical component of the structural system tested in the laboratory and the remainders of the structure simulated analytically—were conducted within UI-SIMCOR and ZEUS-NL, both software

platforms of the University of Illinois. The simulated results closely matched their measured counterparts. Fragility curves were derived using hybrid simulation results along with dispersions from research on similar structures from the literature. Impact assessment results using the generated hazard map and fragility curves correlated very well with field observations following the Northridge earthquake of 17 January 1994.

The novelty of the developed framework is primarily the improvement of every component of earthquake impact assessment and the integration of these components—most of which have not been deployed in such an application before—into a single versatile and extensible platform. To achieve seamless integration and to arrive at an operational and verified system, several components were used innovatively, tailored to perform the role required by NISRAF. The integrated feature brings the most advanced tools of earthquake hazard and structural reliability analyses into the context of societal requirement for accurate evaluation of the impact of earthquakes on the built environment.

ACKNOWLEDGMENTS

TABLE OF CONTENTS

LIST OF TABLES

LIST OF FIGURES

xiii

CHAPTER 1

INTRODUCTION

1.1 Background

"Northridge, United States, 1994—60 died; 7,000 injured; $25 billion economic loss"

"Kobe, Japan, 1995—5,502 died; 36,896 injured; $132 billion economic loss"

"Sichuan, China, 2008—69,195 died; 374,177 injured; $146.5 billion economic loss"

"Haiti, 2010—222,570 died; 300,000 injured; $13.9 billion economic loss"

The above devastating earthquake losses during the past few decades, based on the United States Geological Survey (USGS) Historical Earthquakes, clearly demonstrate the impact of earthquakes on modern, urbanized regions (Figure 1-1). In order to reduce the loss of life and property during earthquakes, practitioners and researchers—through field investigations after damaging earthquakes, along with theoretical and experimental studies—have substantially improved their understanding of the effects of earthquakes in the recent decades. Individual sub-disciplines have been focused on specific problems within the broad field of earthquake engineering. Examples of disciplinary developments are strong-motion measurements, system identification, model updating, structural performance evaluation through experimental and analytical simulations, fragility derivation and the development of earthquake impact assessment software.
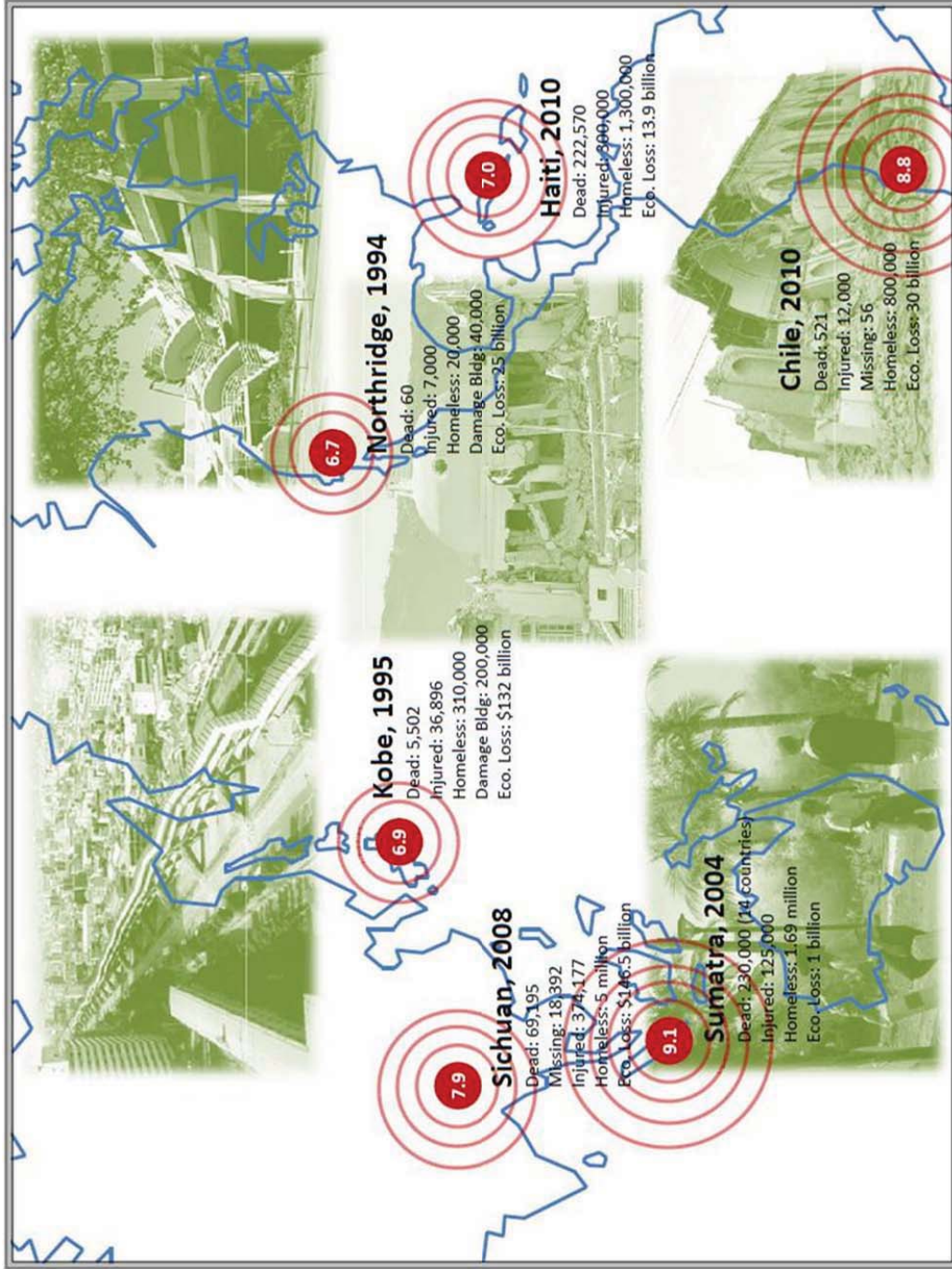
Figure 1-1 Devastating earthquakes in recent decades

The above component-specific studies allow researchers to focus on a particular problem at a fundamental level. For example, high-quality free-field surface and down-hole records are more available than ever. Methods of system identification and model updating have been established and validated with high estimation accuracy. Hybrid simulation, although at its younger age, has showcased its potentials in structural simulation research. Fragility analysis and impact assessment have also reached their own mature stages in their respective fields. More developments in each sub-discipline are detailed in *Chapter 2: Literature Review*.

Even though these specific studies have progressed considerably and produced sophisticated research results, not full utilization of instrumentation data comes into focus and uncertainties remain. For example, in recent years, the utilization of ground motion records for seismic design and site characteristics evaluation is gradually increasing. However, the utilization of data is still a long lag behind the quality and quantity of instruments and captured data. Furthermore, uncertainties remain in the outcomes of sub-disciplines not only because of their inherent characteristics, but also because of the interactions between them. For example, the derivation of fragility curves requires that a large amount of simulations be performed. It is therefore essential to have an accurate structural model which closely represents the response of the real structure. In most fragility simulations, however, either a very simplified structural model is used, or a complicated numerical model is used without being calibrated to the measured response. Such methods introduce significant and by-and-large unquantifiable uncertainties in the derived fragility curves. Moreover, the fragility curves heavily depend on input ground

motions, particularly when the fragility curves are defined in terms of peak ground acceleration (Kwon and Elnashai, 2006). The ground motion is in turn influenced by source, path and site characterization, each of which is a formidable challenge in its own right. The realism of both model and input is therefore a cornerstone in the accuracy and applicability of the ensuing fragility relationships.

Inventory, hazard and fragility (or vulnerability) are the three major components of earthquake impact assessment which aid in emergency planning, mitigation, response and recovery. Inventory includes all the information (such as types, numbers and costs) about the assets in a specific region. Hazard, which can be defined deterministically or probabilistically, represents the ground shaking intensity. The seismic hazard will then result in damage on structures as well as human society directly or indirectly. Finally, the fragility or vulnerability functions relate the probability of structures damaged to specific damage states (light, moderate, extensive and collapse, for example) under a certain seismic hazard. It is evident that the quality of the assessment outcomes is reliant on the accuracy of the components. Among these, the inventory data can be improved with the development and application of survey methods and technologies. This renders the accuracy of the assessment dependent on the reliability of the fragility curves and hazard characterization. Unquantifiable uncertainty and inaccuracies in the two components of hazard and fragility lead to earthquake impact assessments that are unreliable and do not form a viable basis for societal readiness.

1.2 Objective and Scope

To enhance the utilization of instrumentation data and to reduce the above-mentioned uncertainties and unreliability in earthquake impact assessment, an integrated framework is proposed, developed and verified via applications to an actual test bed. Figure 1-2 illustrates the proposed framework and outlines how these components are combined to achieve the main goal of this study. As shown, the proposed framework, referred to as NEES Integrated Seismic Risk Assessment Framework (NISRAF), integrates hybrid simulation with free-field and structure sensor measurements, hazard characterization analysis, system identification-based model updating technology, hybrid fragility analysis and earthquake impact assessment tools. The procedure is specifically proposed and programmed for ease of use.
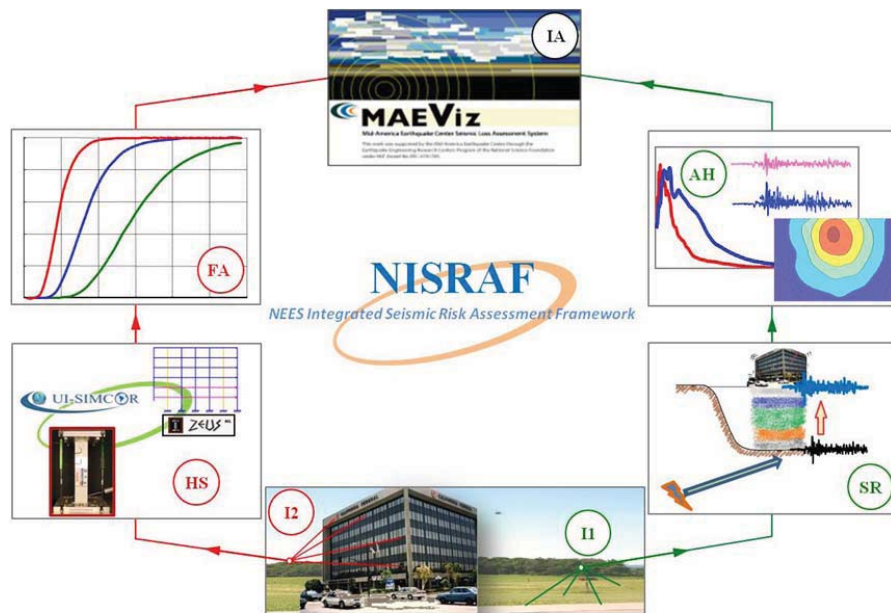
Figure 1-2 Schematic of the proposed integrated framework

The integration feature provides an opportunity to bring together all the sub-disciplines, capitalizing on the respective advances of each sub-discipline. This method of integration is not only intended to provide a tool but also to stimulate the sub-communities of researchers to investigate the problems at the interactions between them.

As part of this study, the following tasks were completed:

- *Task 1:* Literature review of past research and development in earthquake engineering. Focus is given on the sub-disciplines which are needed for the proposed framework.

- *Task 2:* An advanced hazard characterization method, consistent with the above framework, which uses free-field measured data and a 1-D site response analysis program to perform site characterization is proposed, verified and implemented in NISRAF.

- *Task 3:* An advanced hybrid method for fragility derivation, suitable for framework integration, which uses structural responses from hybrid simulation results along with findings from the literature is proposed, verified and implemented in NISRAF.

- *Task 4:* A framework—NISRAF, which combines free-field and structure sensor measurements, system identification-based model updating techniques, hybrid simulation, hybrid fragility analysis and earthquake impact assessment tool, is developed and programmed for ease of use in order to obtain the most reliable earthquake impact assessment results possible.

- *Task 5:* A pilot implementation of this framework and its components using an instrumented structure from which high-quality measurements have been obtained is demonstrated.

- *Task 6:* A pilot implementation of this framework and its components on a modern, urbanized region is demonstrated.

1.3 Organization of Dissertation

This dissertation is conceptually composed of three main parts: namely, (i) introduction and background information, (ii) methodology of the integrated framework and its components, and (iii) case studies. For presentation purposes, the dissertation is comprised of seven chapters:

- *Chapter 1. Introduction:* Introduces the background and objectives, and defines the scope of this study.

- *Chapter 2. Literature Review:* Reviews previous research on all the components implemented in the proposed framework. Discusses the existing methods. Identifies drawbacks and deficiencies in current approaches.

- *Chapter 3. An Advanced Hazard Characterization Analysis Method:* Presents and demonstrates the proposed advanced method for hazard analysis.

- *Chapter 4. Fragility Analysis by Hybrid Simulation:* Presents and demonstrates the proposed advanced method for fragility analysis.

- *Chapter 5. Development of NEES Integrated Seismic Risk Assessment Framework:* Presents the development of the integrated framework—NEES Integrated Seismic Risk Assessment Framework (NISRAF). Discusses its features, potentials, limitations and challenges.

- *Chapter 6. Case Studies:* Presents verifications of NISRAF via an actual test bed in the Los Angeles area, including earthquake impact assessment, both on single building and on an urbanized region.

- *Chapter 7. Conclusions and Recommendations:* Summarizes the major findings from the development of this framework. Limitations are identified and recommendations are made for additional research.

CHAPTER 2

LITERATURE REVIEW

2.1 Introduction

The components of the proposed framework are defined in *Chapter 1*. They comprise free-field and structural instrumentation, seismic hazard characterization, model calibration (including system identification and model updating), hybrid simulation, fragility analysis and impact assessment software. Below, the main components that are implemented in the integrated framework are reviewed.

2.2 Free-Field and Structural Instrumentation

A growing realization of the importance of the physical measurements of the ground motions and response of structures during earthquakes, the number and coverage of free-field and structural response instruments have increased significantly in recent decades. Tens of thousands of free-field strong motions as well as structural instrumented records are archived in many database centers, such as the Advanced National Seismic System (ANSS), the Consortium of Organization for Strong Motion Observation Systems (COSMOS), the Center for Engineering Strong Motion Data (CESMD), the PEER NGA Database, and the California Strong Motion Instrumentation Program (CSMIP) of the

California Geological Survey (CGS). In the following sections, more introductions about the developments for the above instrumentation programs and datacenters are provided.

2.2.1 ANSS, Advanced National Seismic System

Advanced National Seismic System (ANSS) is a national network under U.S. Geological Survey established with the mission to provide real-time records and information products for seismic events through modern monitoring methods and technologies. Four basic goals are made for ANSS: (i) Establish and maintain an advanced infrastructure for seismic monitoring throughout the United States. (ii) Continuously monitor earthquakes and other seismic disturbances, for instance, the tsunami and volcanic eruption, throughout the United States. (iii) Thoroughly measure strong earthquake shaking at ground sites and in buildings and critical structures. (iv) Automatically broadcast information when a significant earthquake occurs. To achieve these goals, over 7000 sensor systems will be established in a nationwide network. The sensors will be both on the ground and in structures (USGS, 1999).

For its monitoring activities feature, as well as making instrumentation data more accessible, several applications based on the measured records have been proposed and released. ShakeMap (http://earthquake.usgs.gov/earthquakes/shakemap/), with real-time seismic intensity information shown in contour map, is generated automatically within minutes after earthquake occurs. PAGER, Prompt Assessment of Global Earthquakes for Response (http://earthquake.usgs.gov/earthquakes/pager/), is a program which uses

ANSS instrumented data along with empirical equations to provide early fatality and economic loss following significant earthquake worldwide.

2.2.2 COSMOS, the Consortium of Organizations for Strong Motion Observation Systems

The Consortium of Organization for Strong Motion Observation System (COSMOS) is an international alliance aiming to maintain, communicate and archive all the earthquake records worldwide. With the contributing members around the world, COSMOS archives a great amount of real-time earthquake records.

Recently, Geotechnical Virtual Data Center has been established and is available to the public for the purpose of increasing the values and use of the archived data by incorporating the data with geotechnical information in an interactive map format. Meanwhile, annual meeting and periodical workshops are held to discuss current developments and applications of the instrumented data.

2.2.3 CESMD, Center for Engineering Strong Motion Data

The Center for Engineering Strong Motion Data (CESMD) is a datacenter established by U.S. Geological Survey (USGS) and California Geological Survey (CGS). The mission of CESMD is to integrate strong-motion data from the CGS California Strong Motion Instrumentation Program, the USGS National Strong Motion Projects and the ANSS. Both raw and processed strong-motion data are stored in the datacenter for earthquake engineering applications.

2.2.4 Pacific Earthquake Engineering Research Center (PEER) NGA Database

The PEER NGA Database is an update and extension to the PEER Strong Motion Database, which was published in 1999. Larger sets of records are stored in the database, but only acceleration time history files are available currently.

For its larger set of records and more extensive data, five sets of ground-motion attenuation models—Next Generation of Ground-Motion Attenuation Models for the western United States (NGA West)—were developed and are available to the public (Power et al., 2008).

2.2.5 CSMIP, California Strong Motion Instrumentation Program

The California Strong Motion Instrumentation Program (CSMIP) was established in 1972 by California Legislation to obtain vital earthquake data for the engineering and scientific communities through a statewide network of strong motion instruments (Naeim, 2005). More than 900 stations, including 650 ground-response stations, 170 buildings, 20 dams and 60 bridges are installed statewide. With the earthquake monitoring devices, accelerographs, real-time records are recorded when earthquakes occur.

With heavily instrumented structures, CSMIP provides case study opportunities for researchers to evaluate structural design procedures as well as to review the design provisions. Performance-based seismic evaluation (Kunnath et al., 2004) and evaluation of building period (Kwon and Kim, 2010) are two examples.

Indeed, with the increase of the real-time records, both quantitatively and qualitatively, researchers and experts in many fields have benefited. For example, the significant earthquakes provide critical information for emergency planning; the structural engineers improve their understanding about the structural responses during earthquakes; while the geotechnical engineers learn more about the site effect based on specific records, and the seismologists, with the high-quality and various records, are capable of investigating the propagation of seismic waves. However, when comparing with the quality and quantity of instruments and captured data, the above benefits are disproportional. That is the reason that focus is given to the applications of these valuable data in recent years.

2.3 Seismic Hazard Characterization

Due to its stochastic nature, it is difficult to predict accurately the occurrence (including the date and location) and the intensity of a future earthquake event. Similarly, for its complicated and nonlinear behavior, it is also formidable to simulate realistically the soil and topographic effects. Researchers have been devoted to the study of seismic hazard characterization analysis to improve their understanding on seismic hazard. Considerable understanding and significant development have been made in the past few decades. In general, earthquake attenuation relationship, synthetic (artificial) ground motion generation, and site response analysis contribute to current developments in seismic hazard analysis. Below, the development of attenuation relationship is reviewed

with a focus given to research specifically addressing from recent comprehensive database. Next, a review of methodology and program of synthetic ground motion generation and site response analysis is provided.

2.3.1 Attenuation Relationship

Attenuation relationship or ground motion prediction equation (GMPE), an empirical equation regressed from a great amount of historical earthquake records, is used to predict the seismic intensity (in peak ground parameters or spectral ordinates). During the past decades, several studies have been conducted which contribute the proposal of various equations to estimate the attenuation of ground motions (Ambraseys and Bommer, 1991; Rinaldis et al., 1998; Tong and Katayama, 1998; Takahashi et al., 2000; Boore et al., 1997; Campbell, 1997; Youngs et al., 1997; Campbell and Bozorgnia, 2003; Ambraseys and Douglas, 2003). Recently, a set of more comprehensive attenuation equations specifically for western United States is presented in a research project, the Next Generation of Ground-Motion Attenuation (NGA) project (Power et al., 2008). This project was coordinated by the Lifelines Program of PEER, in partnership with the U.S. Geological Survey and the SCEC (South California Earthquake Center). The proposed equations are regressed from the numerous records in the PEER NGA Database, as described in the previous section. The objective of this project is to provide new ground motion prediction equations through a comprehensive and highly interactive research program. Five NGA models are presented in this project, namely, Abrahamson and Silva, 2008 (AS08); Boore and Atkinson, 2008 (BA08); Campbell and Bozorgnia, 2008 (CB08); Chiou and Youngs, 2008 (CY08); and Idriss, 2008 (I08). A comprehensive description of

the Campbell and Bozorgnia NGA model (2008) is given below to explain how to perform seismic hazard analysis using NGA models.

The attenuation relationship proposed by Campbell and Bozorgnia (2008) is given by Equation (2.1). $\hat{Y}$ is the median estimate of the geometric mean horizontal component of PGA (g), PGV (cm/s), PGD (cm) or PSA (g). The following section presents the equations for Campbell and Bozorgnia NGA model. More details (regression methodology and procedure, for example) about this model can be found in a related document (Campbell and Bozorgnia, 2008).

$$ln\hat{Y} = f_{mag} + f_{dis} + f_{flt} + f_{hng} + f_{sit} + f_{sed} \tag{2.1}$$

where $f_{mag}, f_{dis}, f_{flt}, f_{hng}, f_{sit}$ and f_{sed} denote the magnitude term, distance term, fault mechanism term, hanging-wall term, shallow site response term and basin response term, respectively.

the magnitude term is given by the expression

$$f_{mag} = \begin{cases} c_0 + c_1 M; & M \leq 5.5 \\ c_0 + c_1 M + c_2(M - 5.5); & 5.5 < M \leq 6.5 \\ c_0 + c_1 M + c_2(M - 5.5) + c_3(M - 6.5); & M > 6.5 \end{cases} \tag{2.2}$$

the distance term is given by the expression

$$f_{dis} = (c_4 + c_5 M)\ln(\sqrt{R_{RUP}^2 + c_6^2}) \tag{2.3}$$

the fault mechanism term is given by the expressions

$$f_{flt} = c_7 F_{RV} f_{flt,Z} + c_8 F_{NM} \tag{2.4}$$

$$f_{flt} = \begin{cases} Z_{TOR}; & Z_{TOR} < 1 \\ 1; & Z_{TOR} > 1 \end{cases} \tag{2.5}$$

the hanging-wall term is given by the expressions

$$f_{hng} = c_9 f_{hng,R} f_{hng,M} f_{hng,Z} f_{hng,\delta} \tag{2.6}$$

$$f_{hng,R} = \begin{cases} 1; & R_{JB} = 0 \\ \left[\max\left(R_{RUP}, \sqrt{R_{JB}^2 + 1} \right) - R_{JB} \right] \Big/ \max\left(R_{RUP}, \sqrt{R_{JB}^2 + 1} \right); & R_{JB} > 0, Z_{TOR} < 1 \\ \dfrac{R_{RUP} - R_{JB}}{R_{RUP}}; & R_{JB} > 0, Z_{TOR} \geq 1 \end{cases} \tag{2.7}$$

$$f_{hng,M} = \begin{cases} 0; & M \leq 6.0 \\ 2(M - 6.0); & 6.0 < M < 6.5 \\ 1; & M \geq 6.5 \end{cases} \tag{2.8}$$

$$f_{hng,Z} = \begin{cases} 0; & Z_{TOR} \geq 20 \\ (20 - Z_{TOR})/20; & 0 \leq Z_{TOR} < 20 \end{cases} \tag{2.9}$$

$$f_{hng,\delta} = \begin{cases} 1; & \delta \geq 70 \\ (90 - \delta)/20; & 0 \leq \delta < 70 \end{cases} \tag{2.10}$$

16

the shallow site response term is given by the expression

$$f_{site} = \begin{cases} c_{10}\ln\left(\dfrac{V_{S30}}{k_1}\right) + k_2\left\{ln\left[A_{1100} + c\left(\dfrac{V_{S30}}{k_1}\right)^n\right] - ln[A_{1100} + c]\right\}; & V_{S30} < k_1 \\ (c_{10} + k_2 n)\ln\left(\dfrac{V_{S30}}{k_1}\right); & k_1 \le V_{S30} < 1100 \\ (c_{10} + k_2 n)\ln\left(\dfrac{1100}{k_1}\right); & V_{S30} \ge 1100 \end{cases} \quad (2.11)$$

the basin response term is given by the expression

$$f_{sed} = \begin{cases} c_{11}(Z_{2.5} - 1); & Z_{2.5} < 1 \\ 0; & 1 \le Z_{2.5} \le 3 \\ c_{12}k_3 e^{-0.75}\left[1 - e^{-0.25(Z_{2.5}-3)}\right]; & Z_{2.5} > 3 \end{cases} \quad (2.12)$$

In the above equations, the empirical coefficients c_i and the theoretical coefficients c, n and k are derived based on regression technique. M is moment magnitude; R_{RUP} is the closest distance to the coseismic rupture plane (km); R_{JB} is the closest distance to the surface projection of the coseismic rupture plane (km) (Figure 2-1); F_{RV} and F_{NM} represent the fault mechanism, $F_{RV} = 1$ for $30° < \lambda < 150°$, $F_{RV} = 0$ otherwise, $F_{NM} = 1$ for $-150° < \lambda < -30°$, $F_{NM} = 0$ otherwise; λ is rake of the fault; Z_{TOP} is the depth to the top of the coseismic rupture plane (km); δ is the dip angle of the rupture plane; V_{S30} is the shear-wave velocity in the top 30 m of the site profile (m/s); A_{1100} is the median estimate of PGA on the reference rock outcrop ($V_{S30} = 1100 m/s$); and $Z_{2.5}$ is the depth (km) to the 2.5 km/s shear-wave velocity.
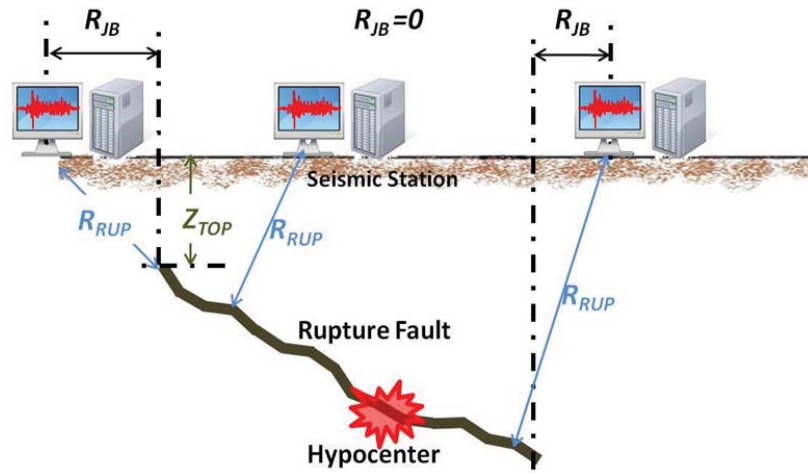
Figure 2-1 Source-to-site distances

The aleatory uncertainty of Campbell and Bozorgnia NGA (2008) model is defined by the following equation.

$$lnY_{ij} = ln\hat{Y}_{ij} + \eta_i + \varepsilon_{ij} \tag{2.13}$$

where η_i is the inter-event residual for event i; $\hat{Y}_{ij}$, Y_{ij} and ε_{ij} are the predicted value, the observed value and the intra-event residual for the recording of event, respectively.

2.3.2 Synthetic Ground Motions Generation

SIMQKE, a program for artificial motion generation in FORTRAN language, was proposed in the literature (Gasparini and Vanmarcke, 1976). Three major steps are implemented in SIMQKE to produce the synthetic ground motions:

(a) First, the spectral density function *G(w)* is generated through the duration and response spectrum which are specified by users.

(b) Next, the peak ground acceleration (PGA) of the event and a deterministic envelope function *I(t)* are defined to reflect the transient characterization of a real earthquake.

(c) Finally, an iterative procedure is implemented in order to smoothen the calculated spectrum and to improve the matching.

As described above, the PGA, response spectrum and duration are the only pre-required information for SIMQKE to produce the synthetic ground motions. Owing to its ease of use and efficiency of computation, it has been a widely used tool for ground motion generation since its release in 1976.

2.3.3 Site Response Analysis

The significance of local site effect on ground shaking and structural response has been known for many years. The surface ground motions may be amplified in some kinds of soil deposits, while attenuated in others. Several clear examples can be found in recent significant earthquakes, such as Mexico City, 1985 (Stone et al., 1987), San Francisco Bay Area, 1989 (Seed et al., 1990) and others.

Generally, the amplitude, frequency and duration of ground shaking are critically affected by the local site condition. The influence of site condition depends on the soil profiles at the site as well as the topography around. In addition, the input motions are believed to have substantial influence upon the results. Two methods are usually used to account for site effects, namely, site-specific development and code-based development (Kramer, 1996). The site-specific approach is based on empirical observation (Figure 2-2)

or analytical simulation (for example, site response analysis). Contrarily, for the code-based development, site specific parameters are provided in the codes on account of the different soil types, such as F_a and F_v in NEHRP recommended seismic provisions (FEMA, 2009). The code-based approach is believed to be relatively conservative due to the application to a broad region with the same soil parameters. In contrast, the analytical approach has the ability to present the complicated and nonlinear behaviors in the soil. Several analytical methods have been proposed in the past decades, varying from three-dimensional (3-D), two-dimensional (2-D), to one-dimensional (1-D) approaches. Generally, the 3-D and 2-D methods can provide the most realistic results. However, their computational costs are relatively higher and the treatment of the finite element models is also questionable. Therefore, the 1-D ground analysis method is currently the most commonly used approach in the geotechnical earthquake engineering. SHAKE91 (Idriss and Sun, 1992) and DEEPSOIL (Hashash et al., 2009) are the two leading site response analysis programs which use the 1-D approach to perform local site effect analyses. In 1-D approach, soil profiles are idealized as many layers of homogeneous soil. Then the response of soil is calculated based on the vertical wave propagation. The continuous solution to the wave equation can be calculated in frequency domain (SHAKE91 and DEEPSOIL) or time domain (DEEPSOIL). Below, a review on the features of these two programs is given.
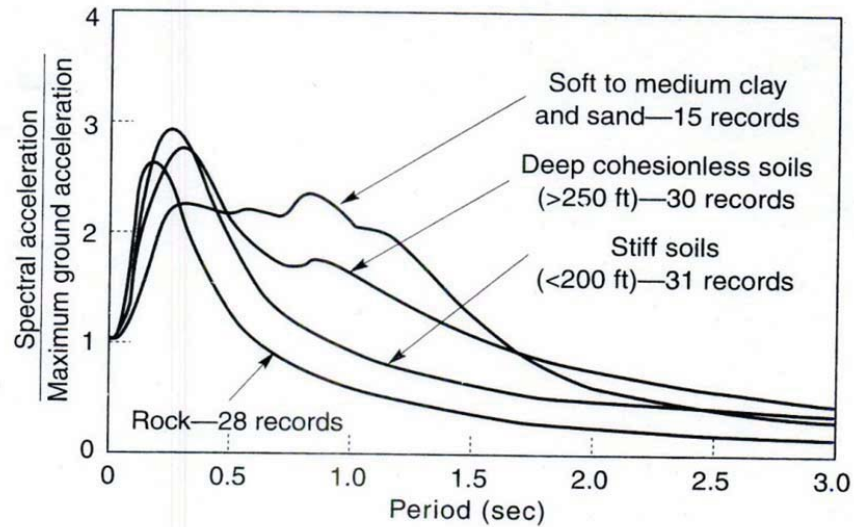
Figure 2-2 Average normalized response spectra (5% damping) for different local site condition

(Kramer, 1996)

2.3.3.1 SHAKE91

SHAKE91 (Idriss and Sun, 1992), modified based on SHAKE (Schnabel et al., 1972), is a computer program for seismic response analysis of horizontally layered soil deposits. When performing SHAKE91, users need to define the soil properties for each sub-layer (shear-wave velocity, shear modulus, damping and total weight, for example) and select the input motions. In addition, the modulus reduction versus shear strain relationship and damping ratio versus shear strain relationship must be specified to represent the soil material properties. An equivalent linear analysis procedure is implemented in SHAKE91 to account for nonlinear response of soil. The outputs of the program are the time histories requested by users. In addition, many associated types of

data can be outputted, upon users' request, such as the maximum shear stress and strain, maximum acceleration, response spectrum, Fourier spectrum and amplification spectrum.

2.3.3.2 DEEPSOIL

DEEPSOIL (Hashash et al., 2009) is a 1-D site response analysis program with an intuitive graphical user interface. Both equivalent linear and nonlinear analysis approaches can be performed in this program. Similar to SHAKE91, the pre-requisite for a site response analysis is the development of a soil column that is fully representative of the study site condition. The major features in DEEPSOIL are (i) both 1-D equivalent frequency domain and nonlinear time domain analysis approaches available, (ii) MRDF pressure-dependent hyperbolic model, (iii) new procedures for nonlinear parameters selection and fitting, (iv) new small-strain damping formulation, (v) the intuitive graphical user interface, and (vi) the batch mode analysis.

Hazard stands for the demand in earthquake impact assessment. The fidelity of hazard characterization, hence, masters the realism and reliability of the assessment results, which underpins the emergency response and recovery planning of stakeholders. Owing to its highly complicated and nonlinear behaviors, many obstacles and uncertainties still need to resolve, even though substantial understanding and various simulation methods have been made. However, the hazard characterization can be more realistic than ever—based on the strength of the mature developments (attenuation

relationship, synthetic ground motion generation and site response analysis), alongside the high-quality and various instrumentation arrays.

2.4 Model Calibration

Finite element (FE) model simulation provides a powerful way to understand the response of buildings and other structures. However, even well constructed models may produce significant differences in some dynamic response predictions, in particular when the structure behaves nonlinearly. The difference results from the uncertainties of the material properties, boundary conditions and the contributions from the non-structural elements in the real structures. In order to resolve this drawback, system identification based on the experimental or real instrumented response, along with model updating techniques, is undertaken to derive the most accurate FE model. A brief review of these two techniques is presented in the next few paragraphs.

2.4.1 System Identification

The basic concept of system identification is using the recorded sensor histories on the structure to identify the mode shapes and frequency of the real structure. Among the state-space based system identification methods, Eigensystem Realization Algorithm, ERA (Juang and Pappa, 1985) is widely adopted for its good performance in multi-input multi-output (MIMO) problems. The basic idea of ERA is to find a minimum realization of system (state-space representation with minimum dimension) using Singular Value Decomposition (SVD) on the Hankel matrix built by Markov parameters (impulse

response functions), so that the modal properties can be extracted from the realized minimum state-space representation.

2.4.2 Model Updating

Model updating aims to minimize the discrepancy between the numerical and the actual model by manipulating the stiffness and mass matrices. An objective function is constructed with modal parameter (such as natural frequencies and mode shapes) residuals which represent this discrepancy. Approaches used for model updating can generally be sub-divided into two groups, namely, the direct method and the iterative method. In the direct method, stiffness and mass matrices are changed directly (Minas and Inman, 1990; Friswel and Mottershead, 1995). While for the iterative method, the physical parameters are updated directly (Wu and Li, 2004).

To keep the sparse feature and physical meaning of the stiffness and mass matrices, structural parameters, instead of the matrices themselves, are modified in an iterative manner automatically through the specified optimization algorithms. Theoretically, all parameters that are potentially inaccurate in the model and, hence, will affect the model properties should be included in the candidates. However, a large number of parameters may issue a huge challenge to the optimization algorithms and also the computation capacity. Therefore, parameters for model updating should be selected carefully based on engineering judgment and sensitivity analysis.

2.5 Dynamic Response Simulation of Structures

Being aware of the vital role of structural response to assessment and mitigation of earthquake loss, advanced simulation techniques have been developed in order to duplicate the real structural behaviors. With the improved knowledge and development in both structural engineering and computation, an evolution has been presented from analytical finite element model simulation to laboratory testing, such as Pseudo-Dynamic Test (PSD) and shaking table testing. Recently, an advanced simulation technique— hybrid simulation—has been proposed and showcased potentials via its coordination and geographically distributed features. Below, a review of the simulation techniques in the order of evolution is given.

2.5.1 Model Analytical Simulation

Analytical model, which is developed based on the principles of mechanics and/or calibrated with the experimental data, provides an alternative way to predict the response of structures efficiently. Several finite element (FE) model simulation programs have been developed and released in the past decades, such as ZEUS-NL (Elnashai et al., 2004), OpenSees (McKenna and Fenves, 2001), ABAQUS (Hibbit et al., 2001), Vector2 (Vecchio and Wong, 2003), PISA3D (Lin et al., 2006) and others. ZEUS-NL, a product of Mid-America Earthquake Center has plate, shell and solid elements. OpenSees, developed by the Pacific Earthquake Engineering Research Center, focuses on the geotechnical constitutive models. ABAQUS, a commercial program, has extensive element libraries, but limited capabilities in conducting reinforced concrete analysis.

In addition to analytical simulation, laboratory (or experimental) simulation provides an alternative to understand structural behaviors. Static, dynamic and shake table testing are the most commonly used simulation techniques for experimental simulations. Among them, shake table testing with a full scale structure can provide the most realistic response. However, most of the tables are small, and their capacities are limited. Moreover, the cost of testing is relatively high. Many alternative methods have been developed and evolved during the past decades with different research purposes as well as the development of computation techniques.

2.5.2 PSD, Pseudo-Dynamic Test

Pseudo-Dynamic Test (PSD) was developed to alternate the real-time shake table testing. In PSD, the inertial and damping force are calculated in the analytical models, and, after that, the corresponding displacements are applied to the structures. The concept of PSD was first proposed by Takanashi in Japan (Takanashi et al., 1975). Since that, several PSD tests have been performed around the world (Mahin and Shing, 1985; Nakashima et al., 1987; Elnashai et al., 1990; Jeong and Elnashai, 2004; Chen et al., 2003).

2.5.3 Hybrid Simulation

Pseudo-Dynamic Test is applicable to large-scale tests in the laboratory. However, PSD may suffer problems due to the limitation of the facility capacity in the laboratory. Meanwhile, as described previously, each FE program has its own strengths and weaknesses. In order to capitalize the strengths of each module (FE program or

laboratory facility), UI-SIMCOR—a hybrid simulation software platform—was proposed and developed (Kwon et al., 2007). Although UI-SIMCOR uses the same integration scheme as that in PSD, its geographically distributed feature allows unlimited modules (analytical or experimental, domestic or international) to be combined within the simulation. Currently, the modules can be experimental specimen or analytical models in OpenSees (McKenna and Fenves, 2001), ZEUS-NL (Elnashai et al., 2004), ABAQUS (Hibbit et al., 2001), FedeasLab (Filippou and Constantinides, 2004) and Vector2 (Vecchio and Wong, 2003). Hybrid simulation—defined as the combination of physical (or experimental) testing and analytical models—is used here to be distinguished from multiplatform simulation, in which all the sub-structures are simulated analytically. Several multiplatform and hybrid simulation tests (including small and large scale) have been conducted and approved its coordination and communication features (Spencer et al., 2006; Spencer et al., 2007).

Analytical and experimental simulation provides a way to understand seismic behavior of structures. Hybrid simulation, indeed, promotes the ability to evaluate structural behaviors never before available. However, at its younger age, more verification about its components as well as the interaction between other sub-disciplines is essential for its integrity and robustness.

2.6 Fragility Analysis

Fragility, or vulnerability is defined as the conditional probability that a structure or a structural component would reach or exceed a certain damage level for a given ground motion intensity. Through the application of fragility curves, loss from earthquake hazard can be easily estimated. Mathematically, a fragility relationship can be defined as:

$$P_f = P\left[\frac{S_d}{S_c} \geq 1\right] \qquad (2.14)$$

where P_f is the failure probability for a specific damage state; S_d is the structural demand, and S_c is the structural capacity. In Equation (2.14), structural demand S_d depends on earthquake ground motion intensity.

Significant contribution has been made in the field of fragility analysis in the past few decades. A comprehensive review on the development of fragility assessment, specifically addressing methodologies over the past 30 years was presented in the literature (Calvi et al., 2006). Generally, fragility curves can be sub-divided into four categories based on data sources, namely, empirical fragility curves, judgmental fragility curves, hybrid fragility curves and analytical fragility curves (Rossetto and Elnashai, 2003).

Empirical fragility curves are developed through field investigations after earthquakes—are the most realistic. However, this observation data is scarce and clustered in the low damaged range. Judgmental fragility curves are based on expert opinion, and are therefore subjective. Unlike the empirical and judgmental fragility curves, analytical fragility curves are more general. Curves can be generated for different

limit states and different structural types, although at a higher computation cost. Meanwhile, the selection of the models and the simulation methods will significantly affect the accuracy of the curves. Due to the above limitations, most analytical fragility curves are generated either by simple models or by complicated models without calibration to measured response, which can result in uncertainties in these curves. Hybrid fragility curves are proposed to compensate the scarcity, subjectivity and modeling deficiency in experimental, judgmental and analytical fragility curves, respectively. Two approaches are generally used to derive hybrid fragility curves, namely, fragility relationships calibrated with other source and fragility relationships combined with others. In the first one, empirical data is generally used to calibrate the judgmental or analytical fragility curves. While in the other one, two different types of fragility curves are combined to derive fragility relationships, such as analytical curves along with empirical curves from historical earthquakes. Presumably, hybrid fragility curves capitalize advantages from different types of fragility curves. Limitations and challenges, however, still remain for the reasons that each type of fragility has its own uncertainties, and the analytical fragility relationships cannot be really improved by only a small portion and maybe clustered of empirical data.

2.7 Earthquake Impact Assessment Tools

Earthquake impact assessment tools have been already extensively adopted by the stakeholders in the community for risk management. The realism of the outcomes, such as the effect on the infrastructure systems, economy and societal activities are the

essential ingredients of the emergency response and recovery planning—which will then adequately protect our vulnerable communities.

In recent years, significant progress has been made in earthquake impact assessment, including consequence estimation methodology as well as developing software that provides decision-makers with a tool to assess the impact. Currently, many software tools using different methodology able to estimate seismic losses have been developed and released. Among the leading software tools are HAZUS-MH (FEMA, http://www.fema.gov/plan/prevent /hazus/), MAEviz (Mid-America Earthquake Center, http://mae.ce.uiuc.edu/software_and_tools/maeviz. html), RMS (Risk Management Solutions, http://www.rms.com/catastrophe/software/), AIR (AIR Worldwide Corporation, http://www.air-worldwide.com/_public/html/modeltech.asp), KOERILOSS (Bogazici University, http://fatin.koeri.boun.edu.tr/depremmuh/EXEC_ENG.pdf), and others. In the following review, a focus is placed on HAZUS-MH (FEMA, 2006) and MAEviz (MAE Center, 2007). The reason underlining this selection is that HAZUS-MH is a public package supported by FEMA, the federal agency responsible for disaster response planning, and MAEviz is the open-source platform of the MAE Center, where new models and linkages can be easily implemented. Moreover, as discussed in *Chapter 1*, the reliability of assessment results is very much dependent on the hazard characterization and fragility curves. Therefore, focus is given to methodology of hazard and fragility components.

2.7.1 MAEviz

MAEviz, an earthquake consequences assessment package, which follows the Consequence-based Risk Management (CRM) paradigm, has been developed by the MAE Center and the National Center for Supercomputing Applications (NCSA) at the University of Illinois (MAE Center, 2007). CRM is a new paradigm for seismic risk reduction across regions or systems that incorporates identification of uncertainty in all components of seismic risk modeling and quantifies the risk to societal systems and subsystems.

MAEviz provides more than 40 types of analysis models from building, bridge, utility and transportation networks, socioeconomic, to decision support analysis. With these various analyses and its interactive-visual feature, MAEviz provides the stakeholders with assessment information for developing plans and mitigation for future seismic events.

Deterministic hazard approach is implemented in MAEviz. Therefore, users are prompted to define seismic parameters and select attenuation equations to generate the seismic hazard. Moreover, the code-based method, i.e. F_a and F_v site specific coefficients in NEHRP provisions (FEMA, 2009) is adopted to account for local site effects. Due to the probabilistic nature and approximate method, uncertainties remain in the procedure and outcome. For the fragility component, numerous fragility models developed by researchers for different types of structures are archived in MAEviz database. A mapping file is therefore required to match the fragility curves with different types of structures.

Among these archived fragility relationships, however, most of them are from simple models (Single Degree of Freedom, SDOF) or complicated models without calibration to the real response of a physical structure. Such methods, therefore, introduces significant and by-and-large uncertainties in the derived fragility curves.

2.7.2 HAZUS-MH

HAZUS-MH, a risk assessment package, is developed by Federal Emergency Management Agency to estimate the potential losses from floods, hurricane winds and earthquakes (FEMA, 2006). The HAZUS-MH earthquake model can provide the estimation of damage and loss to buildings or lifelines under the scenario earthquakes, for example, the damage to the buildings, the direct or indirect cost during events, and displacement of households or the requirement of shelters.

Both deterministic and probabilistic hazard approaches are implemented in HAZUS-MH. For the deterministic method, similar to the procedures in MAEviz, user needs to define the seismic parameters and select attenuation equations. While in the probabilistic method, the hazard maps generated by USGS are implemented in HAZUS-MH, which allows users to select a map specific to different hazard levels for analysis. The code-based method—multiplying by F_a and F_v parameters, same as MAEviz—is adopted in both deterministic and probabilistic approaches.

Unlike the straightforward methodology in MAEviz, capacity spectrum method (CSM) is implemented in HAZUS-MH to calculate the degree of damage of structures as well as the related societal activities. Briefly, the structural capacity and fragility

relationships in HAZUS-MH are defined based on expert opinions and judgments. The assumed bilinear capacity curve and the hazard demand curve, along with CSM, are used to derive the structural response. Structural nonlinear behavior is reflected only by simply scaling the demand curve. Although its efficiency, this simplified approach does not explicitly consider the influence of structural parameters, such as damping, period and yield strength level.

2.8 Summary and Discussion

The components required for this proposed framework are in a sufficiently mature state. The increase in network density and applications reinforces the role of strong-motion instruments in the seismic community. Ground motion prediction equations, synthetic ground motions and site response analysis are all in their mature states, which allow to present hazard characterization probabilistically. The potential of hybrid simulation has been shown previously. Fragility analysis and model calibration techniques both have their substantial development. Impact assessment also has reached its mature state and has been extensively used worldwide.

Nevertheless, uncertainties, simplification and engineering judgment still remain in the procedures and outcomes, as discussed previously. An integrated, transparent and systematic framework, therefore, provides an opportunity to reduce and manage the uncertainties and assumptions. Through the proposed integrated framework—NEES Integrated Seismic Risk Assessment Framework, NISRAF—uncertainties from each sub-

discipline can be managed more effectively and the utilization of the instrumentation will increase. For example, the reliability of probabilistic seismic hazard can be significantly improved through the use of free-field strong-motion measurements. Analytical and hybrid (analytical-experimental) simulations can be realistic due to calibration with system identification results from sensor measurement. The uncertainties from deriving fragility relationships can be greatly reduced through the use of more reliable representation of hazard and more accurate structural models. Confidently, with seismic hazard from field measurements and fragility curves derived from accurate models, NISRAF can significantly improve upon earthquake impact assessment results.

To achieve a seamless integration and to arrive at an operational and verified system, the above components are used innovatively, tailored to perform the role required by NISRAF. The integrated system brings the most advanced tools of earthquake hazard and structural reliability analyses into the context of societal requirement for accurate evaluation of the impact of earthquakes on the built environment.

In the following sections of this dissertation, an advanced hazard characterization method and an advanced hybrid fragility analysis method are proposed and demonstrated first. Development of the proposed framework, which integrates components from sensor data to seismic loss assessment, is then presented, followed by verifications and case studies.

CHAPTER 3

AN ADVANCED HAZARD CHARACTERIZATION

ANALYSIS METHOD

3.1 Introduction

Several countries around the world have to face threatening earthquakes and related hazards, such as tsunami. Historical earthquakes have revealed their power to devastate structures, to cause fatalities and to disrupt human society (Figure 1-1). Owing to the uncertainties from seismo-tectonic, earthquake energy attenuation and site conditions, it is difficult to estimate accurately the ground motion parameters. Many methods for seismic hazard analysis have been developed over the past decades. Among them, Deterministic Seismic Hazard Analysis, DSHA (Reiter, 1990) and Probabilistic Seismic Hazard Analysis, PSHA (Cornell, 1968) are the most commonly used methods, and both are generally implemented within the earthquake impact assessment packages, such as MAEviz (MAE Center, 2007) and HAZUS-MH(FEMA, 2006). Due to the probabilistic nature and the simplified assumption for the local site effect, such as the use of the site coefficients F_a and F_v, uncertainties remain in the procedure and outcome. To reduce these uncertainties, an advanced hazard characterization analysis method is proposed—which uses free-field measured data and 1-D site response analysis program to perform site characterization.

3.2 Overview of the Advanced Hazard Characterization Analysis Method

The advanced hazard approach is mainly composed of four parts: (a) seismic hazard analysis, (b) synthetic ground motion generation, (c) site response analysis and (d) hazard map generation. First of all, the natural records are investigated directly to evaluate the hazard characterization. Synthetic records—with site specific characteristics and different hazard levels—are then generated to present the hazard as well as to provide various ground motions for further use in hybrid simulation and fragility curve derivation. Figure 3-1 shows the methodology and procedures of the advanced hazard characterization analysis approach. The following sections detail the methodology and procedures. Rather, verifications are given via an actual test bed application in the Los Angeles area.
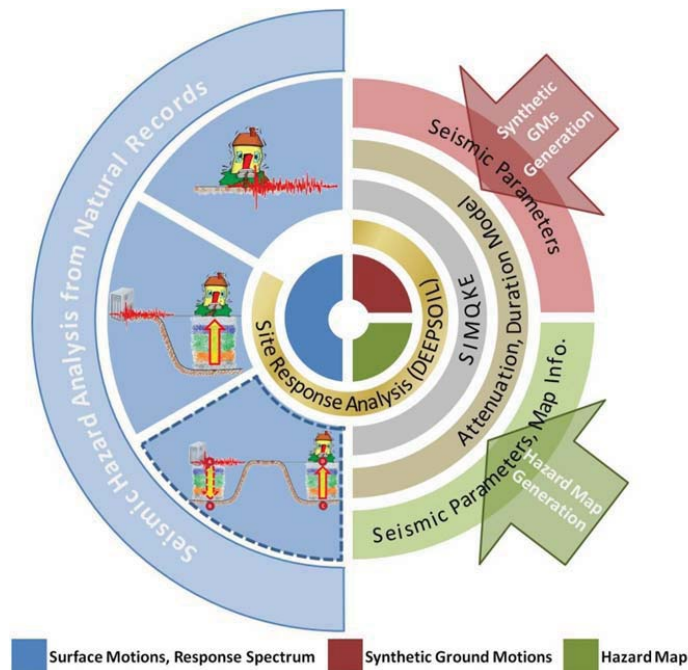
Figure 3-1 Methodology and procedures of hazard characterization analysis

3.3 Seismic Hazard Analysis

Seismic Hazard Analysis is the first step in hazard characterization analysis. In this step, the natural records around the site of interest are investigated comprehensively. Peak ground acceleration (PGA) and response spectra are generated and compared. Furthermore, several tools—such as attenuation model, duration prediction and deaggregation, which are commonly used to evaluate seismic characterization probabilistically —are also included in this step. Seismic information is indispensable for synthetic ground motion generation, particularly in a region where earthquake records are absent or in lower quality. Consequently, seismic hazard characteristics—based on the measured free-field records or deriving from probabilistic tools—are the ingredients in the further synthetic ground motion generation, site response analysis and hazard map generation.

3.3.1 Seismic Hazard Analysis from Natural Records

Generally, strong motion records are subdivided into three different types, namely, (i) Measured structures with instruments on the ground, (ii) Free-field station records on the outcrop, and (iii) Free-field station records on the surface of soil. Different analysis procedures are conducted for different type of records.

(I) Measured structures with instruments on the ground

If the structure instrumented and has sensors installed on the ground (Figure 3-2), the records on the ground level are utilized directly. Seismic parameters (peak ground acceleration (PGA) and response spectra, for example) are calculated and generated

to present the seismic characterization at this site. Meanwhile, the natural records are ready to be used in hybrid simulation and fragility analysis later.

Figure 3-2 Measured structures with instruments on the ground

(II) Free-field station records on an outcrop

Site response analysis is performed on outcrop free-field strong motion records (Figure 3-3), in order to capture the local site effect. DEEPSOIL (Hashash et al., 2009), a 1-D site response analysis program, is used to conduct the site response analysis. As mentioned previously, a representative soil column is the prerequisite for site response analysis. Therefore, user is prompted to define the soil profiles (thickness, shear-wave velocity and unit weight, for example) and the material properties (such as shear modulus reduction versus strain and damping versus strain curves) for different soils. Surface motions with specific site characteristics are then generated and ready for further use later.
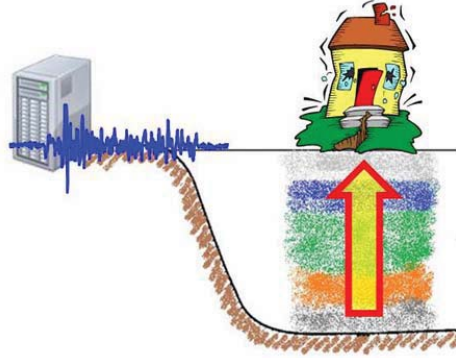
Figure 3-3 Free-field records on an outcrop

(III) Free-field station records on soil surface

When records are on soil deposits surface (point A in Figure 3-4) or within soil deposits, it is more complicated to evaluate site characterization. For record on the surface or within soil deposits, it is first deconvolved through the soil profiles to determine the motion on the bedrock (point B in Figure 3-4). Bedrock motion is then propagated to the bedrock beneath the interested site (point C in Figure 3-4). Finally, the record on the bedrock is convoluted through soil profiles to the surface (point D in Figure 3-4).
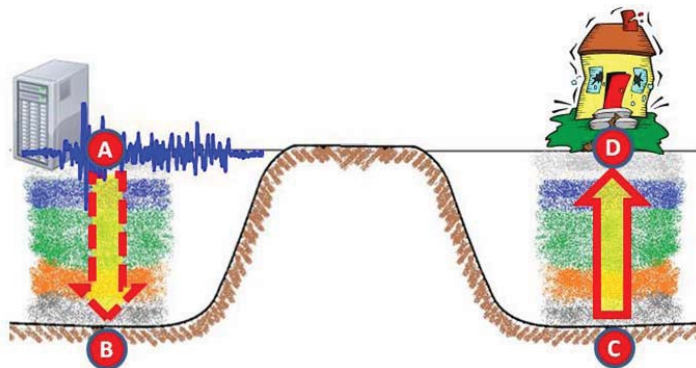
Figure 3-4 Free-field station record on soil surface

Although the deconvolution concept is rational, the technology to deconvolve ground motion through soil is still a challenge and studies are still going. Therefore, the deconvolution procedure is not implemented in the current proposed advanced hazard method, but will be when this technology is ready.

3.3.2 Seismic Hazard Analysis for Scenario Earthquakes

Due to the limited number and narrow intensity distribution of the natural ground motion records, several tools have been developed and are available to derive seismic hazard characteristics for a scenario earthquake. In this study, the latest and the most mature research findings are integrated in a novel manner in order to provide the realistic hazard characteristics as well as reasonable and various synthetic ground motions. NGA attenuation models (Power et al., 2008) and duration prediction equation (Kempton and Stewart, 2006)—both empirical equations regressed from the PEER NGA Database—are used to derive PGA, response spectrum and duration, which are the critical ingredients in seismic hazard analysis. With the above seismic information, SIMQKE (Gasparini and Vanmarcke, 1976)—a widely used synthetic ground motion generation program—is conducted to generate numerous artificial motions. Furthermore, ground motions varying with different hazard levels are essential to capture structural responses in different performance limit states, which in their own right are needed for fragility derivation. For this variation requirement, deaggregation results—which provide earthquake shaking information for different hazard levels—are therefore included in this advanced hazard method.

The NGA attenuation has already been discussed in *section 2.3: Seismic Hazard Characterization*. In the below section, duration proposed by Kempton and Stewart (2006) is detailed, followed by discussion on the deaggregation technology. Rather, SIMQKE is discussed in *section 3.4 Synthetic Ground Motion Generation.*

3.3.2.1 Significant duration prediction equation

Duration, the time for energy release during the ground shaking, varies with the magnitude, distance and also the site condition. Several definitions of ground motion duration have been proposed, such as bracketed duration (Kawashima and Aizawa, 1989), uniform duration (Vanmarcke and Lai, 1980) and significant duration (Trifunac and Brady, 1975). A more comprehensive review on duration of earthquake ground motions can be referred to Bommer and Martinez-Pereira (1999).

To predict the duration, Chang and Krinitszky (1977) first proposed an empirical relationship for duration estimation (bracketed duration with 0.05g threshold acceleration). In the proposed prediction relationship, the duration varies with magnitude under different site condition; i.e. rock and soil site (Figure 3-5). Recently, an equation for significant-duration prediction has been proposed by Kempton and Stewart (2006). This new prediction equation is derived based on the PEER NGA Database through a random-effects regression procedure. This proposed significant-duration prediction equation is given by:

$$\ln(SD)_{ij} = \ln\left[\frac{\left(\frac{\exp(b_1+b_2(M_i-M^*))}{10^{1.5M_i+16.05}}\right)}{4.9 \cdot 10^6 \beta} + r_{ij}c_2 + (c_4 + c_5(V_{S30})_{ij})\right] + \eta_i + \varepsilon_{ij} \qquad (3.1)$$

where SD is the significant duration; M^* is the reference magnitude taken as 6; β is the shear-wave velocity at the source (taken as 3.2 km/s); M_i is the magnitude of event i; r_{ij} is the distance for recording j in event i; η_i is the event term for earthquake event i; ε_{ij} is the residual for recording j in event i; and b_i and c_i are regression coefficients.
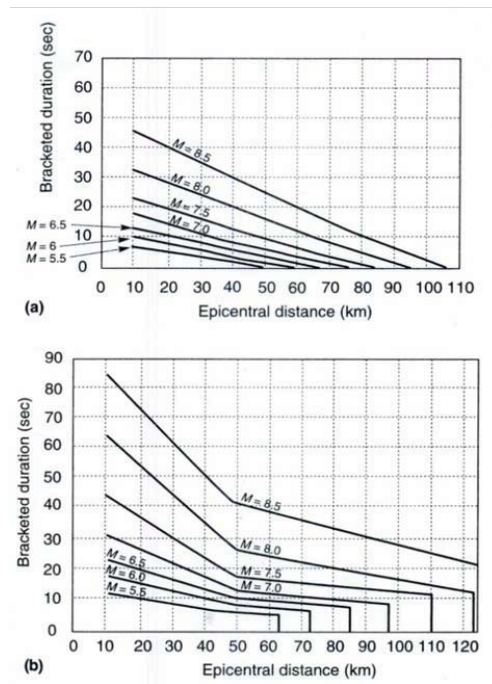
Figure 3-5 Variation of bracketed duration (0.05g threshold) with magnitude and epicentral distance: (a) rock sites; (b) soil sites. (Kramer, 1996)

This significant-duration prediction equation proposed by Kempton and Stewart (2006) is incorporated into the proposed advanced hazard method, not only for its

inherent nature (regressed from a modern database), but also for its ease for implementation (a mathematical equation rather than a plot relationship). Moreover, to account for the uncertainties in duration, in addition to the uncertainty term in Kempton and Stewart's equation, various lengths of duration—the original predicted duration and -5%, +5%, +10%, +20% of the predicted duration—are implemented in the proposed procedure.

3.3.2.2 Deaggregation results from Probabilistic Seismic Hazard Analysis

The probabilistic seismic hazard analysis method provides the annual rate of exceedance at a particular site, which is from the aggregation of the potential earthquakes of different magnitudes and different source-site distances (Kramer, 1996). However, the information about the likely earthquake magnitude and the most likely source-site distance is sometimes more useful for structural designers and decision makers. Deaggregation, a resolution of the above concern, is capable of identifying scenario events. Generally, a set of deaggregation results is composed of three components, namely, (i) magnitude, (ii) distance and (iii) epsilon.

Magnitude (M)

The magnitude term in deaggregation result is referred to the moment magnitude.

Distance (R)

The distance term in deaggregation result means the source to site distance.

Epsilon (ε)

The definition of epsilon is the number of standard deviations by which a given $lnSa$ value differs from the mean $lnSa$ value, based on the given magnitude and distance. Epsilon can be presented as:

$$\varepsilon = \frac{lnSa - \mu_{lnSa}(M, R)}{\sigma_{lnSa}} \tag{3.2}$$

where $\mu_{lnSa}(M, R)$ and σ_{lnSa} are the predicted mean and standard deviation of $lnSa$, respectively. $lnSa$ is the natural logarithm of the spectral acceleration of interest. The first two parameters can be calculated through attenuation equations.

In addition to magnitude, distance and epsilon, information about the contributed fault mechanism is also provided in the deaggregation results. The fault information is also important when performing attenuation models.

3.4 Synthetic Ground Motion Generation

As a feature to provide site specific synthetic ground motions, SIMQKE (Gasparini and Vanmarcke, 1976)—a widely used program for artificial ground motion generation—is incorporated in the proposed hazard method. Step-by-step procedure to generate synthetic ground motion is given below:

Step 1: At the beginning of the analysis, the user is prompted to define the seismic parameters (magnitude, distance, fault mechanism and site condition).

Step 2: Spectra, specified by the user or based on ground motion prediction

equations, such as the Next Generation Attenuation (NGA) models, and

predicted duration are produced.

Step 3: Finally, synthetic ground motions are generated automatically and

efficiently through SIMQKE based on the information defined previously.

Subsequently, both the natural and synthetic records are ready to be modified to reflect the local site condition. DEEPSOIL (Hashash et al., 2009)—a 1-D site response analysis program—is implemented to perform the site response analysis. Site response analysis will be fully illustrated in *section 3.5 Site Response Analysis*.

As illustrated in *section: 2.3 Seismic Hazard Characterization*, in addition to the PGA, response spectrum and duration, an intensity function is needed to define in SIMQKE (Gasparini and Vanmarcke, 1976). Moreover, two additional duration parameters (T_b and T_{total}) are prompted to be defined in the proposed method. Through the definition of intensity function as well as duration parameters, a more realistic and reasonable ground motion is produced. Below, introduction on intensity function and the proposed duration parameters are shown.

3.4.1 Intensity Function

To reflect the transient character of real earthquake records, a deterministic envelope function (intensity function) *I(t)* needs to be defined. Two different intensity functions are implemented—the trapezoidal and exponential functions (Figure 3-6). The user is prompted to select one of them and define the related coefficients.

(a) Trapezoidal   (b) Exponential
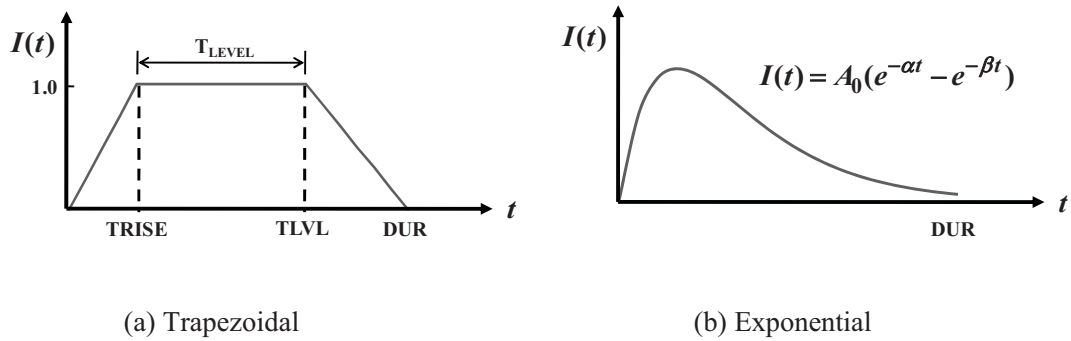
Figure 3-6 Intensity functions implemented in SIMQKE (Gasparini and Vanmarcke, 1976)

3.4.2 Duration Parameters

In SIMQKE (Gasparini and Vanmarcke, 1976), the defined duration is the period of the major vibration of the records (as the 'Duration' range shown in Figure 3-7). In order to simulate the quiet zone or small vibrations in the beginning and end of an earthquake record, T_b and T_{total} are introduced in the proposed method, as shown in Figure 3-7.
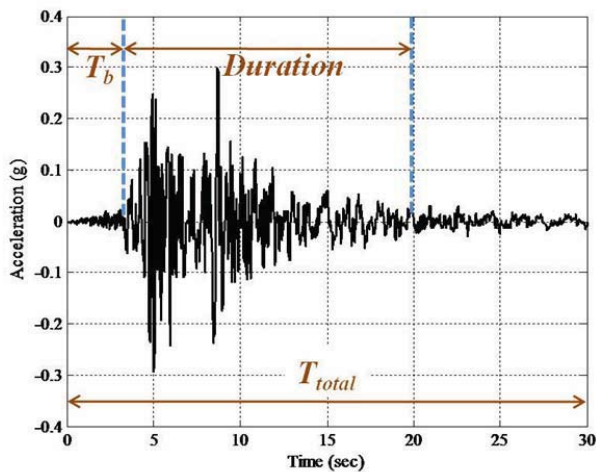
Figure 3-7 Definition of T_b and T_{total}

46

3.5 Site Response Analysis

The influence of soil conditions on ground shaking and structural damage has been understood for several years. Many evidences have also demonstrated the critical role of the local site effect. For example, the 1985 Mexico City earthquake and the 1989 Loma Prieta earthquake in San Francisco Bay Area, both of them illustrated the importance of local site effects.

As discussed in *section 2.3: Seismic Hazard Characterization*, two approaches, the site-specific and code-based methods, are used to simulate the influence of site conditions on a ground motion. Moreover, the code-based method (using F_a and F_v parameters) is implemented in MAEviz (MAE Center, 2007) and HAZUS-MH (FEMA, 2006). This simplified and approximated utilization, different F_a and F_v coefficients for different type of soil, is believed to be more conservative and unable to reflect the real site conditions. For the purpose to reduce the uncertainties and to derive more realistic results, DEEPSOIL, the 1-D site response analysis (site-specific method) is implemented in the advanced hazard analysis method. DEEPSOIL (Hashash et al., 2009), the University of Illinois site response analysis software platform, is featured for its versatile analysis (equivalent linear and nonlinear), sophisticated model (MRDF pressure-dependent hyperbolic model, nonlinear parameters selection and fitting, small-strain damping formulation, and others), and intuitive graphical user interface.

As reviewed in *section 2.3: Seismic Hazard Characterization*, the pre-requisite for a site response analysis is to develop the representative soil column. Soil properties

are defined either from field reports (such as borehole logs) or based on field or laboratory tests (Standard Penetration Test (SPT), for example).

3.6 Hazard Map Generation

Hazard Map—which contains earthquake intensity either with peak ground parameters (PGA, PGV or PGD) or spectral ordinates (S_a, S_v or S_d)—is used to present the hazard at a specific site. Hazard map is essential and widely used in many sub-disciplines. For example, structural engineers use it for seismic design; insurance companies use it to evaluate risk and develop policy. Moreover, it is an essential component of earthquake impact assessment.

Through the tools discussed in previous sections, a hazard map is generated with accuracy in an efficient way. Step-by-step procedure to generate hazard map is given below:

Step 1: At the beginning of the analysis, the user is prompted to define the seismic parameters (epicenter location, magnitude, distance, fault mechanism and site condition, for example) for a scenario event. In addition, map information, such as the cell size of raster data, the location (the latitude and the longitude) of area of interest, are also needed to be specified. Raster data here is a file contained hazard values with location information, which is a commonly used format in Geographic Information System (GIS).

Step 2: PGA, response spectrum and duration are derived by the models specified

by the user. Next, these information for each cell are fed into SIMQKE

along with site response analysis to derive surface ground motions.

Step 3: Hazard Map is finally generated by collecting seismic parameters at each

cell with organization. A visual map and a raster data format file are

generated simultaneously. Raster data format file here is compatible with

MAEviz to perform earthquake impact assessment.

3.7 Verification Studies

As illustrated in previous sections of current chapter, the latest and widely used approaches are utilized in the proposed advanced hazard characterization method. To achieve seamlessness, to conduct the analysis efficiently and to make ease of use, the above tools or methods are integrated in a novel manner and are tailored for user's ease. For example, users are only needed to define the seismic parameters in the beginning step. Synthetic ground motions and hazard map are then generated with site response analysis automatically. More discussion and features of this advanced hazard method is addressed in *Chapter 6 Development of NEES Integrated Seismic Risk Assessment Framework.* In the following parts of this section, several verifications are presented in order to evaluate the achievements of this proposed advanced hazard method.

3.7.1 Introduction

The Burbank Fire Station site at Burbank, California (latitude = 34.181°, longitude = -118.304°)—where the borehole log, and records from free-field stations and

instrumented buildings around are available—was selected to demonstrate the procedures and evaluate the outcomes under the proposed hazard characterization approach.

Based on the SMIP geotechnical report No. 131 (Fumal et al., 1979), the soil deposits at the Burbank site is Pleistocene alluvium. The borehole log (Figure 3-8) shows the soil profile for the top 30 meters at this site. Fine Sandy Loam, Gravelly Sand and Sandy Loam/Loamy Sand are the three soils in the top 30 meters. SPT results range from 10 blows/ft in fine sandy loam to 40 blows/6 inches in Gravelly Sand. The average measured shear-wave velocity is 405 m/s in Fine Sandy Loam, and is 452 m/s in Gravelly Sand and Sandy Loam/Loamy Sand (Table 3-1). The water table is assumed 20 feet below the ground surface, based on the geologic criteria for Burbank with soil deposits of similar Pleistocene age (Department of Conservation, Division of Mines and Geology, 1998).

Table 3-1 Soil properties of Burbank site (Fumal et al., 1979)

Depth (m)	Soil Type	SPT (Blow/ft)	Density (gm/cc)	Shear-wave Velocity (m/s) (avg.)
-12.5	Fine Sandy Loam	10	2.16	405
-18	Gravelly Sand	40/6"	2.16	452
-30	Sandy Loam/Loamy Sand	---	2.16	452

ALTITUDE: 610'	LOCATION:						HOLE No. 31	
	Lat. 34°10'50"						SITE: BURBANK FIRE STATION	
	Long. 118°18'15"							
DATE: 8/1/79	QUADRANGLE:						GEOLOGIC Qc	
	BURBANK, CA						MAO UNIT: Pleistocene alluvium	

SAMPLE DESCRIPTION	Density (gm/cc)	Blows/ Foot	Sampling	Graphic Log	Depth (meters)	DESCRIPTION
					0	FINE SANDY LOAM, dk. Brown, some v. coarse sand and fine gravel, medium plasticity, moist, loose.
FINE SANDY LOAM, dk, bBrown, occasional v. coarse sand and gravel, medium plasticity, moist, loose.		10			5	
					10	
SANDY LOAM, brown, poorly sorted, mostly finer than coarse sand, some granitic gravel, v. dense.		40/6"				
	2.16				15	GRAVELLY SAND, granitic.
SANDY LOAM and LOAMY SAND, dk. Brown, poorly sorted, slight plasticity, quick, moist, occasional fine gravel to 5 mm.			P		20	SANDY LOAM and LOAMY SAND, dk. Brown, poorly sorted, slight plasticity, quick, moist, occasional fine gravel to 5mm.
					25	
					30	

COMMENTS:	LOGGED BY: T. Fumal
Figure 22 39	

Figure 3-8 Borehole log of the Burbank site (adapted from Fumal et al., 1979)

3.7.2 Hazard Models Calibrated with Measured Records

As shown in Figure 3-9, numerous free-field stations (circle) and instrumented buildings (square) are around the study site (Burbank, California). Meanwhile, a great number of records are available for past earthquakes, including the Northridge earthquake on January 17th, 1994. The hazard model may therefore be more realistic by calibration with the measured free-field records. In the following sub-sections, comparisons are undertaken between seismic parameters from the measured records during the Northridge earthquake and those derived from Campbell and Bozorgnia NGA model (Campbell and Bozorgnia, 2008)—using the Northridge earthquake mechanism along with site information from the SMIP geotechnical report.
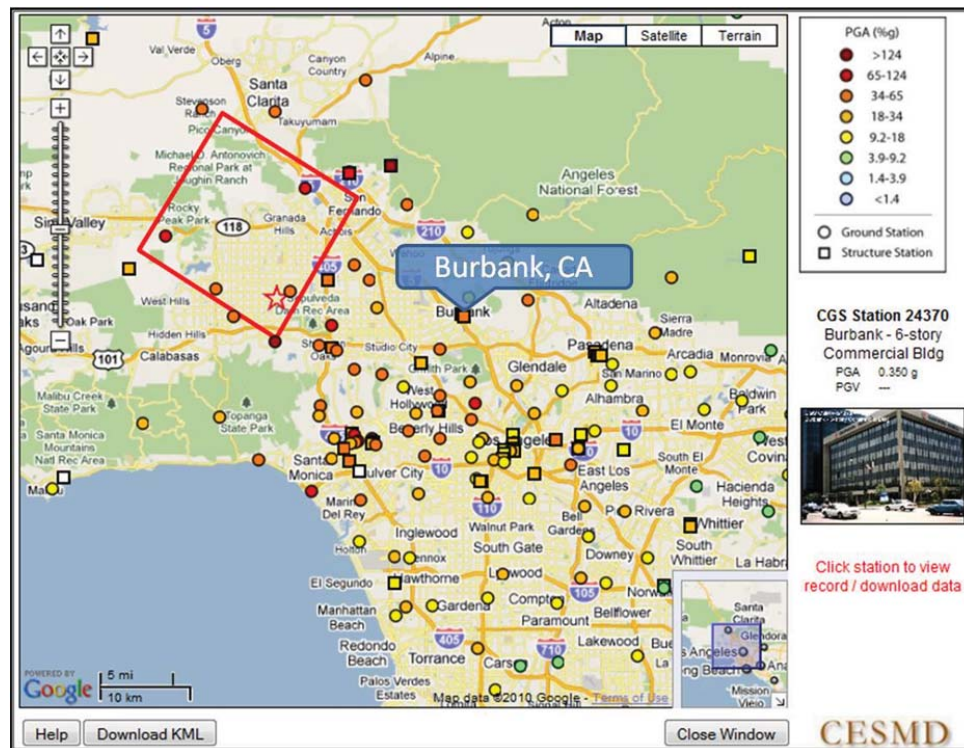
Figure 3-9 Free-field and structural instruments around the Burbank site (CESMD)

Nineteen borehole logs are available in the SMIP report. Eight of them were selected to calibrate the Campbell and Bozorgnia NGA model, CB-NGA (2008) for the reason that there is at least one instrument station (CSMIP station) which is close to the borehole site (less than 5 kilometers). Records during the 1994 Northridge earthquake in the instrument stations were used for this calibration. Consequently, site conditions from the borehole logs and seismic mechanism of the Northridge earthquake (Table 3-2, Figure 3-10) were used to tune the CB-NGA model. $Z_{2.5} = 2km, (f_{sed} = 0)$ was assumed for the absence of this information in SMIP report. Table 3-3 lists the parameters of the borehole sites required for the CB-NGA model.

Table 3-2 Seismic parameters of the 1994 Northridge earthquake (USGS, 1996)

Magnitude (Mw)	Dip (degree)	Rake (degree)	Z_{TOP}(km)	Fault Mechanism
6.7	40	104	5	Reverse
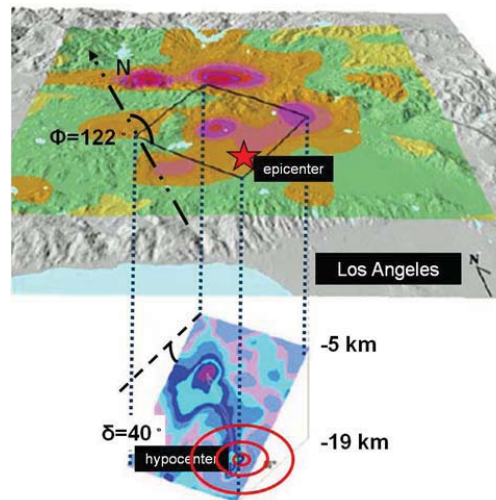
Figure 3-10 Portrayed buried fault plane of the Northridge earthquake (USGS, 1996)

Table 3-3 Parameters from SMIP report required for the CB-NGA model

Borehole ID	R_{JB}(km)	R_{RUP}(km)	V_{S30}(m/s)	$Z_{2.5}$(km)*
#31	18.7	22.0	430.1	2
#32	84.9	87.0	324.8	2
#34	53.3	56.6	407.3	2
#36	48.8	52.3	221.1	2
#38	63.1	65.9	275.1	2
#41	6.0	7.8	790.6	2
#42	5.1	7.2	453.3	2
#44	5.1	7.2	531.0	2

* No information about $Z_{2.5}$ from SMIP report, $Z_{2.5} = 2km$, $(f_{sed} = 0)$ was assumed.

To calibrate the NGA model, two approaches are considered, namely, calibrating the regression coefficient c_i or checking the sensitivity of seismic parameters (for example, V_{S30}, $Z_{2.5}$ and others). Due to the limited stations and records, the second approach was conducted in this study. Sensitivity analyses of V_{S30} and $Z_{2.5}$ were performed, for the absence of $Z_{2.5}$ and the use of average V_{S30} values. Figure 3-11 shows a comparison using different V_{S30} and $Z_{2.5}$. The difference was defined as the square root of sum of squares (SRSS) of the discrepancy between the measured value and the predicted median value (CB-NGA, Campbell and Bozorgnia, 2008) at each station. Clearly, the result was significantly affected by the $Z_{2.5}$ value rather than V_{S30}. To reduce the uncertainties, more investigation was conducted. Table 3-4 lists $Z_{1.0}$, $Z_{1.5}$ and $Z_{2.5}$ information of the 8 selected stations. This information is from stations in the PEER NGA Database, which are close to the 8 selected CSMIP stations (within 5 kilometers). For sites where only $Z_{1.5}$ is available (for example, #42 and #44), the Equation (3.3) was

used to predict $Z_{2.5}$ (Campbell and Bozorgnia, 2007). If $Z_{1.0}$, $Z_{1.5}$ and $Z_{2.5}$ are unavailable,

$Z_{2.5} = 2km$, $(f_{sed} = 0)$ was assumed. Table 3-5 lists the final values of $Z_{2.5}$.

$$Z_{2.5} = 0.636 + 1.549Z_{1.5} \qquad (3.3)$$
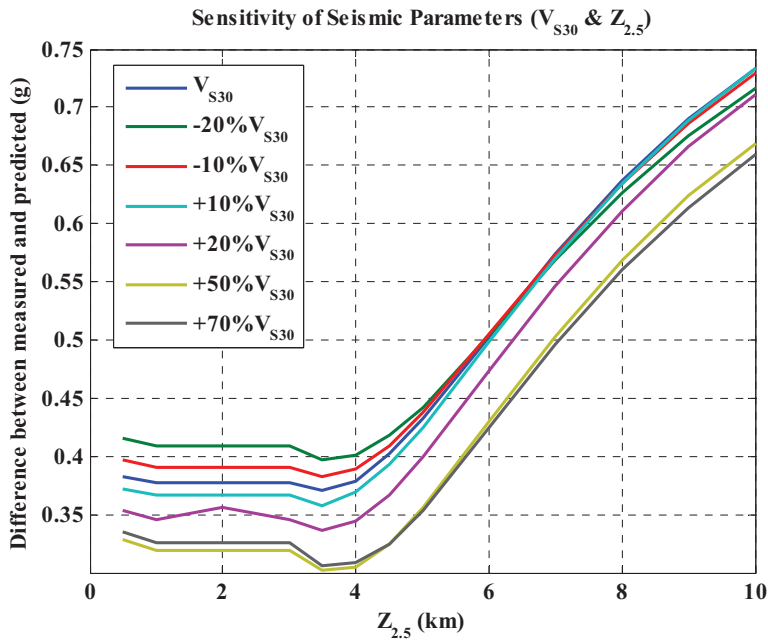
Figure 3-11 Comparison of the difference (SRSS of the difference between the measured value

and the predicted value (CB-NGA)) using different V_{S30} and $Z_{2.5}$

Table 3-4 $Z_{1.0}$, $Z_{1.5}$ and $Z_{2.5}$ values of stations close to the borehole site

Borehole ID	$Z_{1.0}$ (km)	$Z_{1.5}$ (km)	$Z_{2.5}$ (km)
#31	---	---	---
#32	~ 0.32	~ 0.54	~ 2.74
#34	~ 1.28	~ 3.05	~ 5.48
#36	~ 0.90	~ 1.90	~ 2.41
#38	~ 0.80	~ 1.67	~ 3.43
#41	~ 0.13	~ 0.23	~ 1.30
#42	---	~ 3.04	---
#44	---	~ 3.04	---

*$Z_{1.0}$, $Z_{1.5}$ and $Z_{2.5}$ are values of stations in PEER NGA Database

which are close to the selected borehole (within 5 kilometers)

Table 3-5 $Z_{1.0}$, $Z_{1.5}$ and $Z_{2.5}$ values after modification

Borehole ID	$Z_{1.0}$ (km)	$Z_{1.5}$ (km)	$Z_{2.5}$ (km)
#31	---	---	2
#32	~ 0.32	~ 0.54	~ 2.74
#34	~ 1.28	~ 3.05	~ 5.48
#36	~ 0.90	~ 1.90	~ 2.41
#38	~ 0.80	~ 1.67	~ 3.43
#41	~ 0.13	~ 0.23	~ 1.30
#42	---	~ 3.04	~ 5.34
#44	---	~ 3.04	~ 5.34

Figure 3-12 and Figure 3-13 show the difference between assuming $Z_{2.5} = 2km$, $(f_{sed} = 0)$ and using $Z_{2.5}$ from the PEER Database. The difference reduced from 0.377 to 0.269. Figure 3-14 shows the sensitivity of average shear-wave velocity. Various

V_{S30} values were investigated to account for the uncertainty from measurement. The comparison shows that a value of $+70\%V_{S30}$ leads to best results.
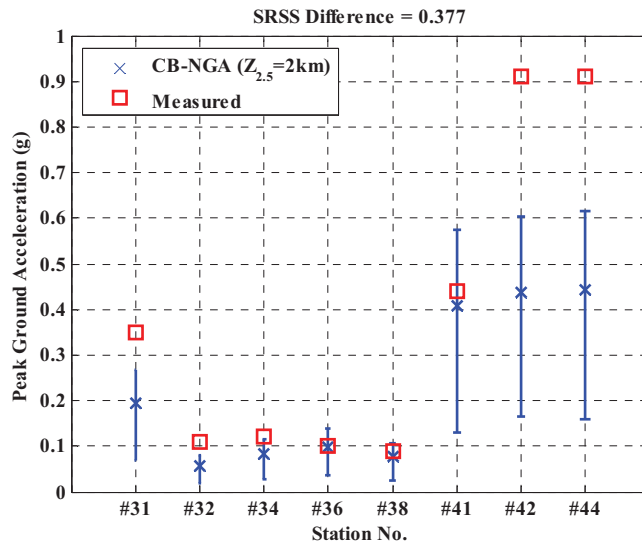
Figure 3-12 Difference when assuming $Z_{2.5} = 2km$ for all the borehole sites
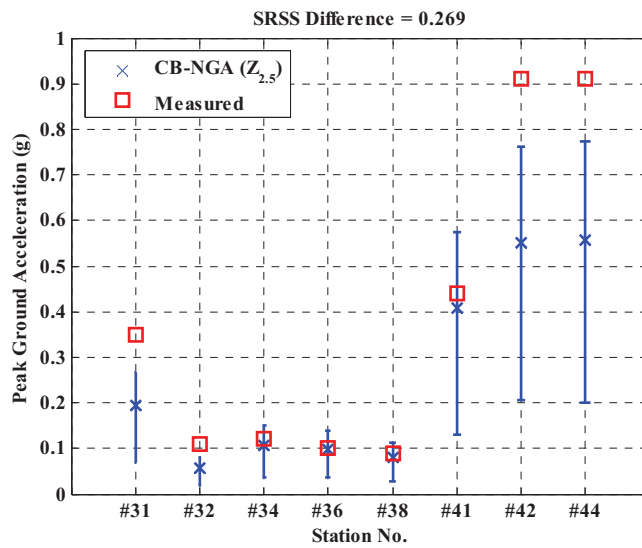
Figure 3-13 Difference when using $Z_{2.5}$ value from PEER NGA Database
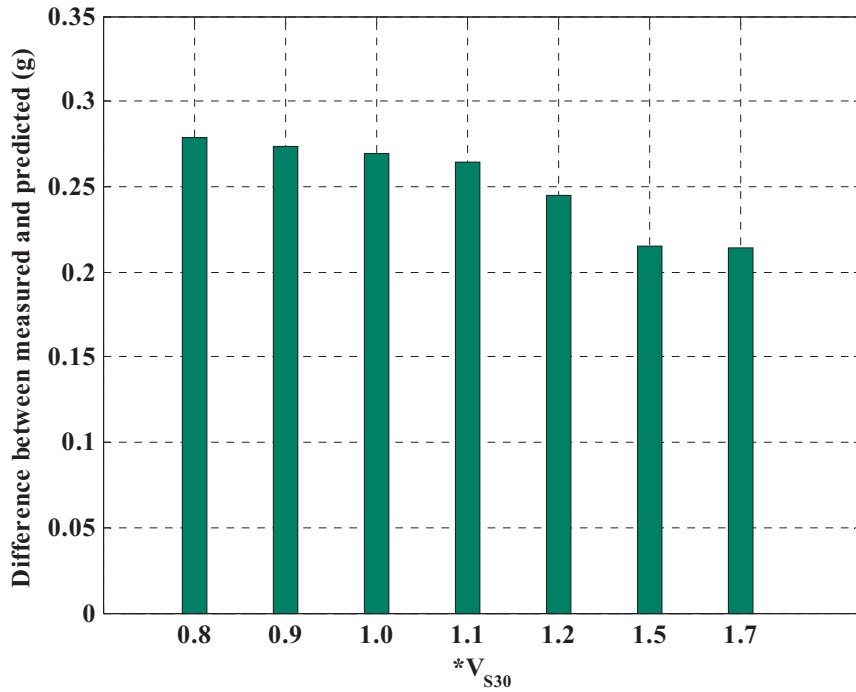
Figure 3-14 Sensitivity of shear-wave velocity to the PGA predicted by CB-NGA

Based on the above comparisons, the median value of the CB-NGA model is sensitive to both V_{S30} and $Z_{2.5}$. When $Z_{2.5}$ value is available, the predicted value (PGA) from the CB-NGA is improved. Meanwhile, the sensitivity analysis of the shear-wave velocity illustrates that the use of average shear-wave velocity is unrealistic. Hence, the CB-NGA model along with site response analysis is performed in the following applications in order to reflect the more realistic local site effects.

3.7.3 Application Examples

Three applications are performed to demonstrate the methodology and procedures of the advanced hazard analysis approach.

Application 1: Synthetic ground motions are generated based on earthquake
mechanism of the 1994 Northridge earthquake, followed by the
comparisons between the natural and synthetic records.

Application 2: Synthetic ground motions with various hazard levels are generated,
using deaggregation results and local site conditions.

Application 3: A site specific hazard map under the Northridge earthquake in Los
Angeles area is generated. Comparison is made with the ShakeMap
released by USGS.

3.7.3.1 Application 1—synthetic ground motions through the Northridge earthquake mechanism

The procedure to generate the synthetic ground motions at a specific site (the Burbank site) was verified through a historical event (the Northridge earthquake of January 17th, 1994). In the beginning of this application, seismic information from the Northridge earthquake (Figure 3-10) and the site condition of the SMIP #31 borehole log (Figure 3-8) were fed into this approach. PGA and response spectra from the CB-NGA (Campbell and Bozorgnia, 2008) model and the predicted significant duration were then generated, as shown in Table 3-6 and Figure 3-15. Finally, SIMQKE (Gasparini and Vanmarcke, 1976) with the above prerequisite parameters was conducted to generate synthetic ground motions automatically. Figure 3-16 lists 3 of the 30 synthetic ground motions generated by SIMQKE varying with different durations, PGA and spectral

acceleration intensities (i.e. median minus one std., median and median plus one std.).

Moreover, Figure 3-17 presents the comparison between one of synthetic ground motions

and the natural record, which illustrates that the PGA value and the transient

characteristic are acceptable. Figure 3-18 shows the comparison of response spectra

between the natural record and all the synthetic records.

Table 3-6 Comparison between the measured and predicted seismic parameters

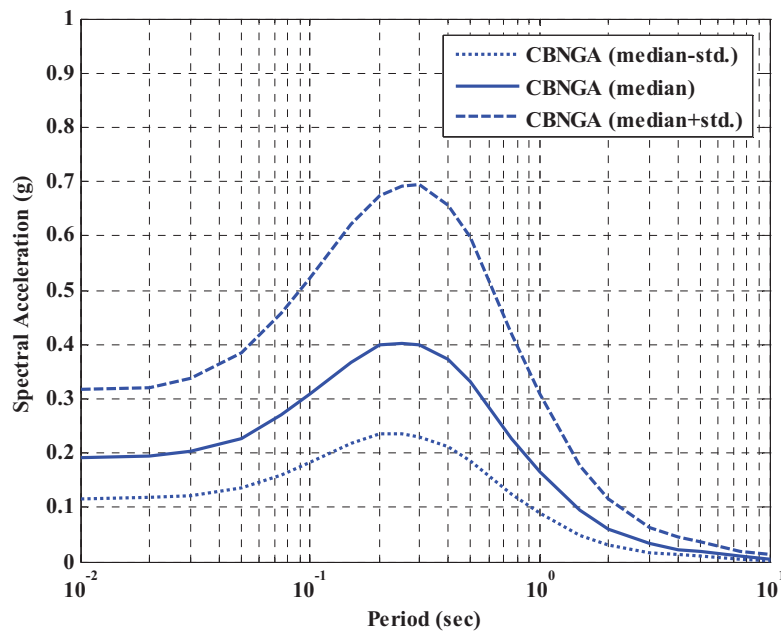|	Measured	Predicted*
Peak Ground Acceleration (g)	0.30	0.11/0.19/0.32
Significant Duration (s)	10.4	9.73/15/23.5

median-std./ median/ median+std.

Figure 3-15 Response spectra generated through CB-NGA model
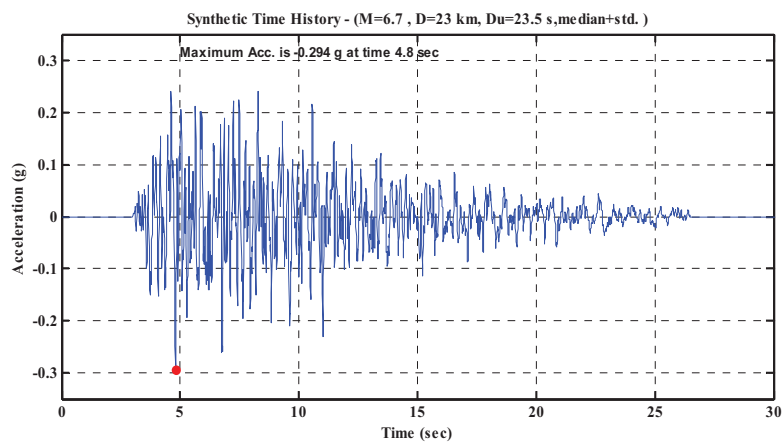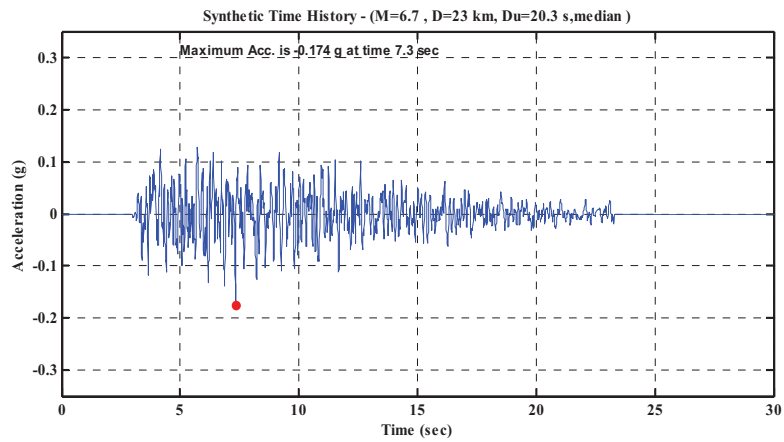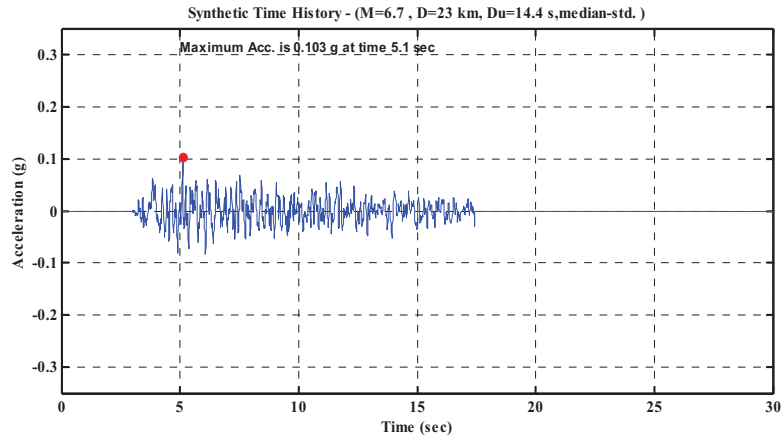
Figure 3-16 Synthetic ground motion with different duration and PGA
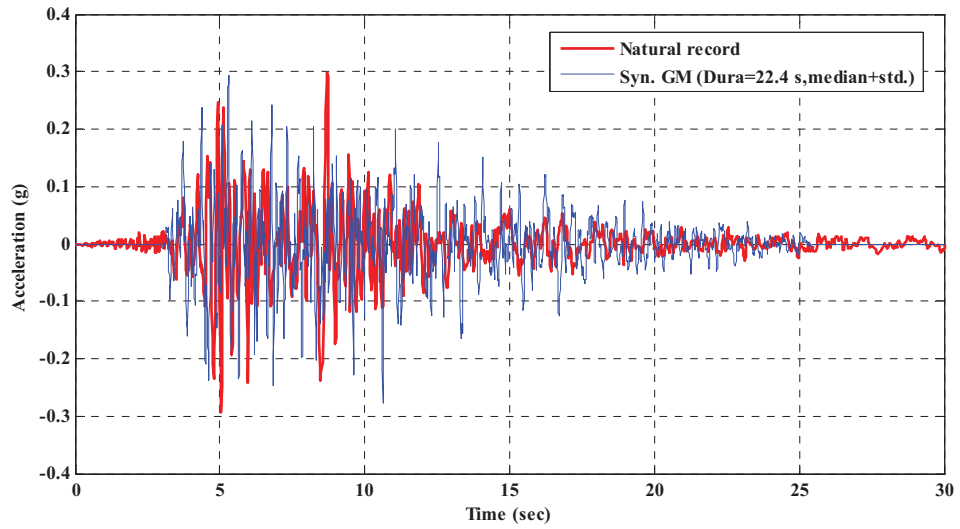
Figure 3-17 Comparison between the natural and synthetic record
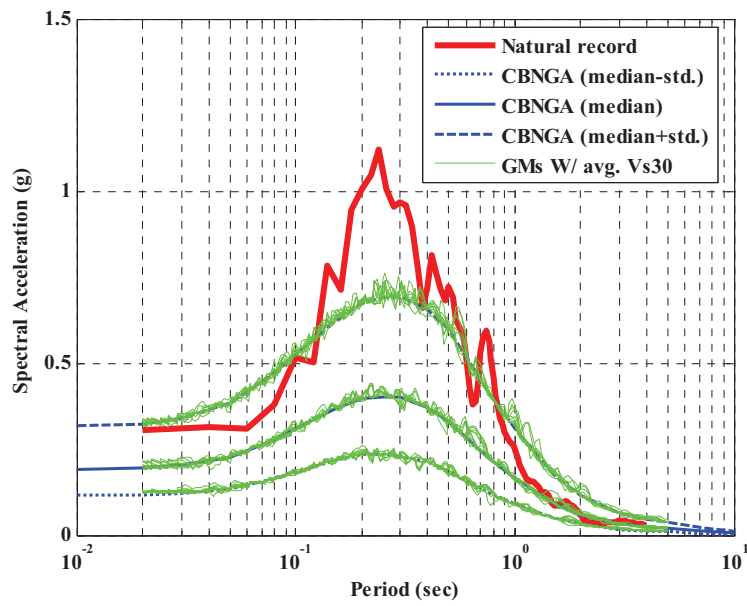
Figure 3-18 Comparison of response spectra

As shown in Figure 3-18, there is a significant difference of the spectral acceleration value between the natural and the synthetic records. At least two reasons are given to explain this difference. First of all, the NGA model is an equation which provides the median estimate of the spectral acceleration. Response spectra generated through SIMQKE based on the NGA model, therefore, cannot always be corrected well with one specific record. Secondly, the difference is more significant for periods range from 0.15 to 0.8 seconds, apparently, due to an amplification of the time history in this range. In this application, the average shear-wave velocity is used to account for the local site effect when applying the NGA equation. The soil condition therefore may not be reflected appropriately with the use of the average shear-wave velocity only. To investigate the local site effect, a soil column representative of the Burbank site was developed. The period of this soil column was around 0.3 seconds, which was calculated based on Equation (3.4):

$$T_i = \frac{4 \cdot h_i}{V_{S,i}} \tag{3.4}$$

where T_i, h_i and $V_{S,i}$ are period, height and shear-wave velocity of the ith soil layer, respectively.

Clearly, the time history is to be amplified around the period equal to 0.3 seconds. This provides exactly one of the reasons to explain the large difference between the natural record and the synthetic records at the Burbank site in the period range from 0.15 to 0.8 seconds. To quantify further the local site effect, site response analysis was

performed using the 1-D site response analysis program, DEEPSOIL. Figure 3-19 shows the comparison of the response spectra between the natural record and the synthetic records after site response analysis. It is evident that the generated ground motions, including site response analysis, can represent the actual hazard characterization. Another time, the importance of the local site effect is emphasized based on the above investigation.
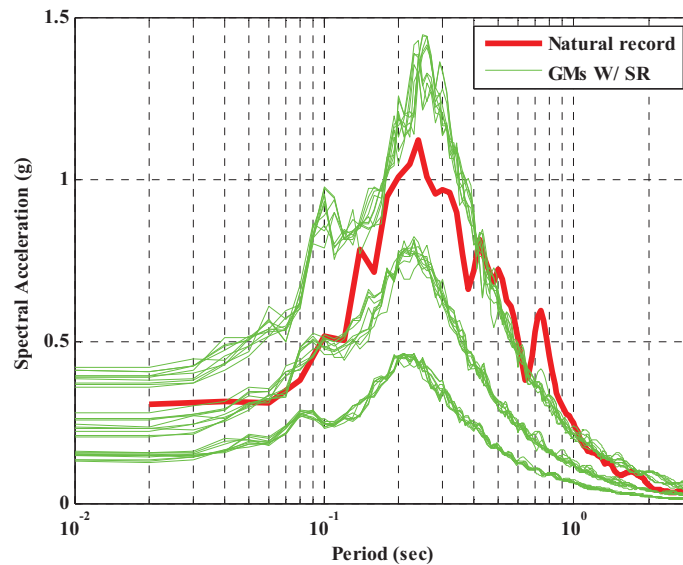
Figure 3-19 Comparison of response spectra with site response analysis (SR)

3.7.3.2 Application 2—synthetic ground motions with various hazard levels

In this verification, ground motions with various hazard levels were generated based on the seismic information specified by the users. The deaggregation results for different hazard levels (10%, 5%, and 2% probability of exceedance in 50 years), as

shown in Table 3-7 and Table 3-8, at the Burbank site were fed into this advanced hazard method. Next, sets of synthetic ground motions, including site response analysis and varying with duration and hazard levels were generated automatically. These motions with compatible format were further used in the hybrid simulation and fragility analysis. Figure 3-20 lists 3 of the 27 generated synthetic ground motions. Rather, Figure 3-21 shows the response spectra in different hazard levels. For completeness, a summary of the procedure and all the generated ground motions are given in Appendix A.

Table 3-7 Deaggregation results at Burbank site

	Return Period (yrs)	M	R (km)	Epsilon
2%/ 50yrs	2475	6.73	6.9	1.18
5%/ 50yrs	975	6.71	8.5	0.91
10%/ 50yrs	475	6.71	10.6	0.63

Table 3-8 Contributed fault information based on deaggregation results

Name	Type	F_{RV}	F_{NM}	$f_{hng,\delta}$	f_{sed}
Verdugo Char	Reverse	1	0	1	0
Elysian Park Char	Blind trust (reverse)	1	0	1	0

*assume $\delta = 90°$, $Z_{2.5} = 2km$
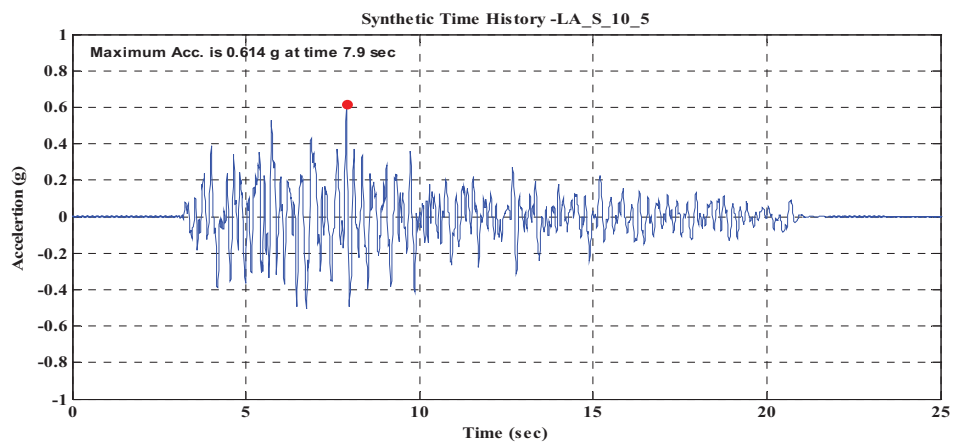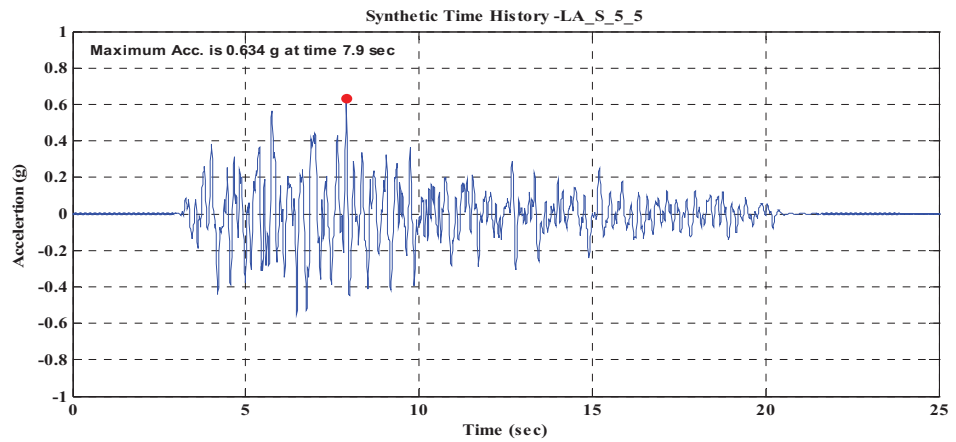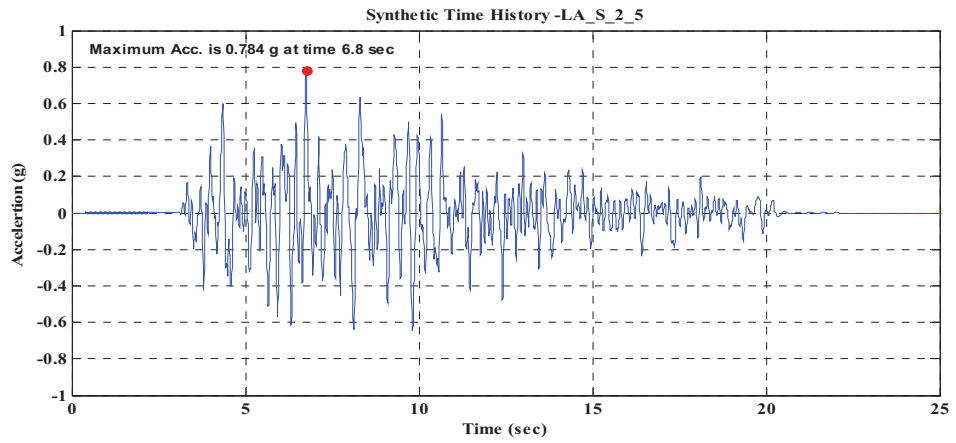
Figure 3-20 Synthetic ground motions for different hazard level and duration
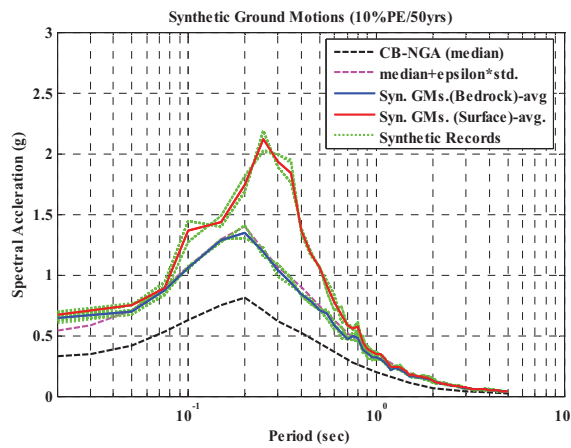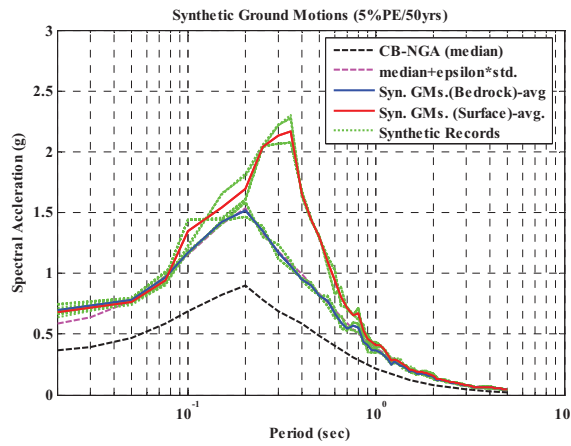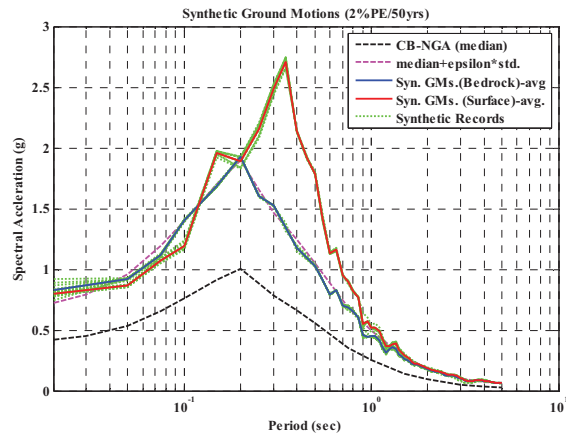
Figure 3-21 Response spectra for different hazard level

3.7.3.3 Application 3— a site specific hazard map under the Northridge earthquake in

LA area

Hazard map, the exposure when calculating earthquake loss, is one of the indispensable components of regional impact assessment. The map of PGA for the 1994 Northridge earthquake in the Los Angeles area in standard gravity (g) was generated in this application. This map is not only served to demonstrate the proposed method, but also used for regional impact assessment in Los Angeles area, which is presented in *Chapter 6: Case Studies.*

SMIP geotechnical report (Fumal et al., 1979) was used again to illustrate local site characteristics. As mentioned previously, 19 borehole logs are available in SMIP report. Figure 3-22 shows the locations of these 19 boreholes (black cross) and the epicenter of the 1994 Northridge earthquake (red star). In order to provide more realistic site conditions, the Los Angeles area was subdivided into 6 smaller regions, as shown in Figure 3-23. One of the boreholes in each region was selected to represent the site condition in that area. Therefore, 6 different site conditions along with earthquake mechanism of the Northridge earthquake contributed the map of PGA for the 1994 Northridge earthquake in Los Angeles area.

Step-by-step procedures to generate the hazard map (described previoulsy in *section 3.6 Hazard Map Generation*) were then performed. The Northridge earthquake mechanism (Figure 3-10), the site conditions (soil profiles and material properties) and map information (such as interested region scope and cell size) were defined in the first

step. Next, the CB-NGA (Campbell and Bozorgnia, 2008) and duration prediction equation along with SIMQKE (Gasparini and Vanmarcke, 1976) and DEEPSOIL (Hashash et al., 2009), were performed for each cell. Finally, PGA values were collected and hazard map of the Los Angeles area was presented, as shown in Figure 3-24.
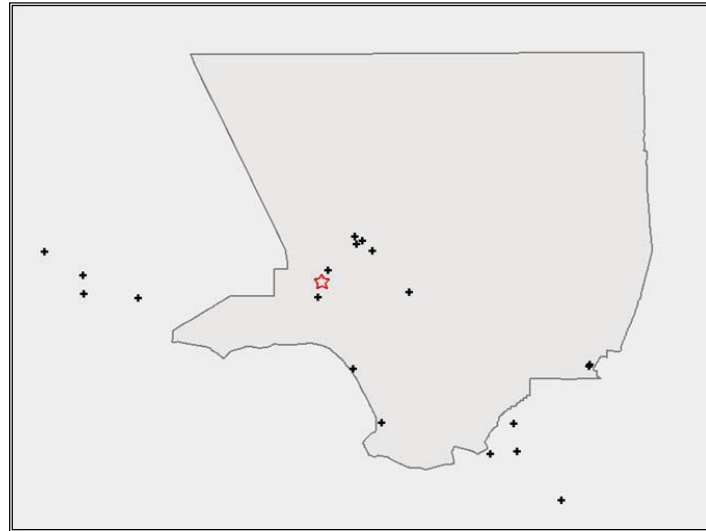
Figure 3-22 Locations of boreholes (black cross) in the SMIP geotechnical report
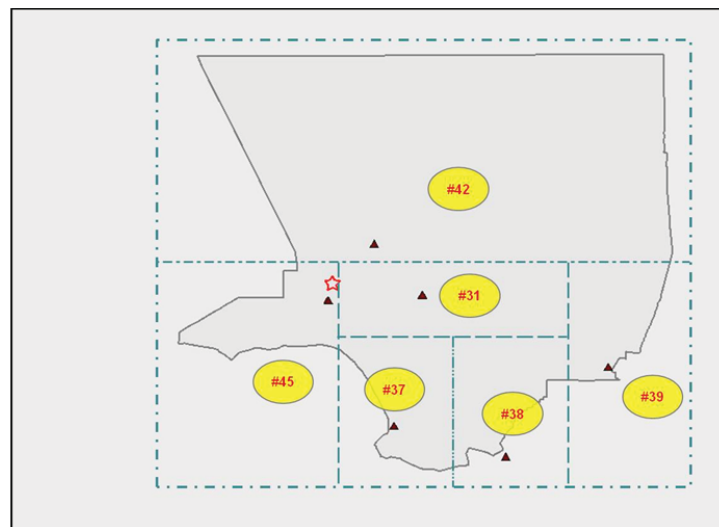
Figure 3-23 Subdivided areas and the selected boreholes in the Los Angeles area
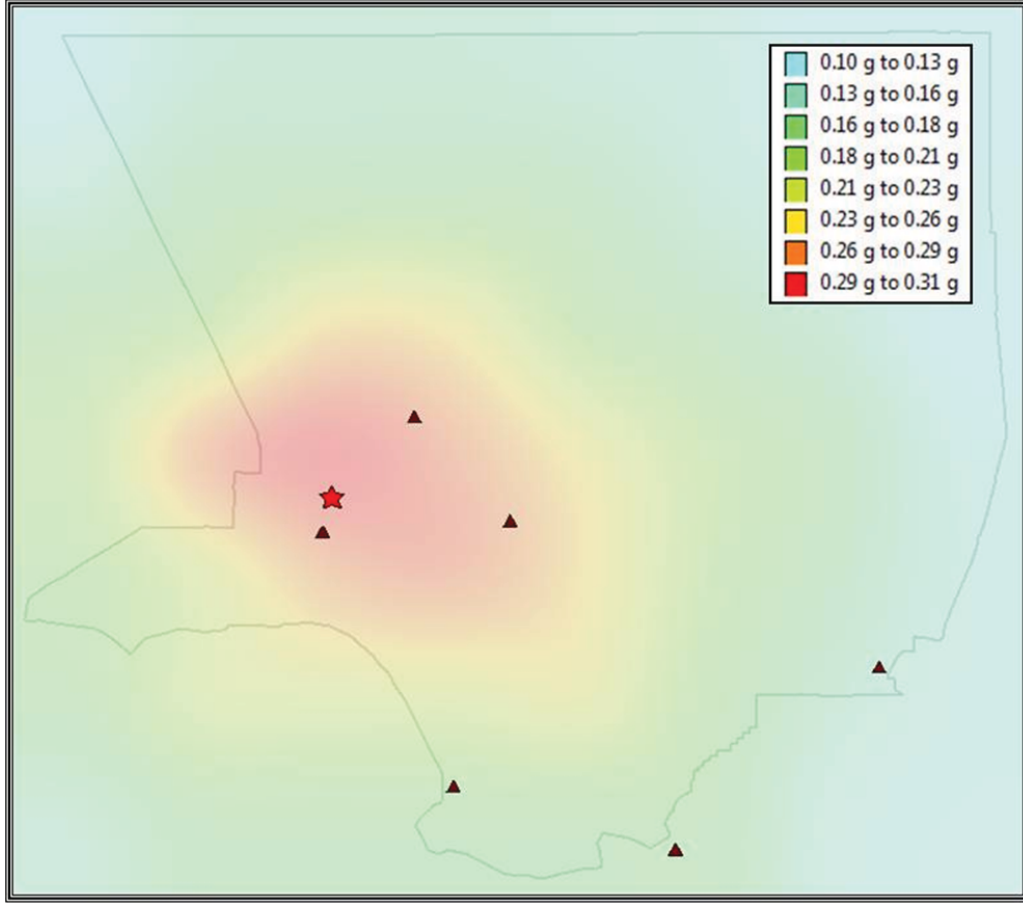
Figure 3-24 Map of PGA for the 1994 Northridge earthquake in the Los Angeles area in standard gravity (g)

To evaluate the improvements of proposed hazard analysis method, comparisons were made between hazard maps generated by different approaches, such as ShakeMap, deterministic hazard map in MAEviz, and the generated map. Figure 3-25 is the ShakeMap published by USGS for the 1994 Northridge earthquake (http://earthquake.usgs.gov/earthquakes/shakemap/sc/shake/Northridge/). It was made by using the instrumented records along with interpolation and extrapolation techniques.

Therefore, the ShakeMap is relatively realistic. When comparing with ShakeMap, the generated map is qualititatively reasonable and acceptable.

Figure 3-25 ShakeMap for the 1994 Northridge earthquake (USGS)

(Pink county border is added by the writer)

Moreover, a quatitative comaprison was made among ShakeMap, map generated by MAEviz and map generated by the proposed method (represented by NISRAF in the following). Figure 3-26 and Figure 3-27 show the generated map as well as differences between the calculated and the measured PGA values during the 1994 Northridge earthquake by NISRAF and MAEviz, respectively. Due to the limited site informaiton, only 6 sites, which were used previously to represent 6 different site conditions, were discussed here. Generally, the map generated by NISRAF is more reasonable and realistic than the one from MAEviz. Site response analysis is one reason for this difference—MAEviz uses a simple approach, the F_a and F_v site coefficients, while NISRAF uses 1-D site response analysis to account for soil nonlinear behavior.

Between these 6 sites, Tarzana and Sylmar show large differences for both NISRAF and MAEviz map, even though they have higher estimated PGA values (Table 3-9). Several studies have been devoted to investigate the high PGA values in these two sites (Hartzell et al., 1996; Vahdani and Wikstrom, 2002). Generally, it is believed that the local geology and topography, the near-fault, basin and the directivity effect of the earthquake contribute to the higher response. Among them, topography, near-fault and directivity effects are not included in current attenuation models and 1-D site response analysis program.
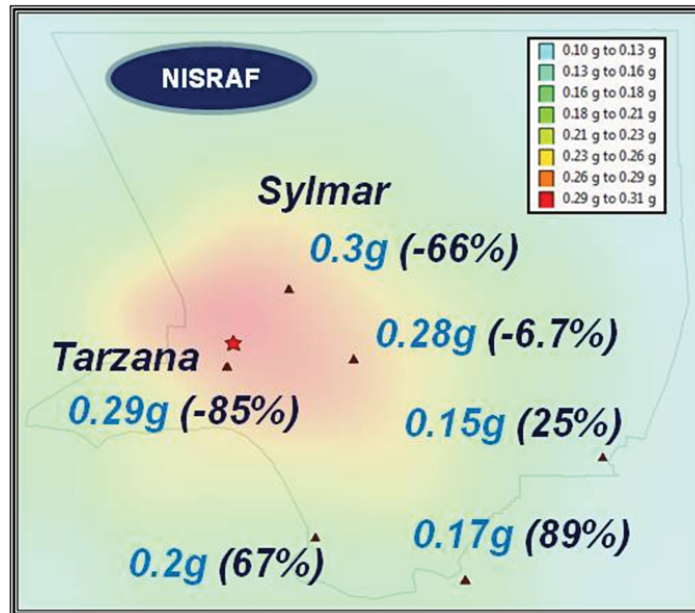
Figure 3-26 Hazard and difference of PGA between NISRAF and measured one
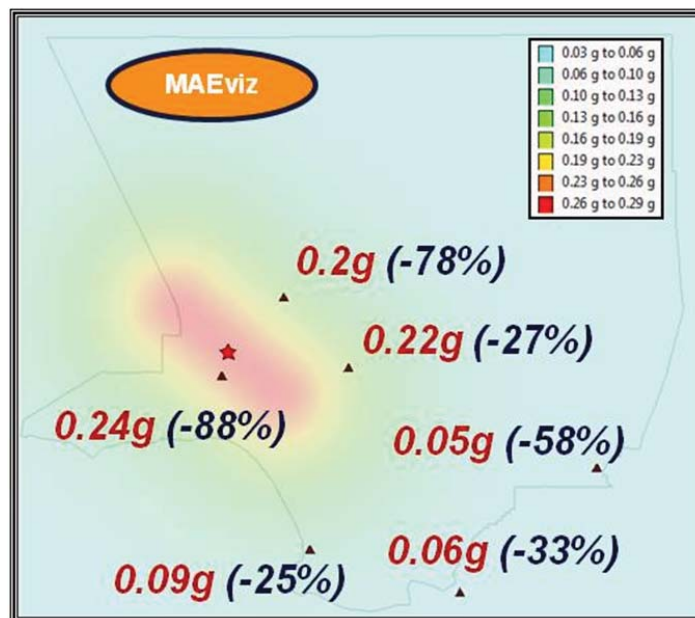
Figure 3-27 Hazard and difference of PGA between MAEviz and measured one

Table 3-9 Comparisons of PGA value between the measured and the calculated

PGA (g)	Tarzana*	Sylmar**
Measured	1.93	0.89
NISRAF	0.29	0.3
MAEviz	0.24	0.2

Tarzana-Cedar Hill Nursery A (CSMIP #24436)

**Sylmar-6-story County Hospital (CSMIP #24763)*

3.8 Summary and Discussion

In conclusion, the above three applications demonstrate the methodologies and procedures of the proposed advanced hazard analysis method, including seismic hazard analysis, synthetic ground motions, site response analysis and hazard map generation. The use of instrumentation data provides an opportunity to calibrate the hazard models, which, therefore, improve the reliability of the hazard characterization used in the further analyses, such as synthetic ground motion and hazard map generation. Meanwhile, the incorporation of site response analysis improves the accuracy in synthetic ground motions as well as in hazard maps. Moreover, the proposed method simplifies tedious and complicated procedures in each hazard model, solves the compatibility between them, and provides an interactive interface for ease of use. This advanced method has already been implemented in NISRAF successfully, which cooperates with other sub-disciplines toward the purpose to provide more reliable earthquake impact assessment results.

.

CHAPTER 4

FRAGILITY ANALYSIS BY HYBRID SIMULATION

4.1 Introduction

Fragility, or vulnerability, presents the probability of reaching or exceeding a specific performance level under a specific seismic hazard. Fragility curves relate the effects of seismic hazard to the damage of the structures. Therefore, fragility curves (sensitivity) along with hazard (exposure) are used to assess earthquake impact on the built environment.

As discussed in *section 2.6: Fragility Analysis*, four categories are generally used to classify fragility curves—empirical fragility curves, judgmental fragility curves, analytical fragility curves and hybrid fragility curves. Through development in the past few decades, the fragility analysis has reached its mature state and also has been widely accepted by the community. Nevertheless, uncertainties and limitations remain for their own inherent nature (such as scarcity in empirical fragility curves and subjectivity in judgmental fragility curves) or modeling deficiencies (analytical fragility curves, for example). Even the hybrid fragility curves have flaws since different uncertainties sources exist between different types of fragility relationships.

4.2 Overview of the Advanced Hybrid Fragility Analysis Method

In order to reduce the uncertainties and to improve reliability, an advanced hybrid fragility analysis method is proposed. In this approach, fragility is represented by a lognormal distribution as shown in Equation (4.1) (Wen et al., 2004).

$$P_f = P\left[\frac{S_d}{S_c} \geq 1\right] = 1 - \Phi\left(\frac{\ln(1) - \lambda}{\beta}\right) = \Phi\left(\frac{\lambda}{\beta}\right) \tag{4.1}$$

where λ and β denote the mean and standard deviation of $\ln(S_d/S_c)$. If S_d and S_c follow lognormal distributions, then lnS_d and lnS_c follow normal distributions and the function $\ln(S_d/S_c)$ also follows a normal distribution. This is, therefore, consistent with the lognormal distribution assumption for S_d and S_c, which is commonly assumed for fragility analysis. The parameter λ is expressed as a function of the earthquake intensity parameter, such as PGA, which is derived through testing in the laboratory. The standard deviation β represents uncertainties in both demand and capacity in the analysis, which is from the literature.

As shown in Figure 4-1, through scaling seismic inputs (ground motions), several tests (hybrid or conventional simulation) are conducted in the laboratory in order to reach the target structural response. The seismic intensity (PGA, for example) of the scaled ground motion is then assigned to the mean seismic intensity for current limit state. The target structural response is defined for different limit states, such as interstory drift angle (ISDA) of 0.7% for the immediate occupancy limit state for steel moment frame building.

Therefore, with λ derived from laboratory testing and β from literature, the fragility relationships is derived through this advanced hybrid manner.
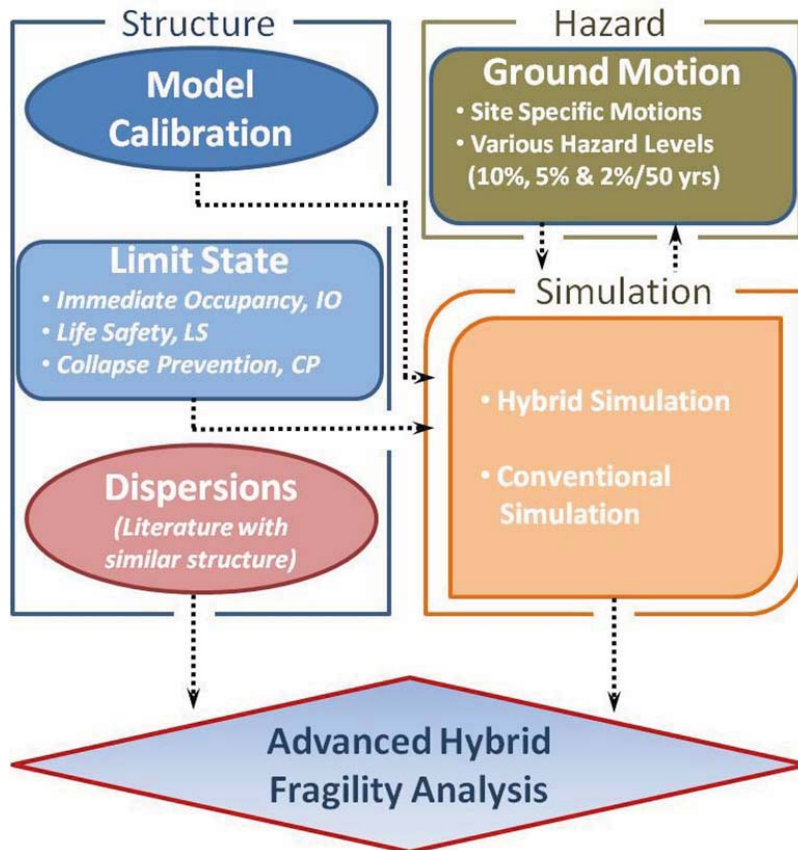
Figure 4-1 Flow chart for the advanced hybrid fragility analysis

4.3 Verification Studies

Fragility curves of three performance limit states (namely, immediate occupancy, life safety and collapse prevention) for a mid-rise steel moment resisting frame building in Los Angeles area were generated through hybrid simulation (with calibrated finite

element model along with experimental simulation and site specific ground motions) and dispersions from similar structures found in the literature.

4.3.1 Structural Model and Seismic Input

4.3.1.1 Building Description and Structural Model

A six-story instrumented building in Burbank, California was selected for this verification. This is a steel moment resisting frame structure, in which the perimeter frames are the primary lateral load resisting system and the internal frames are only resisting gravity load. This building was instrumented by California Strong Motion Instrumentation Program (CSMIP) in 1980 with 13 sensors. A 2-D finite element model was built in ZEUS-NL (Elnashai et al., 2004) and tuned using the measured structural responses (Figure 4-2). More descriptions and discussions of this building, as well as finite element model construction and model updating results, are detailed in *Chapter 6: Case Studies*.
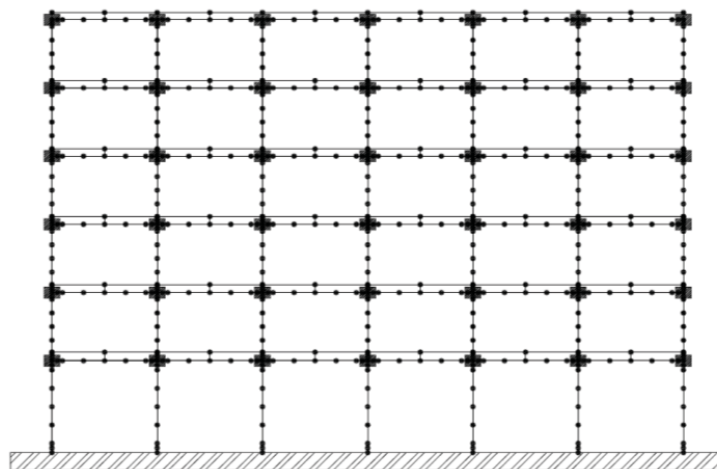
Figure 4-2 Analytical model configuration for Burbank building

4.3.1.2 Performance Limit State

Three performance limit states are specified in this study, namely, the immediate occupancy (IO), the life safety (LS) and the collapse prevention (CP). Interstory drift angles (ISDAs) 0.7%, 2.5% and 5% are assigned to IO, LS and CP performance level, respectively (FEMA, 2000b).

4.3.1.3 Seismic Input

Ground motions representative of the local hazard characterization are essential in order to capture the realistic structural response. In addition, various ground motions should be considered to avoid excessive scaling on them. Excessive scaling is unrealistic and unreasonable particularly when motion has higher earthquake intensity. Based on the above considerations, the 27 site specific synthetic ground motions with various hazard levels, generated for the Burbank sits (Appendix A), were selected as the earthquake demand in this verification. To avoid excessive scaling, records related to 10%, 5% and 2% probability of exceedance in 50 years hazard level are used to derive fragility curves for immediate occupancy, life safety and collapse prevention performance limit state, respectively.

4.3.2 Hybrid Simulation

The calibrated Burbank building model and ground motions from hazard characterization analysis were used to verify the extension of the hybrid simulation to fragility analysis as well as the integration of hybrid simulation in earthquake impact assessment. The calibrated 2-D structure model was divided into two sub-structures,

namely, the column (the lower part of the left exterior column at the first floor) and the frame (the remaining structure). The frame module was simulated using ZEUS-NL (Elnashai et al., 2004), while the column module—replaced by a small scale aluminum specimen (Figure 4-3)—was tested in the laboratory.
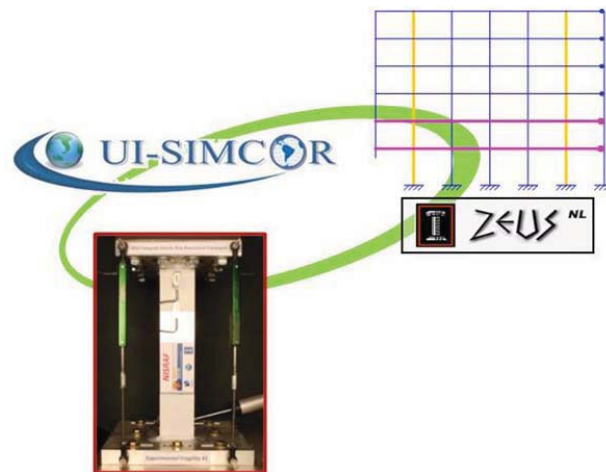
Figure 4-3 Hybrid simulation with two sub-structures (column and frame)

4.3.2.1 Testing Facility

George E. Brown, Jr. Network for Earthquake Engineering Simulation (NEES) equipment site in the University of Illinois at Urbana-Champaign, the Multi-Axial Full-Scale Sub-Structured Testing and Simulation (MUST-SIM) facility is selected as the experimental facility. The MUST-SIM facility consists of an L-shaped strong wall, three large loading and boundary condition boxes (LBCBs) and advanced non-contact measurement systems (Krypton, for example). In addition to the large-scale facility, a $1/5^{th}$–scale model laboratory (including wall-floor system, three boxes, and a portable and self-reacting LBCB) is available for training, for verifying control algorithms and for

investigating structural behaviors in small scale. In this study, the portable LBCB (pLBCB), as shown in Table 4-1 and Figure 4-4, is employed since the tests are a proof-of-concept study—to demonstrate the extension and integration of hybrid simulation in fragility analysis and impact assessment, respectively. Therefore, meeting similitude requirement is not necessary.

Table 4-1 Force and displacement capacities of portable LBCB (Holub, 2010)

Type	Axis	Capacity	Type	Axis	Capacity
Displacement* (inch)	X	±2	Rotation* (degree)	X	±11.7
	Y	±1		Y	±9.7
	Z	±1		Z	±22.6
Force* (kip)	X	±6	Moment* (kip-inch)	X	±28.9
	Y	±3		Y	±58.8
	Z	±9		Z	±28.9

Note the values provides here do not reflect interaction amongst the platen DOF. X actuators have a force capacity of ±3 kips and a displacement capacity of ±2 inch. Y and Z actuators have a force capacity of ±3 kips and displacement capacity of ±1 inch.

Figure 4-4 Portable LBCB at MUST-SIM 1/5th-scale model laboratory

4.3.2.2 Specimen Design

A small scale aluminum column was selected to represent the real steel column in the building. Similitude relationships (Harris and Sabnis, 1999) shown below were used to design the small specimens.

$$M_B = S_E S_L^3 M_S \qquad (4.2)$$

$$F_B = S_E S_L^2 F_S \qquad (4.3)$$

$$S_E = \frac{E_B}{E_S} \qquad (4.4)$$

$$S_L = \frac{L_B}{L_S} \qquad (4.5)$$

In the above equations, M_B and M_S are the large and small-scale moments; F_B and F_S are the large and small-scale forces; E_B and E_S are the large and small-scale moduli of elasticity; and L_B and L_S are the large and small-scale lengths, respectively.

Through the above relationships, $1/6.25^{th}$ scale models of the original column were designed and constructed within the limitation of the pLBCB capacity. The scale factors and the dimensions of the original column and small-scale specimen are listed in Table 4-2 and Table 4-3, respectively. Figure 4-5 is the elevation view of the small-scale aluminum specimen. As shown in the drawing, rigid end plates are included to facilitate connection of specimen to the LBCB platen and reaction frame.

Table 4-2 Scale factor for design small scale specimen

S_E	S_L
2.9	6.25

Table 4-3 Dimension and material properties of real column and small-scale specimen

	d (in)	b_f (in)	t_w (in)	t_f (in)	Elastic modulus E (ksi)	Yield strength f_y (ksi)
Real column (W14x184)	15.38	15.66	0.84	1.378	29000	40
Small-scale specimen (Alloy 6061-T6)	3	2.509	0.349	0.26	10000	36
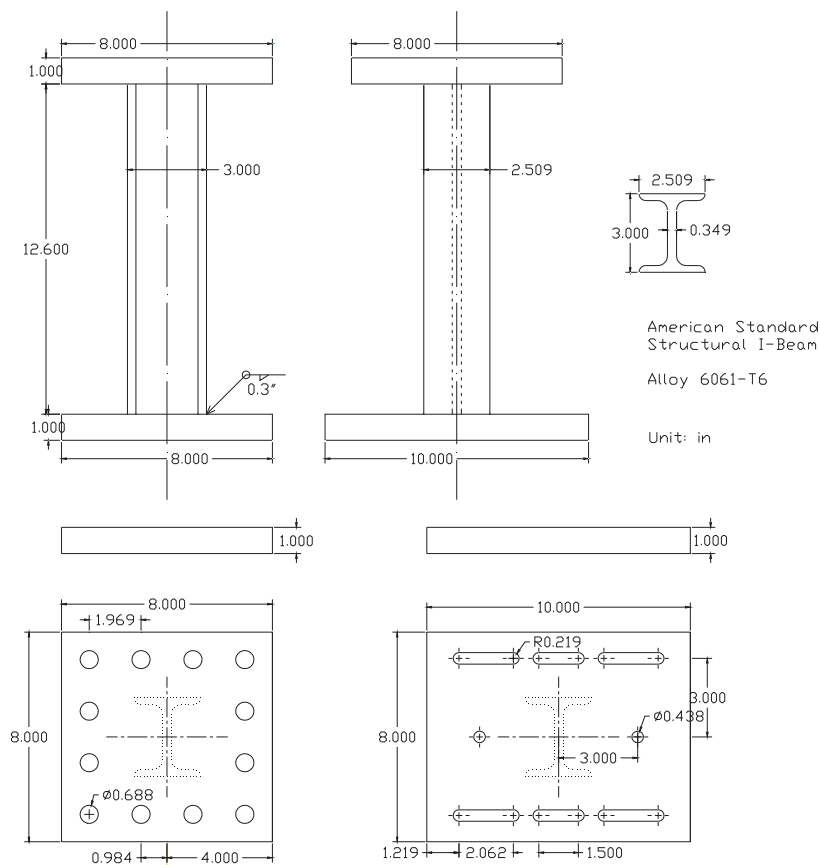
Figure 4-5 Aluminum column specimen elevation, unit: in.

(a) Front side view   (b) Right side view

Figure 4-6 Completed small-scale specimen

4.3.2.3 Software Environment

4.3.2.3.1 UI-SIMCOR

 UI-SIMCOR (Kwon et al., 2007), the University of Illinois software platform for hybrid simulation, is adopted to coordinate all the sub-structures (modules) during the testing, such as the communication and interaction between the experimental (column) and analytical (frame) modules (Figure 4-3). The α-Operator Splitting (α-OS) method is implemented in UI-SIMCOR to conduct time integration. Generally, three stages, namely, stiffness evaluation, static loading and dynamic loading are undertaken step by step to finish a hybrid testing.

4.3.2.3.2 ZEUS-NL

The frame sub-structure model was simulated in ZEUS-NL platform (Elnashai et al., 2004), a nonlinear FE analysis program, developed by the MAE Center. In this analytical model, section and material properties were based on design documents, lumped mass was used and applied at each beam-column connection, and concrete slabs were modeled and connected to steel girders using rigid elements, to account for their contribution of stiffness. More details about construction of this analytical model are illustrated in *Chapter 6: Case Studies*.

4.3.2.3.3 LBCB Operation Manager

The LBCB Operation Manager is a program developed to control the Load and Boundary Conditions Boxes (LBCB) of MUST-SIM facility. Three control algorithms are implemented in this program, namely, displacement, force and mixed mode control. In this study, the displacement control algorithm in Operation Manger is used to control the portable LBCB during the testing.

4.3.2.3.4 LBCB-Plugin

The LBCB-Plugin was original developed as the intermediary between UI-SIMCOR and the LBCB Operation Manger. Recently, a new developed LBCB Plugin is released, which serves as the master program for all the software used during the testing. Therefore, except the communication between UI-SIMCOR and Operation Manger, this program synchronizes data collected and pictures taken and stored from data acquisition program and Camera-Plugin program, respectively.

4.3.2.3.5 Data Acquisition

Instrumented data was collected continuously through a custom LabViw program. In addition to the traditional data (displacement, force and strain), photos were taken automatically at each time step through Camera-Plugin program developed at MUST-SIM facility.

4.3.2.4 Experimental Setup

4.3.2.4.1 Testing Configuration

All the small-scale aluminum columns were tested on the portable LBCB. Figure 4-7 presents the experimental setup. As shown in Figure 4-7 (b), the top-end plate of specimen is attached to the steel frame (fixed end); while the bottom-end plate is attached to the LBCB platen (flexible (control) end). The control algorithm for this study is based on the external feedback of linear potentiometers installed on the specimen. Four linear displacement LVDTs (Liner Variable Differential Transformer) were installed, as shown in Figure 4-7 (b) (another vertical one is behind the specimen), which provided feedback on DOF X (in-plane horizontal), Z (vertical) and R_y (out-of-plan rotation). These 3 DOFs were assigned as the control DOFs in hybrid simulation tests.

(a) Overall view
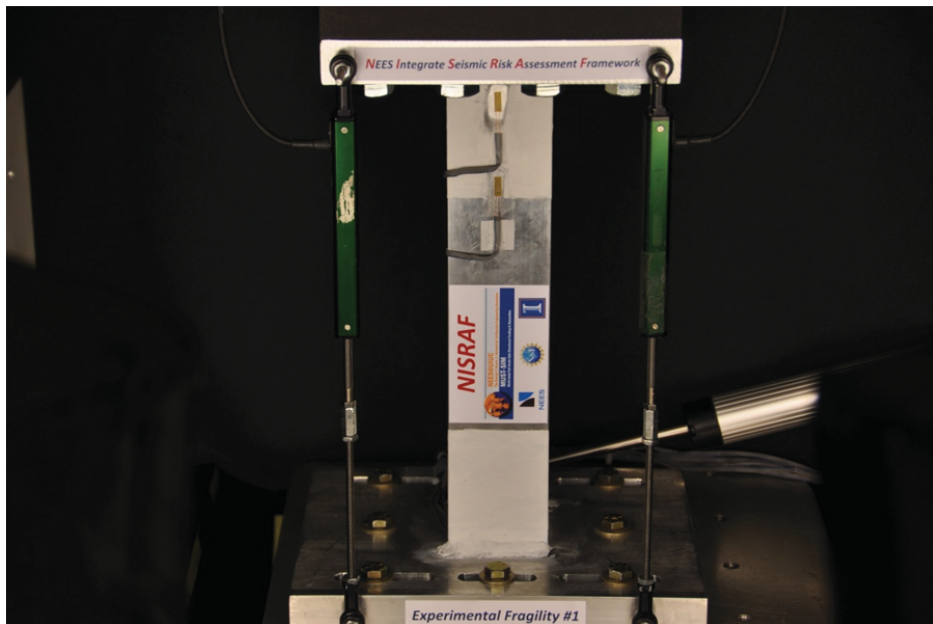
(b) Close view

Figure 4-7 Small-scale experimental setup

4.3.2.4.2 Instrumentation

Six actuator displacements, 6 actuator forces, 6 Cartesian displacements and 6 Cartesian forces from portable LBCB were recorded. Instrumentation from external measurements was also collected, such as displacements from 4 LVDTs and strain values from 6 strain gauges. High resolution photos from three angles (namely, front, right and left side) of the specimen were taken and stored at each time step.

4.3.2.5 Hybrid Simulation Results

Hybrid simulation coordinated by UI-SIMCOR using the Northridge earthquake record (Figure 4-8) as the ground acceleration was first conducted as a proof test of the hybrid model prior to the generation of the hybrid fragility curves. As shown in Figure 4-9, good agreement was found between the measured response (CSMIP Station No. 24370 record of the 1994 Northridge earthquake) and the response from the hybrid simulation testing. With this confidence in the hybrid model and experimental setting, 7 additional hybrid simulation tests with various ground motions were performed in order to generate the hybrid fragility curves. Details and results of these hybrid simulation tests are presented in the following section.
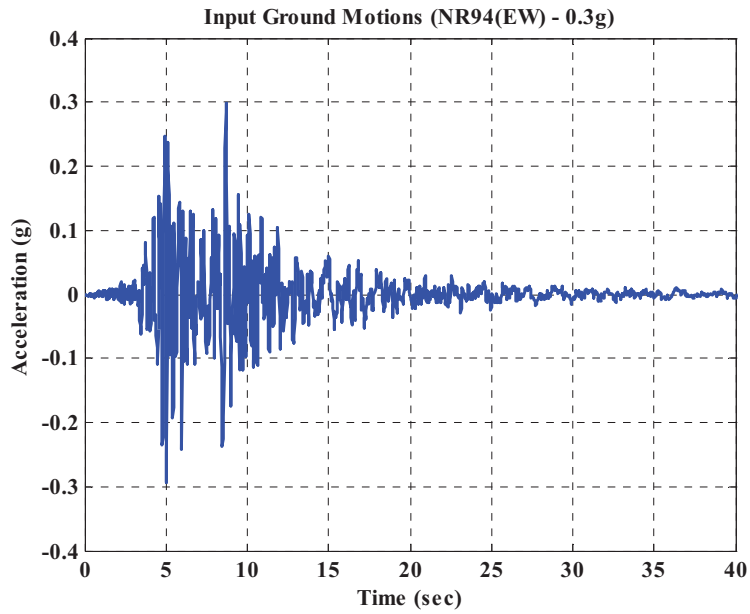
Figure 4-8 Ground motion record of the 1994 Northridge earthquake (CSMIP # 24370)
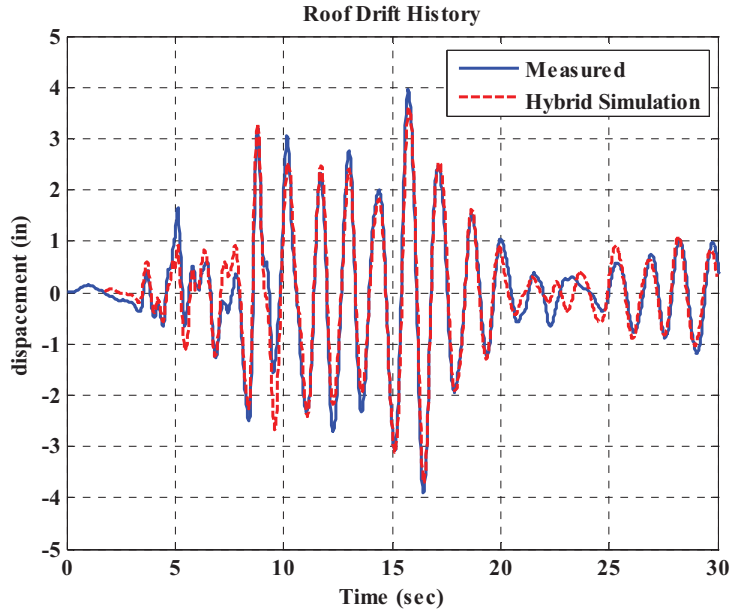
Figure 4-9 Comparison of the roof drift between the measured and the hybrid simulation

4.3.3 Hybrid Fragility Analysis

Based on the lognormal distribution assumption, mean value of seismic intensity from testing along with dispersions from literature are used to derive the hybrid fragility curves. In this study, mean value of PGA from hybrid simulation tests and dispersions from literature (FEMA, 2000a; Cornell et al., 2002; Yun and Foutch, 2000) were used to derive the fragility curves for this 6-story steel building in Los Angeles area. In the following section, mean PGA values from hybrid simulation tests are presented first, followed by discussions on the dispersions found in literature. Moreover, a comprehensive uncertainty review was also included.

4.3.3.1 Mean PGA Values from Hybrid Simulation

Hybrid simulation results under different synthetic ground motions (10%, 5% and 2% probability of exceedance in 50 years for immediate occupancy, life safety and collapse prevention performance levels, respectively) were used to derive the mean PGA value for each performance level. Step-by-step procedure to derive mean PGA value is given below, also shown in Figure 4-10:

Step 1: 10% probability of exceedance in 50 years ground motion is selected as seismic input for hybrid simulation to derive mean PGA value for immediate occupancy limit state.

Step 2: Interstory drift angle (ISDA) is calculated based on testing results. Comparison of ISDA between the calculated one and the target one (0.7% ISDA for immediate occupancy performance limit state, for example) is then made.

Step 3: Hybrid simulation is resumed (replaced with new specimen if nonlinear behavior occurs in previous test) with seismic input multiplied by a scale factor (calculated based the difference in *Step 2*), if the difference exceeds criterion ($\pm$5% difference, for example).

Step 4: Iterations from *Step1* to *Step 3* continues till the criterion is met.

Step 5: Once the calculated ISDA matches the defined ISDA, PGA value of current (scaled) record is assigned as the mean PGA value for immediate occupancy performance limit state.

The above procedure is an example of how to drive the fragility curve for IO limit state, while similar procedures were applied to derive curves for LS and CP limit states using 5% and 2% probability of exceedance in 50 years ground motions, respectively.
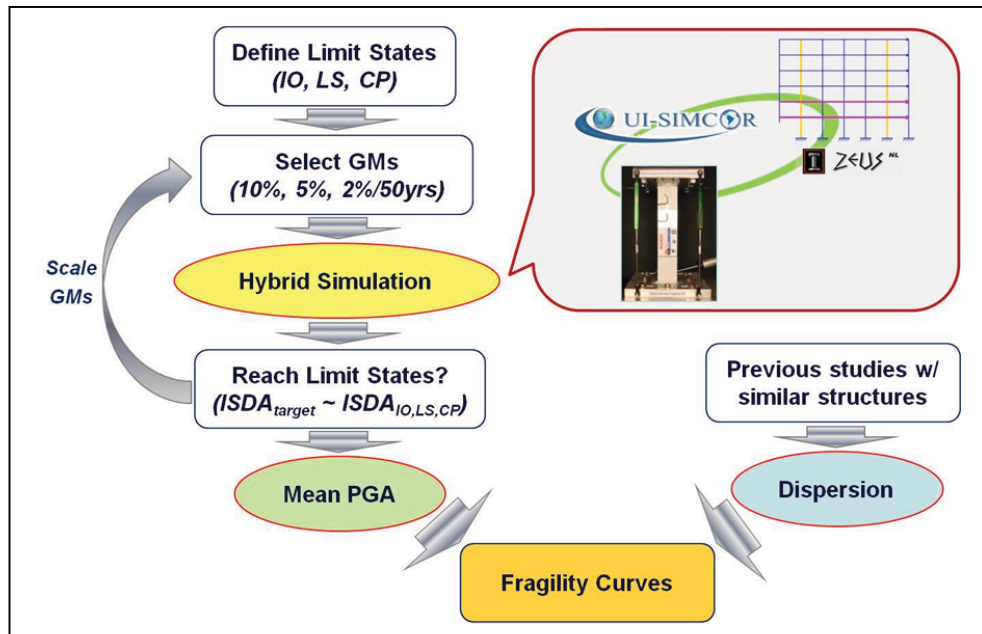
Figure 4-10 Methodology and procedures for the advanced hybrid fragility analysis

Figure 4-11 shows the number of hybrid simulation tests used to derive the mean PGA values. Table 4-4 lists the target ISDA (ISDA, interstory drift angle, are defined in previous section for this study) as well as the mean PGA values from hybrid simulation tests.
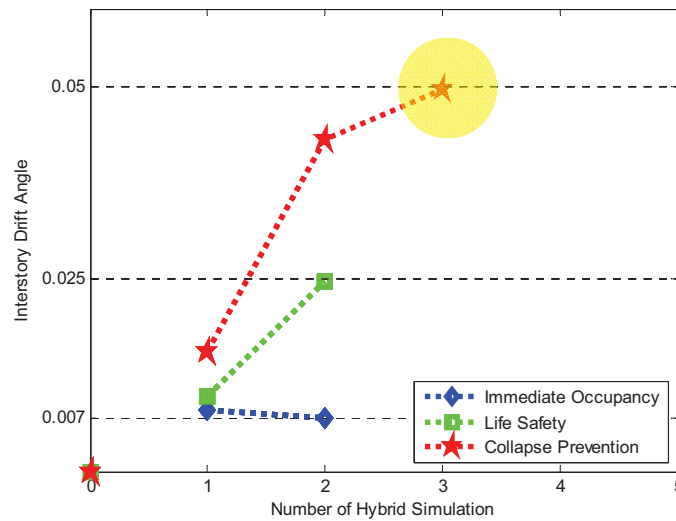
Figure 4-11 Number of hybrid simulation tests to derive fragility curves

Table 4-4 Interstory drift angle (target ISDA) and PGA from hybrid simulation tests

Performance Level	Immediate Occupancy	Life Safety	Collapse Prevention
Interstory drift angle (%)	0.7	2.5	5.0
Mean PGA (g)	0.545	1.627	2.777

Figure 4-13, Figure 4-14 and Figure 4-15 show one simulation result (the red star highlight with yellow circle area in Figure 4-11, 2% probability of exceedance in 50

years multiplied by scale factor equal to 3.54, as shown in Figure 4-12). The other

simulation results can be found in Appendix B.
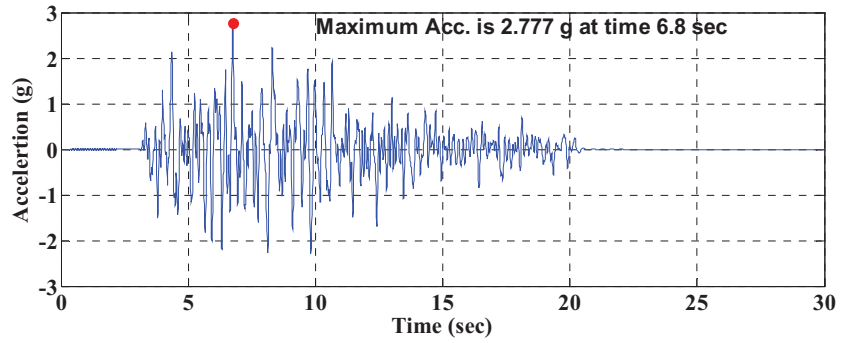
Figure 4-12 Synthetic Ground motion (2% PE/50yrs with scale factor = 3.54)
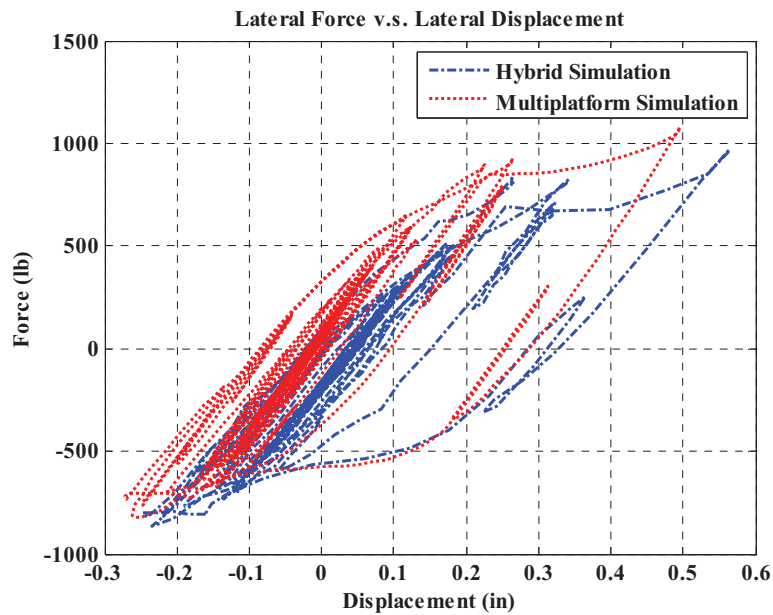
Figure 4-13 Comparison of column response between hybrid and multiplatform simulation
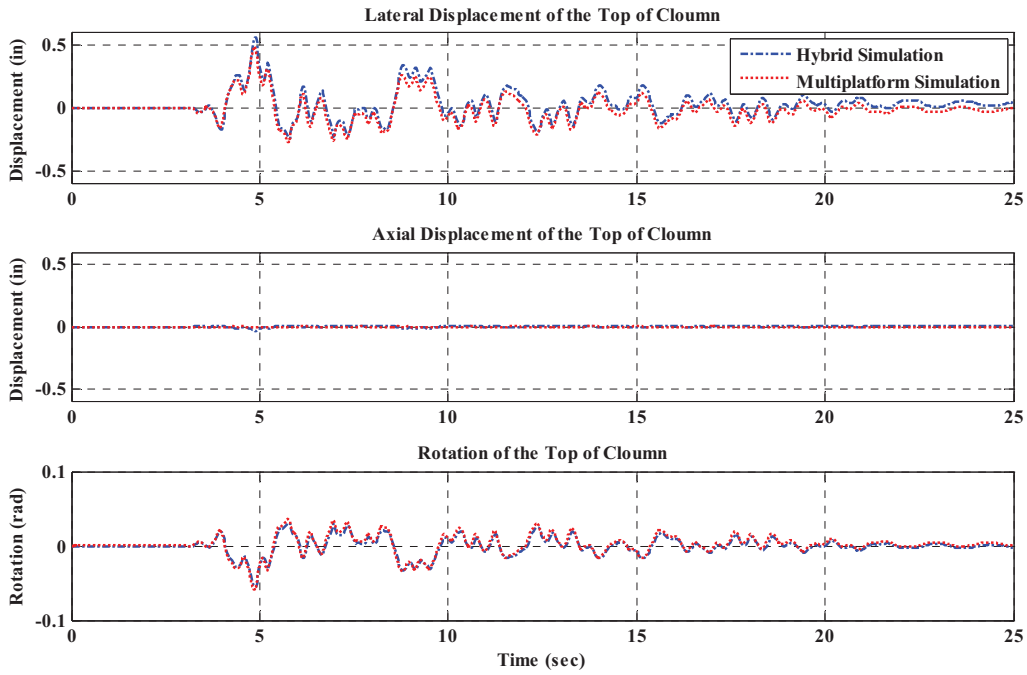
Figure 4-14 Comparison of displacement between hybrid and multiplatform simulation
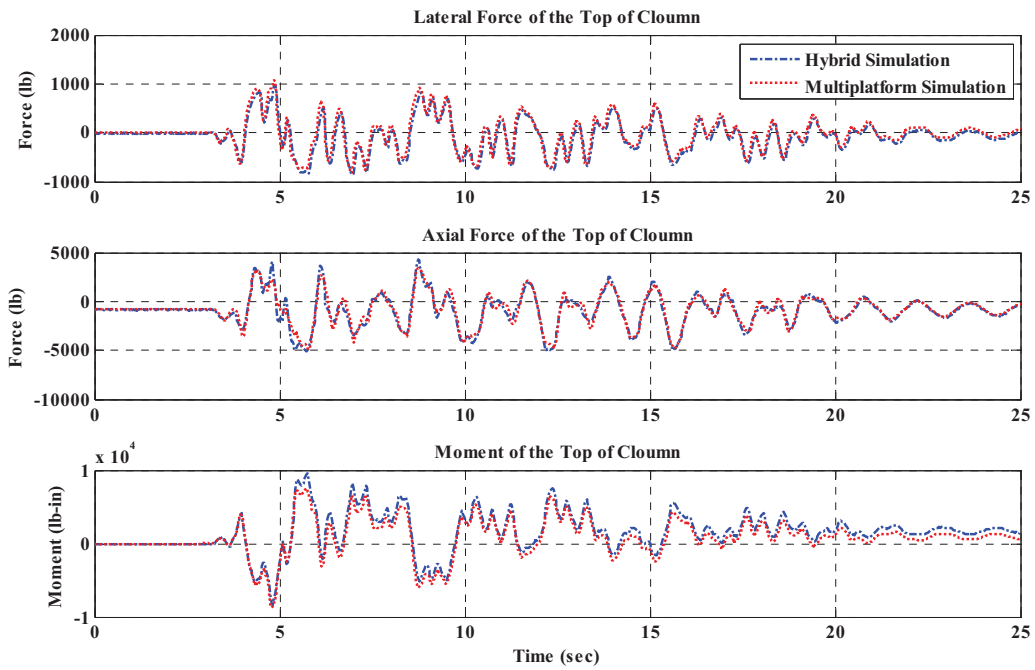
Figure 4-15 Comparison of displacement between hybrid and multiplatform simulation

94

4.3.3.2 Dispersions from Literature

Dispersion, a statistics vocabulary, represents the uncertainty term in fragility relationships. Due to the limited number of tests in the hybrid fragility analysis, it is unreasonable and also unrealistic to regress dispersion based on few testing results. Therefore, dispersions of the proposed hybrid fragility analysis are found from the literature.

Generally, uncertainties are divided into two categories, namely, aleatoric and epistemic uncertainties. Aleatoric uncertainties are inherent, such as occurrence of earthquakes and material properties (Young's modulus, yielding strength in steel and compression strength in concrete, for example). By contrast, epistemic uncertainties are from the absence of knowledge, such as analytical model selection and construction, ground motion selection and others) (Wen et al., 2004). Consequently, a comprehensive review is needed to derive reasonable and representative dispersions.

FEMA 350 (FEMA, 2000a), the recommended seismic design criteria, is specially developed for new steel moment frame buildings. In FEMA 350, as well as in the literature (Cornell et al., 2002; Yun and Foutch, 2002), a method used to evaluate seismic behavior of steel moment frame buildings is proposed. Within this method, uncertainties for different building height, beam-connection type, analysis procedure (linear or nonlinear, static or dynamic), and local and global failures under different performance levels (IO and CP) are tabulated (*Table A-3 in FEMA 350*) or illustrated in the content. The uncertainty is therefore calculated using the following equation (*Equation (A-4) in FEMA 350*).

$$\beta_{UT} = \sqrt{\sum_i \beta_{ui}^2} \qquad (4.6)$$

where β_{ui} are the standard deviations of the natural logarithms of variation from various uncertainty sources. Three sources of uncertainties are included, namely, various analysis methods, beam-column connection behavior and global building stability capacity prediction. Table 4-5 summaries logarithmic uncertainties for mid-rise steel buildings obtained from FEMA 350.

Table 4-5 Logarithmic uncertainties for mid-rise building (FEMA, 2000a)

Uncertainty Source	Immediate Occupancy	Collapse Prevention
Analysis Method*	0.13	0.20
Beam-Column Connection	0.2	0.2
Global Stability Capacity	0.2	0.2

Nonlinear Dynamic Analysis Method

It is evident that, uncertainties from seismic hazard and material properties are missing. Although they somehow may be included in the analysis method uncertainty term, it is unclear here. Meanwhile, uncertainties are available only in two performance levels; uncertainty for LS is missing.

However, for the proposed advanced hybrid fragility analysis, the above two missed uncertainties have already been included in the procedures. Uncertainty in seismic input is captured by using sets of site-specific ground motions and avoiding likely excessive scale effects. Uncertainty in material properties is covered by calibrating the FE model in the beginning. Therefore, uncertainties for hybrid fragility curves were

calculated by using uncertainties listed in Table 4-5 and Equation (4.6). The uncertainty for Life Safety performance level was then interpolated. Table 4-6 lists the mean PGA values and dispersions derived from the proposed hybrid fragility analysis method.

Table 4-6 Mean PGA value and dispersions for mid-rise steel building fragility curves

Performance Level	Immediate Occupancy	Life Safety	Collapse Prevention
Mean PGA (g)	0.545	1.627	2.777
Dispersion	0.311	0.328	0.346

4.3.3.3 Hybrid Fragility Curves

Finally, based on Table 4-6 and lognormal distribution assumption, fragility curves were generated and are shown in Figure 4-16.
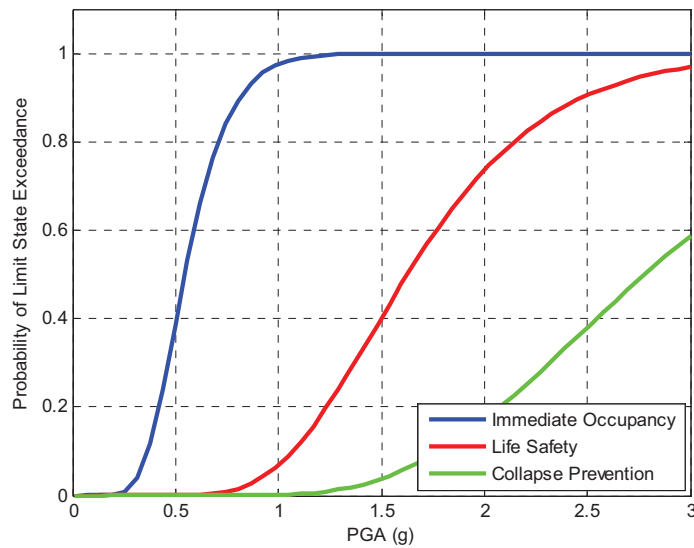
Figure 4-16 Hybrid fragility curves for mid-rise steel moment resisting frame building in Los Angeles area

A Comparison of fragility relationship between the generated (NISRAF) and the default fragility curves in MAEviz (the S1M High-Code category, S1M: mid-rise (4-6 stories) steel moment frame) was made and shown in Figure 4-17. As shown, MAEviz fragility curves are more vulnerable with higher uncertainties. The difference between them is from different fragility analysis approaches and different seismic inputs. The MAEviz default fragility relationships are derived analytically (SDOF (single degree of freedom) dynamic time history analysis). Meanwhile, the ground motions used in MAEviz are synthetic motions special for Central and Eastern United States (CEUS).

Figure 4-17 Fragility relationship comparison between NISRAF and MAEviz

4.4 Fragility Relationships for Other Building Types

A database contained fragility relationships for all building types is an essential ingredient of regional impact assessment. The proposed advanced hybrid fragility analysis provides an alternative method to derive more reliable fragility relationships. Definitely, this hybrid approach can be applied to any other building types. However, considerable time and effort are requ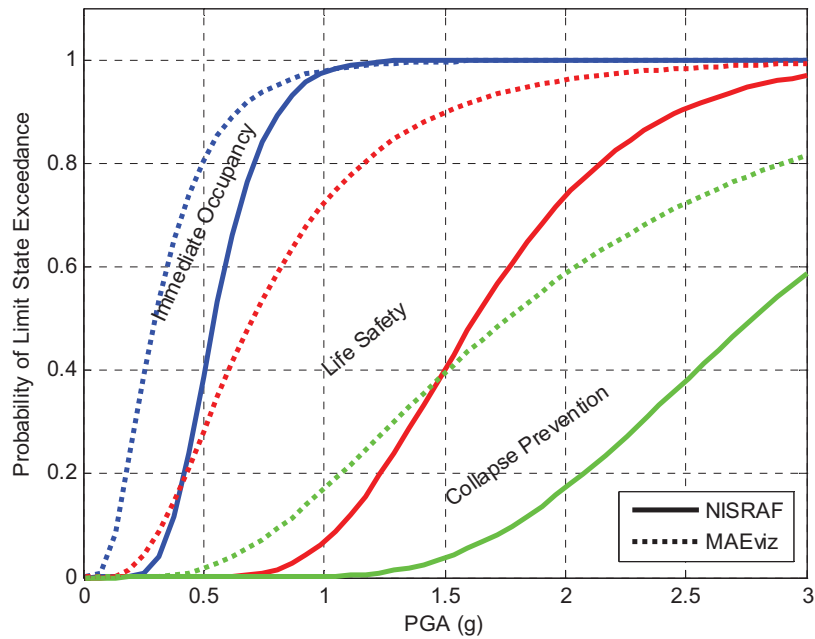ired. For the mid-rise steel moment resisting frame building in Los Angeles area, its fragility relationships have been generated in order to demonstrate fully the hybrid fragility analysis provided in this study. Extension of the database for fragility relationships to other building types is underway although it is out of the scope of this study. Currently, an alternative method to derive fragility relationships for other building types is the Parameterized Fragility Method, PFM (Jeong and Elnashai, 2006). In the following section, PFM is reviewed first, followed by the derivation of fragility relationships for other building types using PFM.

4.4.1 Parameterized Fragility Method

Parameterized Fragility Method (Jeong and Elnashai, 2006), an analytical fragility analysis approach, derives fragility curves through dynamic time history analysis on a SDOF FE model. It is, therefore, parameters corresponded with structure types and ground motions representative of site hazard characterization are essential for this methodology's use in regional impact assessment.

In HAZUS-MH, 36 building types (from W1: wood, light frame to MH: mobile homes) are defined (FEMA, 2006). Meanwhile, structural parameters (period, yield and

ultimate strength) for 36 building types under 4 code levels (pre-code, low-code, moderate-code and high-code) are tabulated. However, the majority of these parameters are based on engineers' opinions and experts' judgment. To be more realistic and reasonable, the latest research findings on structural capacity are incorporated. For example, parameters for wood frame and unreinforced masonry buildings are replaced according to the more comprehensive investigations (Gencturk and Elnashai, 2008; Frankie, 2010).

In addition, sets of site specific ground motions (Appendix A) are used as earthquake demand when performing dynamic time history analysis in PFM.

4.4.2 Fragility Relationships for Los Angeles area

Consequently, fragility relationships for 36 building types under 4 code levels particularly for the Los Angeles area were generated based on structural parameters and ground motions discussed in previous section. Procedure and results of using PFM to derive fragility relationships for other building types are detailed in Appendix C. Figure C-2 tabulates structural fragility parameters for all building types. Comparisons for S1M, W-series (wood frame) and URM-series (unreinforced masonry building) between different approaches were made and discussed below.

Figure 4-18 shows comparison of S1M (High-Code) fragility relationships. It is evident that fragility relationships from PFM are more vulnerable than that from NISRAF, but less vulnerable than that from MAEviz. SDOF dynamic time history analysis is used to derive fragility relationships in both PFM and MAEviz, the only difference between

them is the seismic inputs. Synthetic motions for the Los Angeles area are used in PFM, while synthetic motions for CEUS are used in MAEviz. Therefore, the difference between curves results from seismic inputs. The importance of seismic inputs is therefore emphasized again.
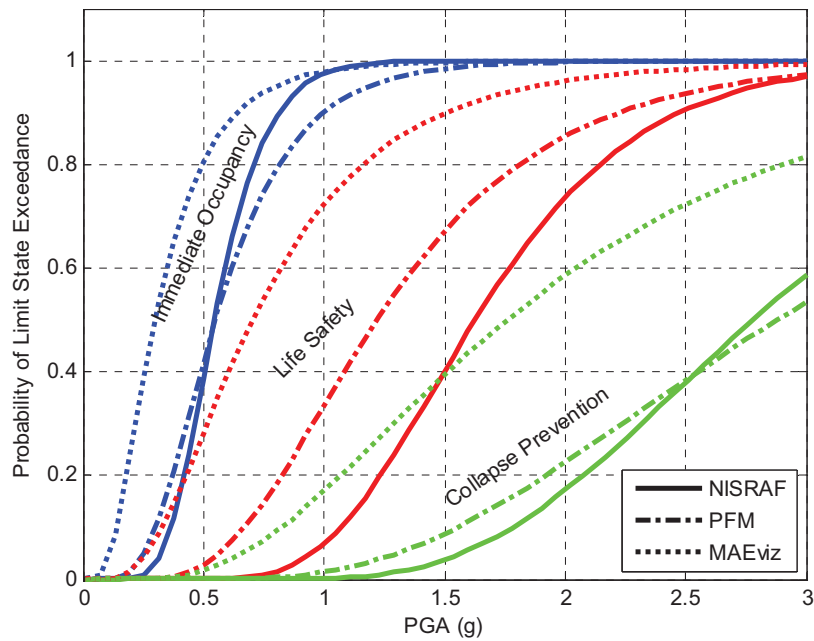
Figure 4-18 Comparison of S1M (High-Code) fragility relationships

Figure 4-19 and Figure 4-20 show comparison of W1 (wood, light frame), High-Code and URMM (mid-rise, unreinforced masonry building), Pre-Code between PFM and MAEviz. Clearly, fragility relationships in PFM are more vulnerable in both W1 and URMM. In addition to the different seismic input, structural parameters in PFM are updated by the latest research instead of using parameters listed in HAZUS-MH, which is in MAEviz. The observation of more vulnerable behavior in both wood frame and

unreinforced masonry building responses matches well to same findings in recent studies (Gencturk, 2007; Frankie, 2010).

Figure 4-19 W1 (High-Code) fragility relationships comparison between PFM and MAEviz

Figure 4-20 URMM (Pre-Code) fragility relationships comparison between PFM and MAEviz

4.5 Summary and Discussion

In conclusion, fragility relationships for a steel moment resisting frame building in the Los Angeles area are developed, which demonstrates the methodologies and procedures of the proposed a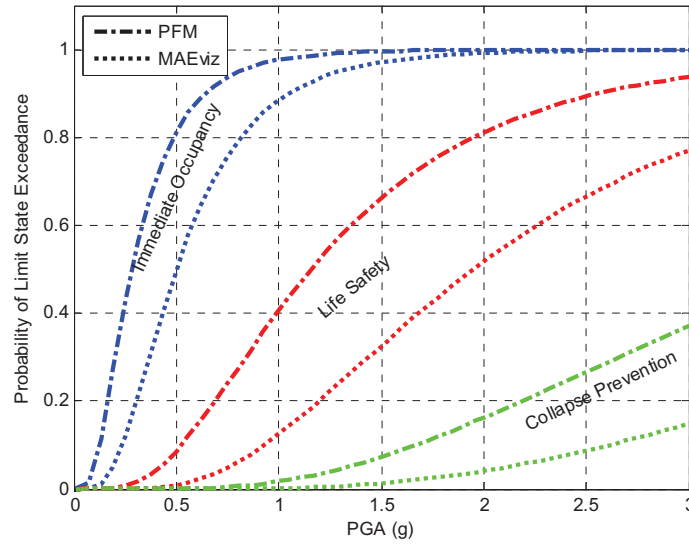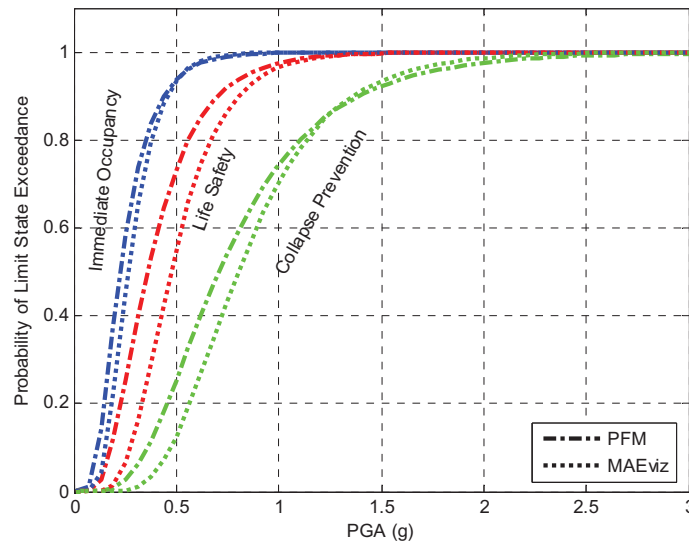dvanced hybrid fragility analysis method, including the incorporation of hybrid simulation into fragility analysis and uncertainty consideration. The incorporation of hybrid simulation test provides a chance to capture real structural responses, which therefore improves the reliability of the fragility relationship. Meanwhile, the comprehensive consideration of uncertainties increases the confidence when using the generated fragility relationships. Moreover, fragility relationships for 36 building types under 4 code levels in the Los Angeles area are provided by combining the generated hybrid fragility relationships (S1M, High-Code) with others through PFM method. In the future, when more and more experimental data are available, fragility relationships can continue being updated and improved through Bayesian method or other statistic approaches.

Finally, this advanced hybrid method to derive fragility relationships has already been implemented in NISRAF successfully, which cooperates with other sub-disciplines toward the purpose to provide more reliable earthquake impact assessment results.

.

CHAPTER 5

DEVELOPMENT OF NEES INTEGRATED SEISMIC RISK

ASSESSMENT FRAMEWORK

5.1 Introduction

NEES Integrated Seismic Risk Assessment Framework (NISRAF), a completed MATLAB (The MathsWork, Inc.) GUI-driven software platform, has been developed for the purpose of making impact assessment more efficient and more reliable. Several components—instrumentation, advanced hazard characterization, system identification, model updating, hybrid simulation, advanced hybrid fragility analysis and impact assessment tool—have been implemented and tailored with novel methods to build the seamless, transparent and extensible framework. Below, the architecture, methodologies, communication protocols and analysis platforms of NISRAF are discussed first. Next, the discussions are focused on features, potentials, limitations and challenges of NISRAF.

5.2 Architecture of NISRAF

As shown in Figure 1-2 and Figure 5-1, free-field measurements (**I1**) along with nonlinear site response analysis (**SR**) are used to generate the advanced hazard map and ground motion records (**AH**). The measured and synthetic records are then used in hybrid simulation and fragility analysis. Meanwhile, the structural model is calibrated with the measured structural response (**I2**). Next, hybrid simulations (**HS**) are performed with the

most critical component of the structural system tested in the laboratory and the remainder of the structure simulated analytically. These simulations are conducted to derive the mean seismic intensity value (PGA, for example) of the corresponding performance limit state. The fragility curves (**FA**) of the structure are then generated using the hybrid simulation data and the dispersions from the literature. Finally, the hybrid fragility curves and the calibrated hazard map are fed into the impact assessment tool, such as MAEviz or HAZUS-MH (**IA**).
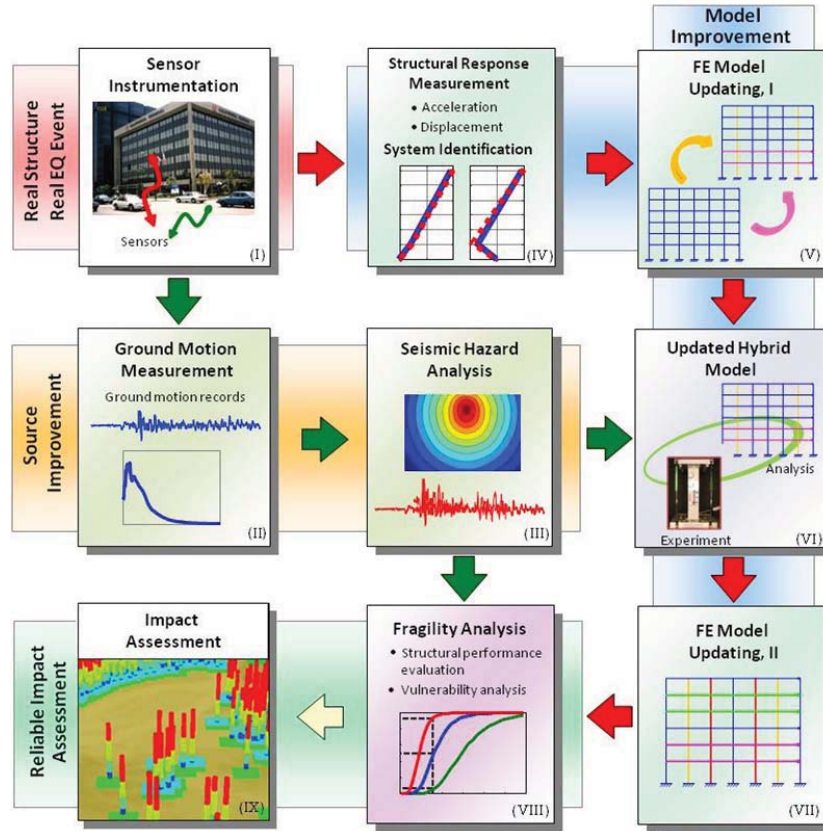

Figure 5-1 Architecture of NISRAF

Clearly, NISRAF is composed of five main parts: namely, (i) instrumentation (**I1**, **I2**), (ii) seismic hazard analysis (**AH**), (iii) model calibration and hybrid simulation (**HS**), (iv) fragility analysis (**FA**) and (v) earthquake impact assessment (**IA**). For ease of use, nine main menus with submenus are designed and arranged, following the analysis sequences (Figure 5-2):

- ***File:*** Contains general menus (such as *Open, Save, Save As, Page Setup, Print Review, Print* and *Exit*).

- ***Strong Motion****:* Provides an interface to download measured data from instrumentation databases (ANSS, COSMOS, CESMD and PEER).

- ***Hazard Characterization***: Contains three menus (*Seismic Hazard Analysis*, *Synthetic Time Histories* and *Hazard Map Generation*) to perform hazard analysis.

- ***Structure Model:*** Contains five menus (*Import from ZEUS File*, *New Model from Template*, *New Model*, *View* and *Structure Model*) to import, develop and view the FE model.

- ***Model Calibration:*** Contains three menus (*Modal Analysis*, *System Identification* and *Model Updating*) to improve the FE model.

- ***Hybrid Simulation:*** Contains five menus (*Dynamic Load*, *Static Load*, *Hybrid Model*, *Simulation* and *Results*) to develop the hybrid model, run simulation and check results.

- *Fragility Analysis:* Contains three menus (*Define Limit States*, *Run Hybrid Simulation* and *Hybrid Fragility Curves*) to derive hybrid fragility relationships through hybrid simulation testing.

- *Impact Assessment:* Contains two menus (*MAEviz* and *HAZUS*) to perform the earthquake impact assessment.

- *Help:* Contains three menus (*NISRAF Manual*, *UI-SIMCOR Manual, SimBuild Manual* and *About NISRAF*) to assist users in performing the analysis. Copyright and version information are also included here.
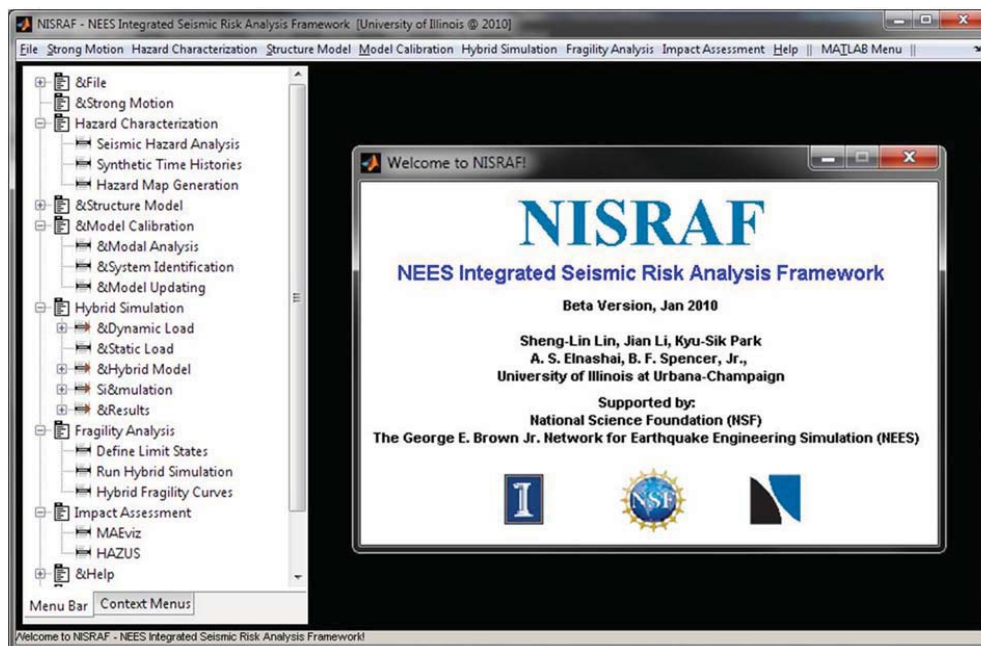

Figure 5-2 Welcome window and main window of NISRAF

In NISRAF, each main menu is modularized. Moreover, each method and algorithm implemented in sub-menu is also developed in module unit. This module feature makes it easy to understand analysis algorithms as well as to maintain this

versatile and integrated program. Most importantly, it enables the latest research finding and computation techniques to be easily implemented. Below, development of each main menu is presented with a focus on the novel manners used to tailor and integrate components to build the seamless framework.

5.2.1 File Menu

File menu contains the general menus, such as *Open*, *Save*, *Save As*, *Page Setup*, *Print Review*, *Print* and *Exit*, as shown in Figure 5-3. These submenus provide the basic functionalities to manage files, such as opening an existing file, saving and printing the current working file, and exiting and closing NISRAF.
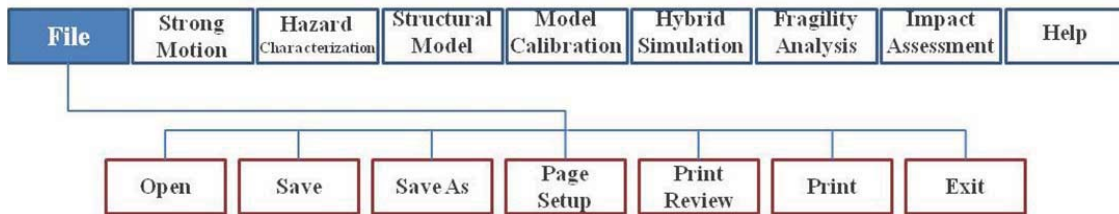
Figure 5-3 File submenus in NISRAF

5.2.2 Strong Motion Menu

In *Strong Motion* menu, as shown in Figure 5-4 and Figure 5-5, the user is prompted to connect to a web-based instrumentation database. Through this linkage, the user can easily download records. Meanwhile, NISRAF allows the user to create a new folder to deposit the downloaded records as well as other basic project information, which facilitates maintenance. Two different types of records are required to perform analysis in NISRAF (Figure 5-6). Ground motion (free-field) records are used to calibrate

hazard models, while structural measurements are used to calibrate structural models. The incorporation of the instrumented data into NISRAF is not only to increase its usage, but also to improve hazard and structural model.
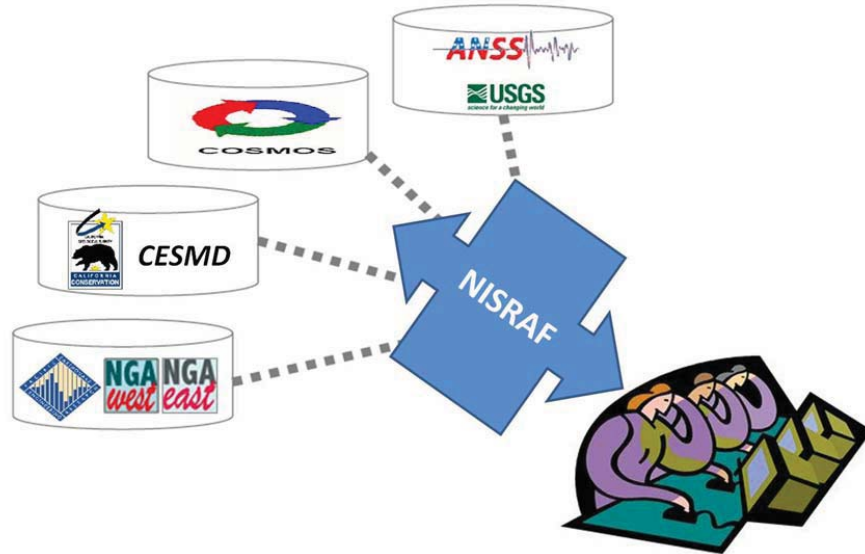

Figure 5-4 Schematic of *Strong Motion* menu in NISRAF

Figure 5-5 Strong Motion menu in NISRAF

Figure 5-6 Strong motion data GUI in Strong Motion menu

5.2.3 Hazard Characterization Menu

Hazard characterization menu is composed of three main parts: namely, *Seismic Hazard Analysis*, *Synthetic Time Histories* and *Hazard Map Generation*, as shown in Figure 5-7. Methodologies and analysis procedures of hazard characterization analysis have already been illustrated and verified in *Chapter 3: An Advanced Hazard Characterization Analysis Method*. One of the features of the proposed advanced hazard analysis approach is its ease of use. By tailoring the hazard models as well as ensuring connection and compatibility between them, it simplifies the complicated and tedious procedures in the conventional analysis. Consequently, with an interactive interface to define inputs, hazard analysis becomes efficient and straightforward. Below, analysis procedures in the three submenus are presented with GUIs and illustrations.
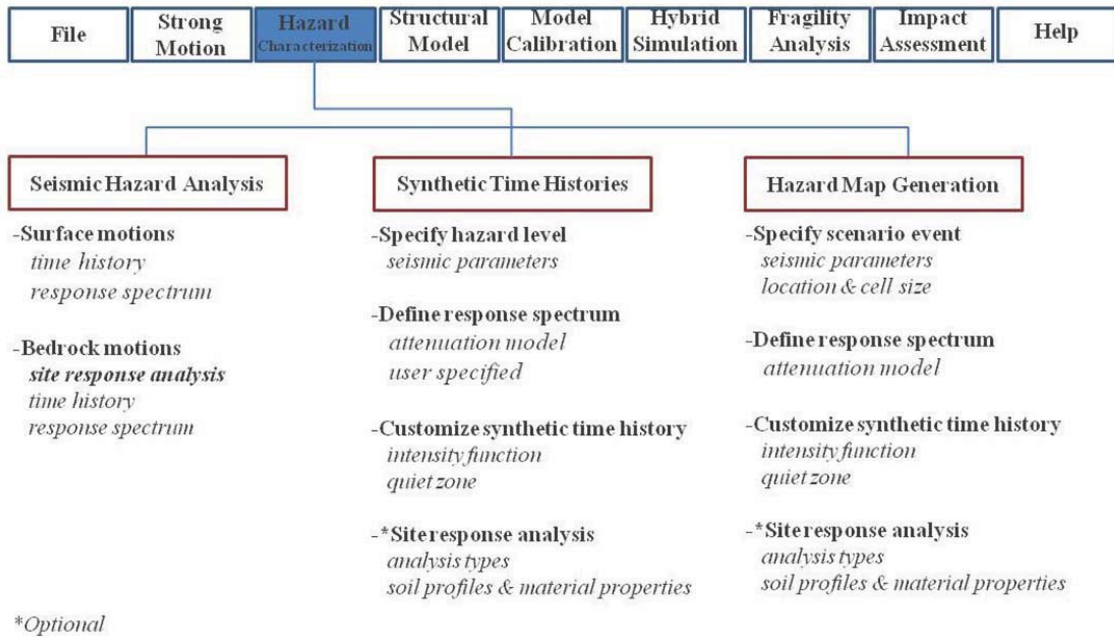
Figure 5-7 Hazard Characterization submenu in NISRAF

5.2.3.1 Seismic Hazard Analysis

Two hazard analysis approaches for natural records are available, namely, surface motions and bedrock motions, as shown in Figure 5-8. GUI for time history and response spectrum checking is available each time when the analysis is finished (Figure 5-9). Site response analysis is required for bedrock motions analysis. As mentioned previously, DEEPSOIL is implemented as the site response analysis platform. To maintain consistency and ease of use, a GUI interface for creating a representative soil column (soil profiles and material properties, for example) is developed (Figure 5-10). With the input file generated by NISRAF, DEEPSOIL is therefore executed in console mode without its user interface.
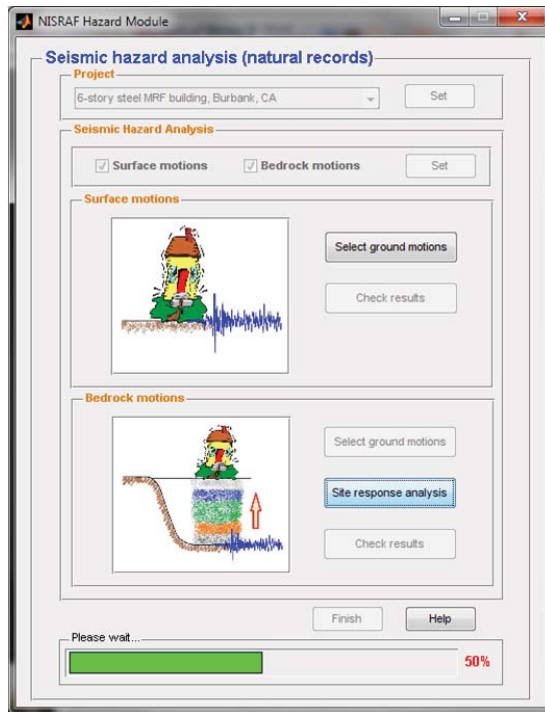
Figure 5-8 Seismic hazard analysis GUI in Hazard Characterization menu
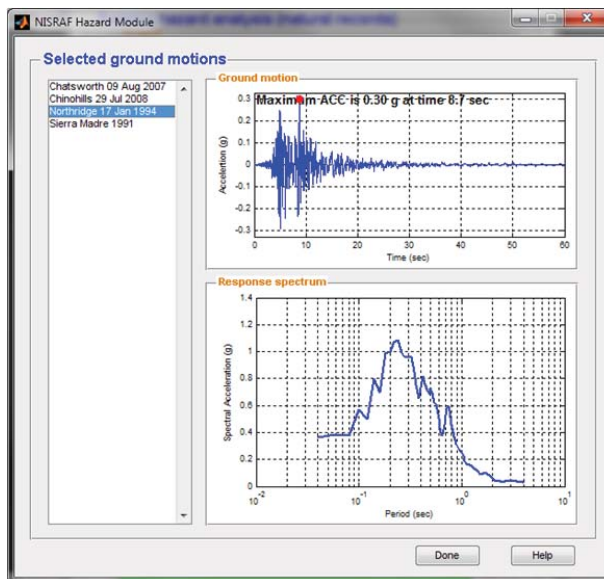
Figure 5-9 Time history and response spectrum checking GUI
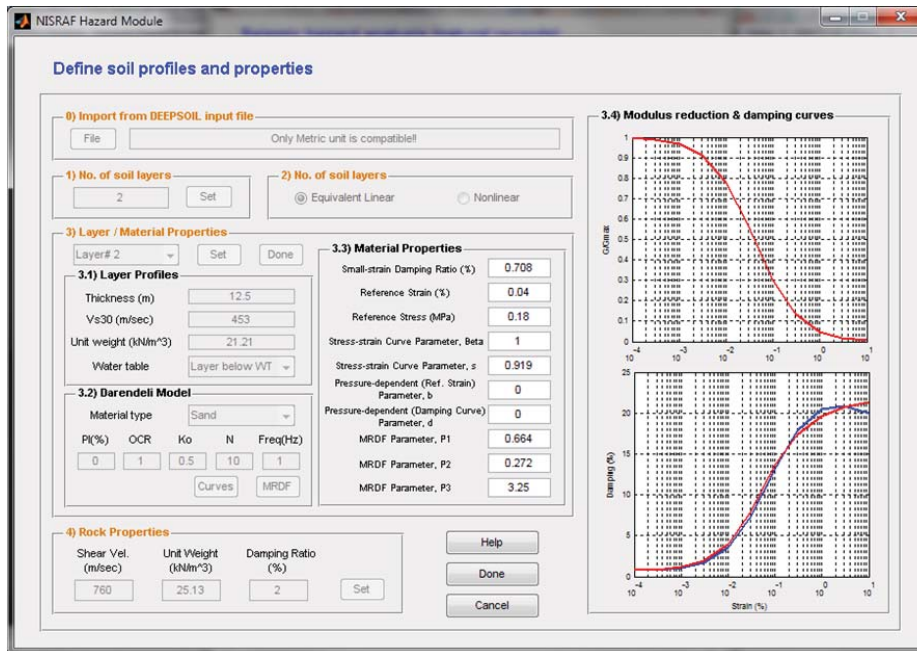
Figure 5-10 Define soil profiles and material properties GUI in NISRAF

5.2.3.2 Synthetic Time Histories

Synthetic time history is essential for seismic engineering, particularly in regions where natural records are absent or insufficient. SIMQKE is the platform implemented in NISRAF to generate artificial motions. Again, for ease of use, parameters needed for SIMQKE are generated using the latest attenuation and duration equations (detailed in *Chapter 3*) through an interactive interface (Figure 5-11). Meanwhile, a GUI for customizing the time history is also developed (Figure 5-12). After that, NISRAF generates the input file (based on user inputs or results from hazard models) and executes SIMQKE in the console mode (Figure 5-13). Eventually, sets of synthetic ground motions are generated and are ready for check or use (Figure 5-14).
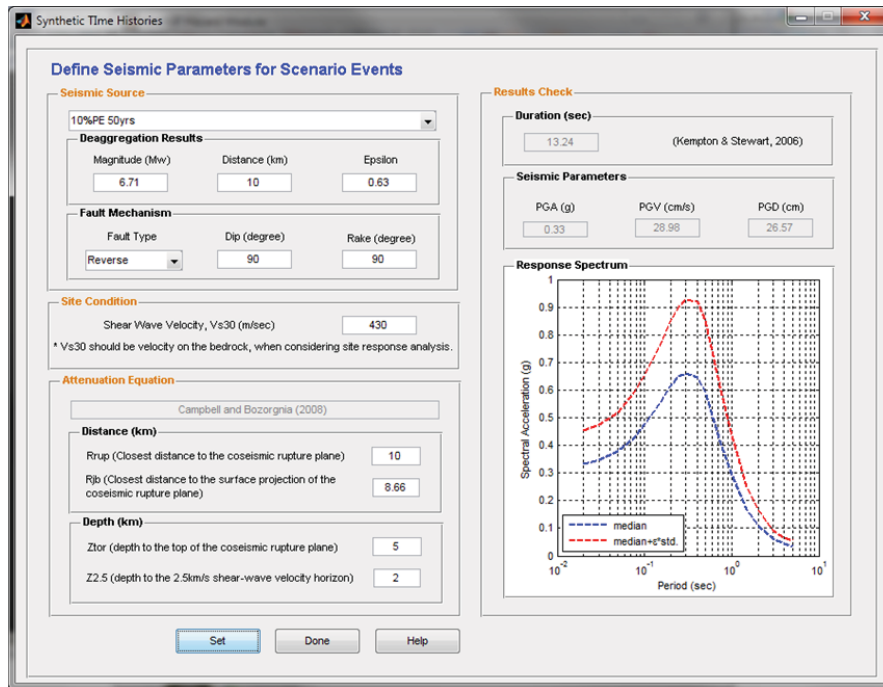
Figure 5-11 GUI to define seismic parameters
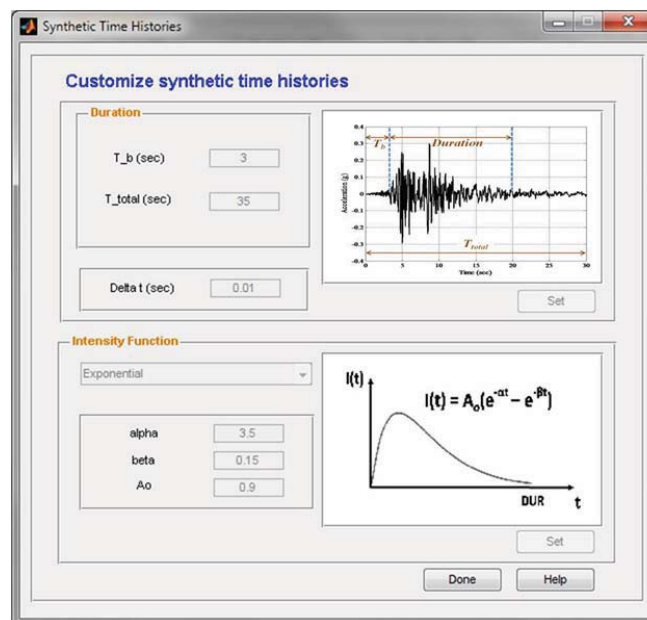
Figure 5-12 GUI to customize synthetic time history
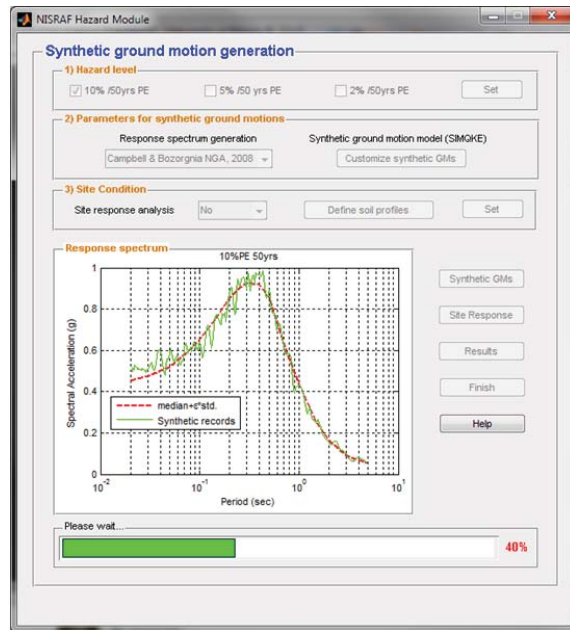
Figure 5-13 GUI to show analysis progress and response spectrum
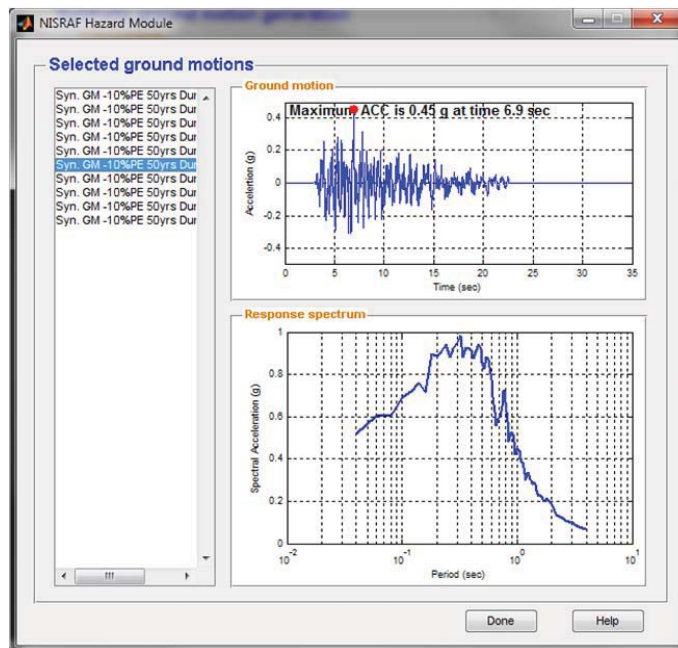
Figure 5-14 Suites of generated synthetic time histories

5.2.3.3 Hazard Map Generation

Similar to the case of procedures for synthetic time histories generation, the user is prompted to specify seismic information in the beginning. Additional information (the interested area and the cell size used in map) particular to hazard map generation is then needed to be specified (Figure 5-15). After that, NISRAF calculates seismic intensity (PGA, for example) at the center of each cell (Figure 5-16). Eventually, a hazard map is generated by collecting results at each cell along with location information (Figure 5-17).
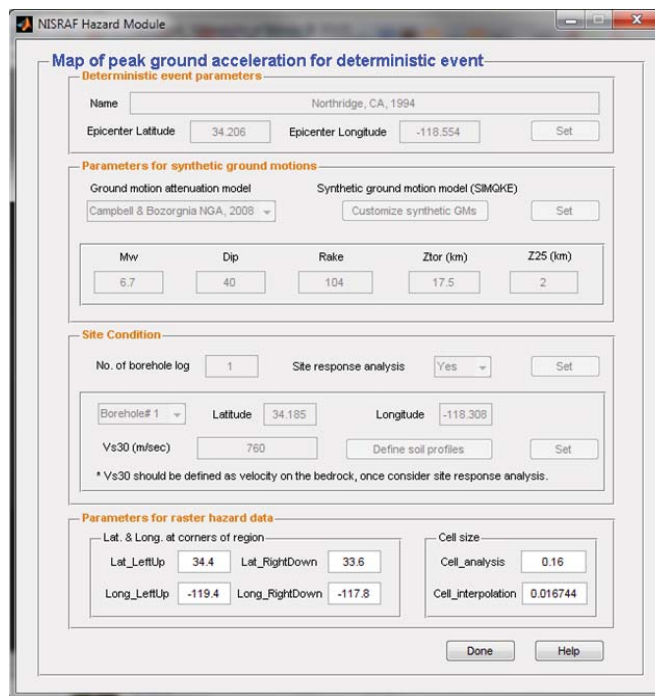
Figure 5-15 GUI to specify information for hazard map generation
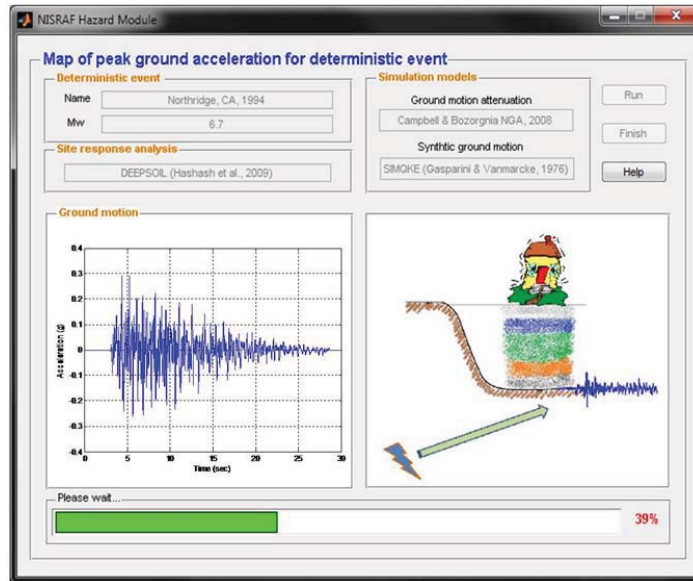
Figure 5-16 Hazard map generation in NISRAF
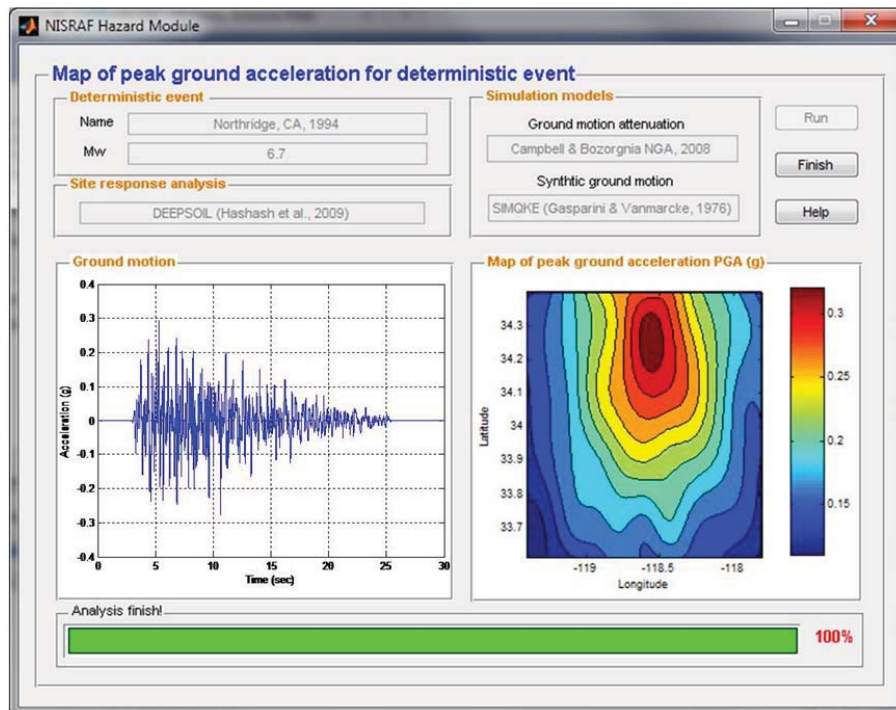
Figure 5-17 Hazard map generated by NISRAF

5.2.4 Structural Model Menu

The finite element model is a prerequisite for model calibration. To create an FE model, the user is allowed to import an existing ZEUS-NL model (Figure 5-19) or create a new model (Figure 5-20) in NISRAF. Submenus for creating an FE model (such as *New Model from Template*, *New Model*, *View* and *Structural Model*) are based on SimBuild (Park et al., 2007), a pre- and post-processor for UI-SIMCOR. Below, only GUIs for importing a ZEUS-NL model and creating a new model are shown. Details and procedures to create a model are referred to SimBuild manual.
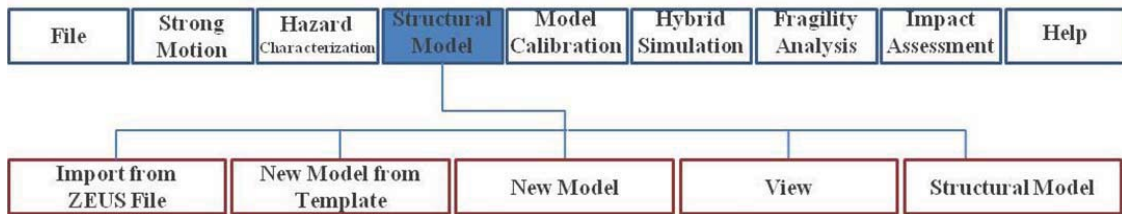
Figure 5-18 Structural Model submenus in NISRAF
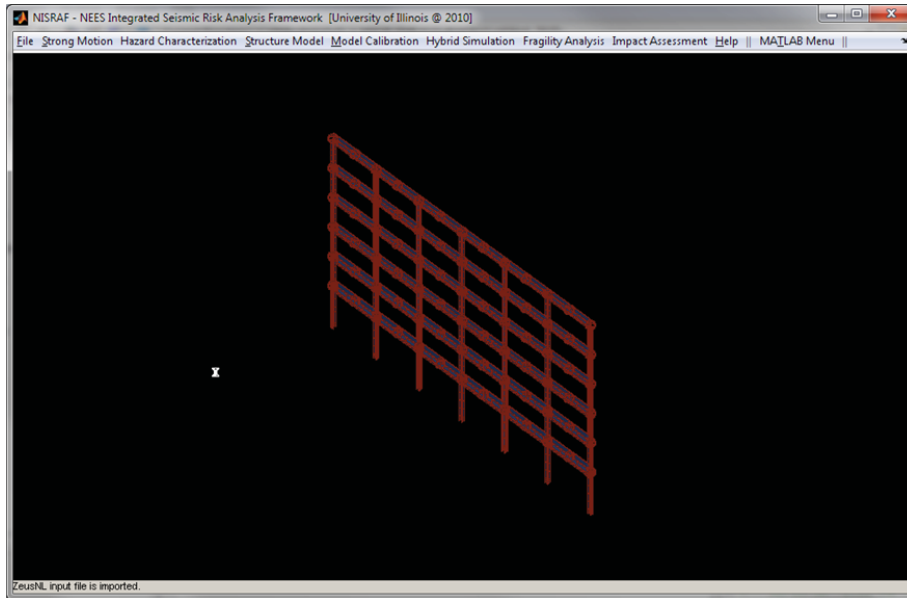
Figure 5-19 Imported ZEUS-NL model in NISRAF
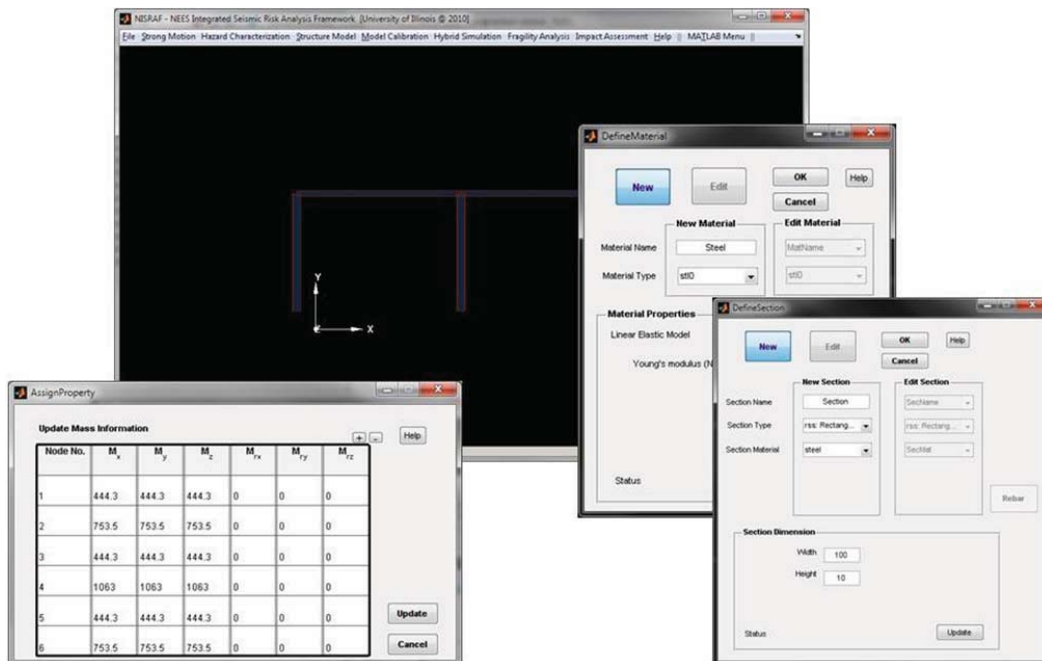
Figure 5-20 NISRAF allows user to create FM model

5.2.5 Model Calibration Menu

An automatic approach for system identification and model updating is developed and incorporated into NISRAF. Methodology, procedures and GUIs of this method are developed by Jian Li at the University of Illinois (Li et al., 2009). Below, brief introduction of this method is given. A more comprehensive illustration is available in Appendix D.

As shown in Figure 5-21, Eigensystem Realization Algorithm (ERA) is implemented in NISRAF due to its wide application and good performance in multi-input multi-output (MIMO) problems (Figure 5-22). Additionally, the modal updating tool implemented in NISRAF is featured by its integration with the finite element modeling capability of NISRAF. Therefore, NISRAF can collect all structural parameters automatically for the user to select as candidate parameters. Moreover, the objective function can be customized by defining different numbers of modes and different weighting factors for frequency and mode shape (Figure 5-23).
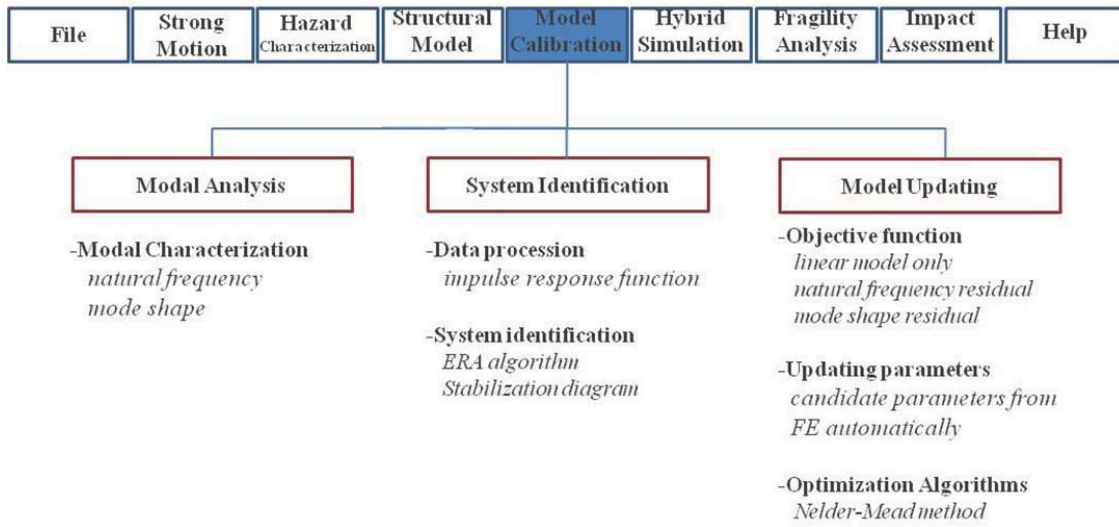
Figure 5-21 Model Calibration submenus in NISRAF
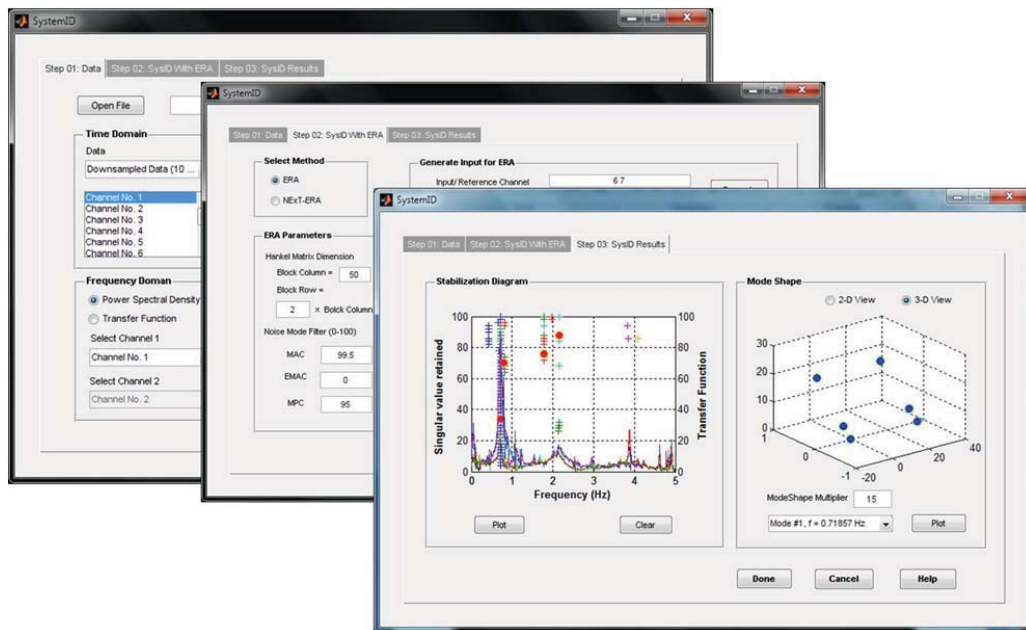
Figure 5-22 GUIs for system identification in NISRAF
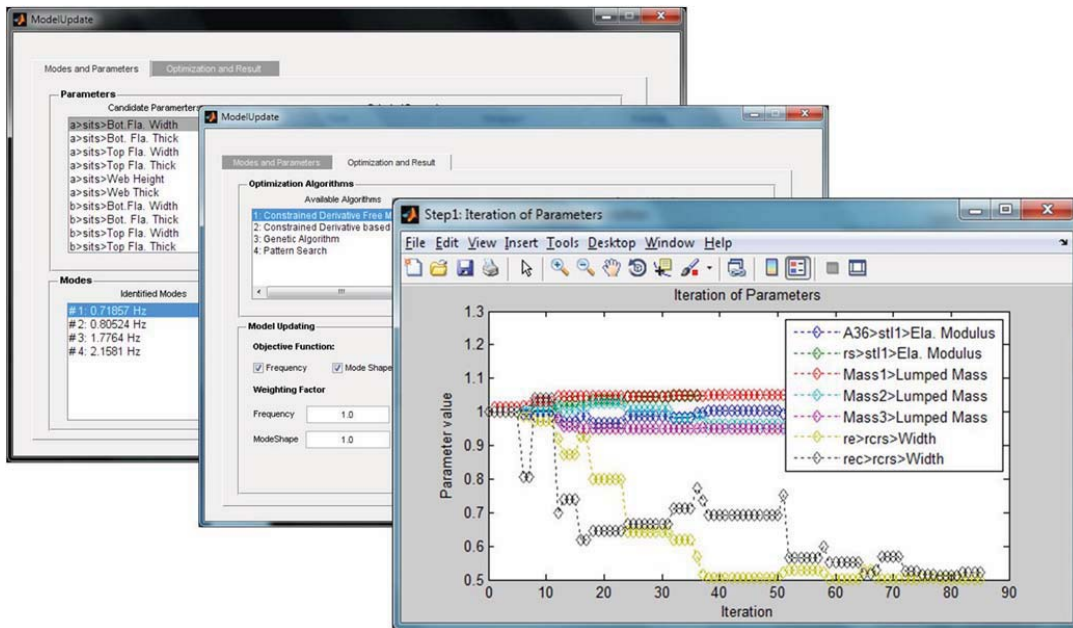
Figure 5-23 GUIs for model updating in NISRAF

5.2.6 Hybrid Simulation Menu

UI-SIMCOR is implemented in NISRAF to coordinate hybrid simulation tests. The selected ground motions from *Hazard Characterization* and the calibrated structural model from *Model Calibration* are fed into UI-SIMCOR to perform the hybrid simulation. The GUIs of *Hybrid Simulation* are based on SimBuild. Through the use of GUIs, the user can easily develop the sub-structures for the analytical platform or laboratory (Figure 5-25), run hybrid simulation (Figure 5-26) and check results.
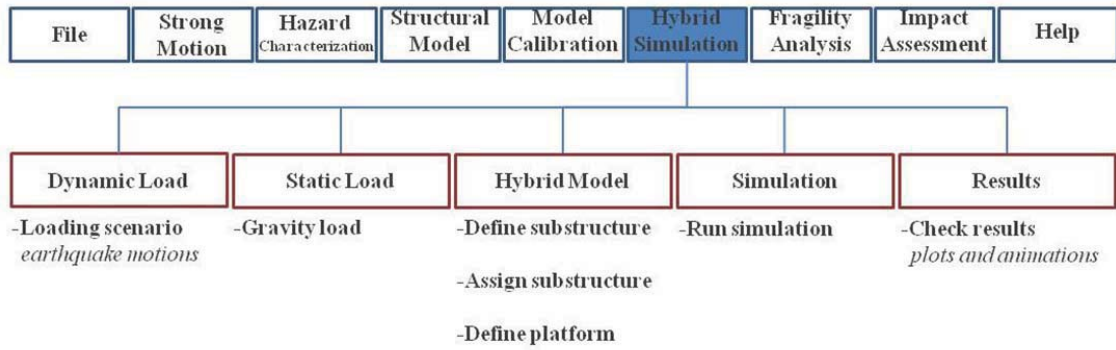
Figure 5-24 Hybrid Simulation submenus in NISRAF
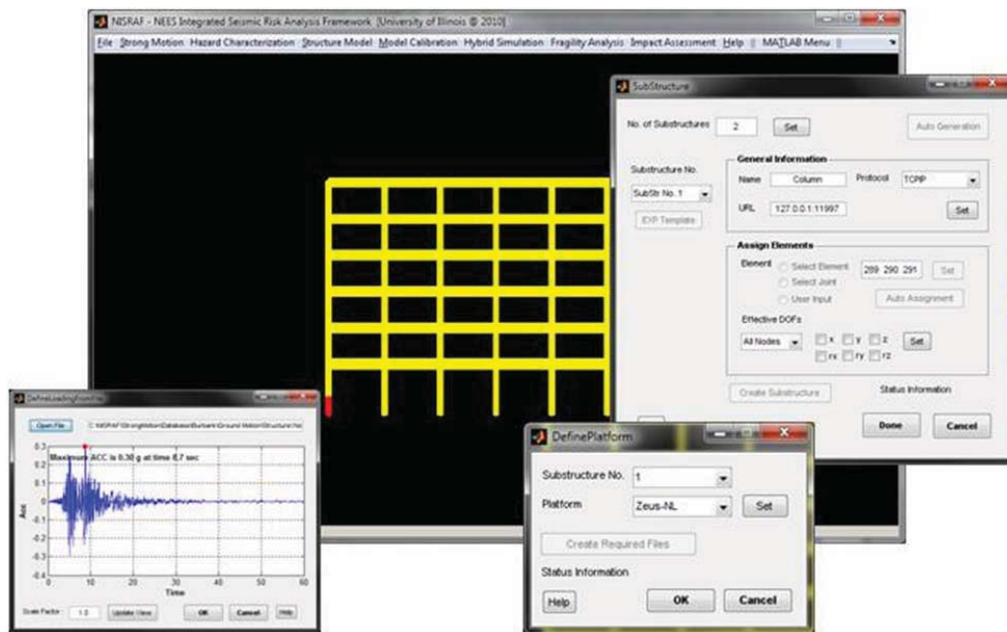
Figure 5-25 GUIs to define sub-structures in NISRAF
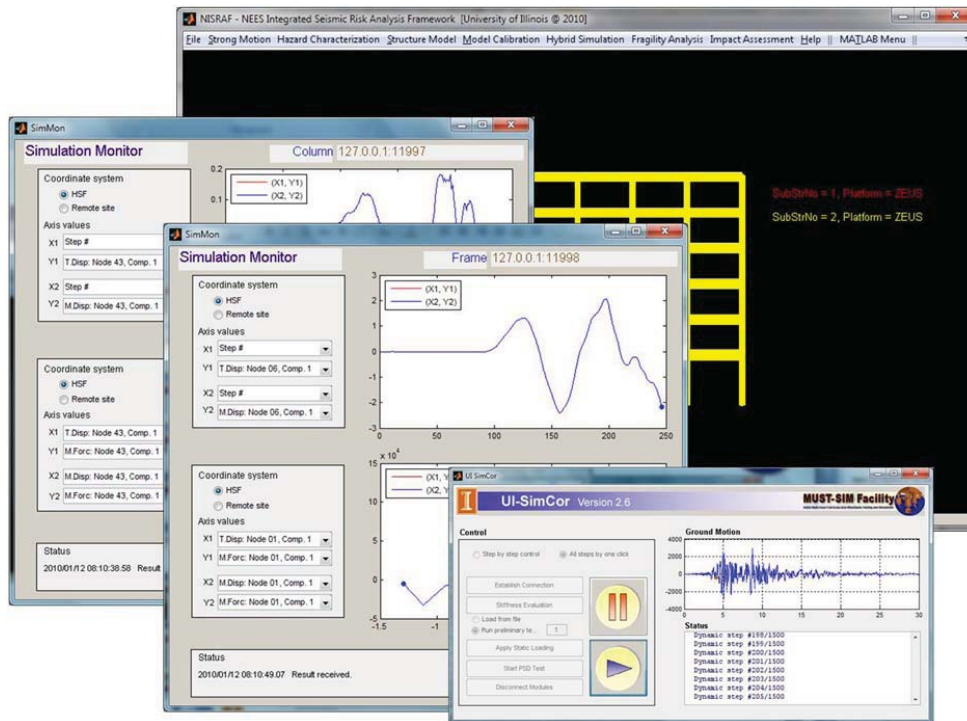
Figure 5-26 GUIs to run hybrid simulation in NISRAF

5.2.7 Fragility Analysis Menu

Fragility Analysis menu is composed of three main parts: namely, *Define Limit States*, *Run Hybrid Simulation* and *Hybrid Fragility Curves*, as shown in Figure 5-27. Methodologies and analysis procedures of fragility analysis have already been illustrated and verified in *Chapter 4: Fragility Analysis by Hybrid Simulation*. One of the features of the proposed advanced fragility analysis approach is its ease of use. With structural information available from *Structural Model*, the user defines interested Interstory drift angle (ISDA) through the interactive structural model (Figure 5-28). Meanwhile, when performing hybrid simulation in order to derive mean seismic intensity, NISRAF calculates ISDAs, compares with target ISDA, calculates scale factor, and asks to

continue the next simulation (Figure 5-30). The above designs avoid the heavy and tedious calculations. The "hold on" feature allows the user to have time to replace the experimental specimen in the laboratory, which is really a useful and practical design (Figure 5-30). Eventually, fragility relationships compatible with MAEviz are generated (Figure 5-31).
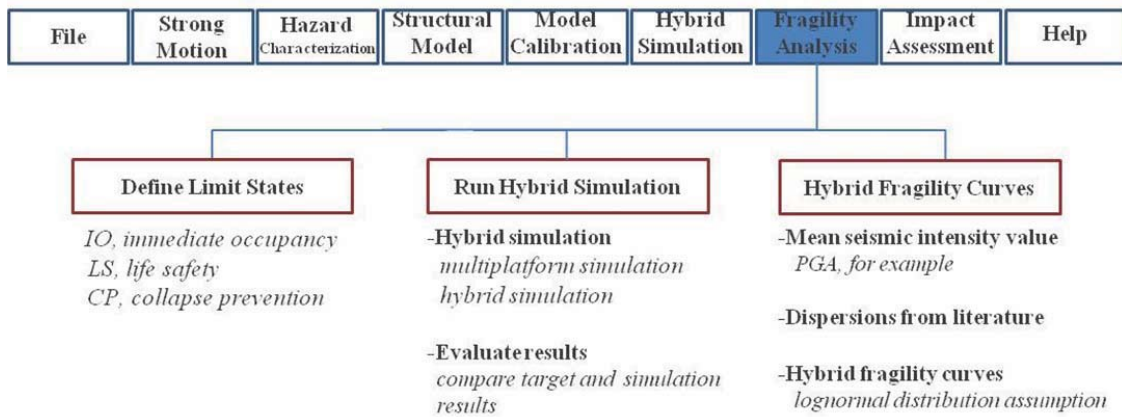
Figure 5-27 Fragility Analysis submenus in NISRAF
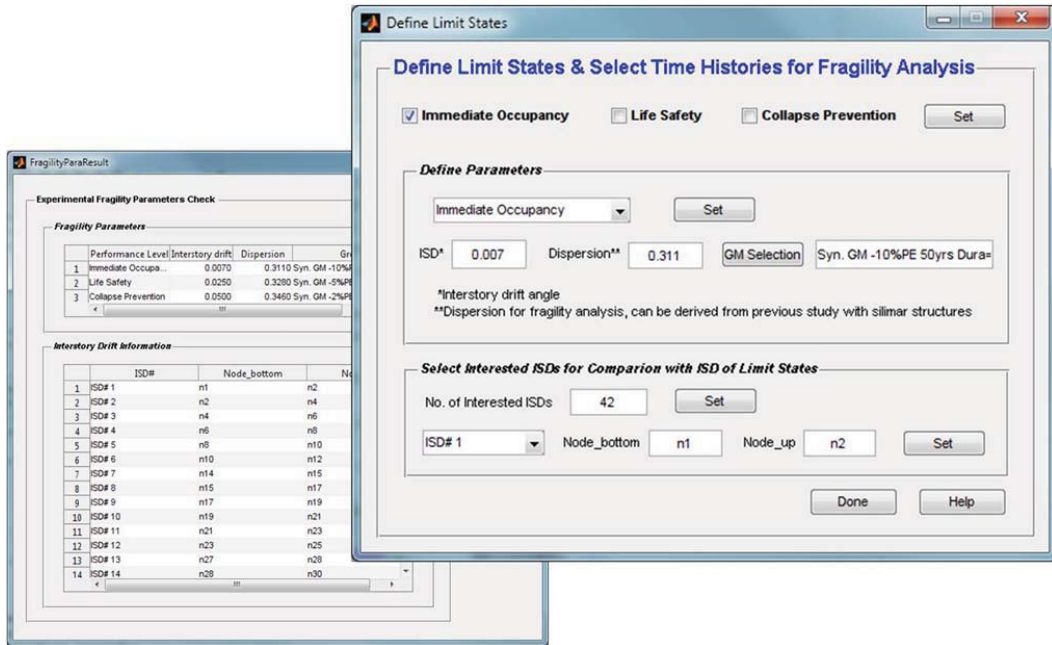
Figure 5-28 GUIs to define limit states, select time history and specify ISDA
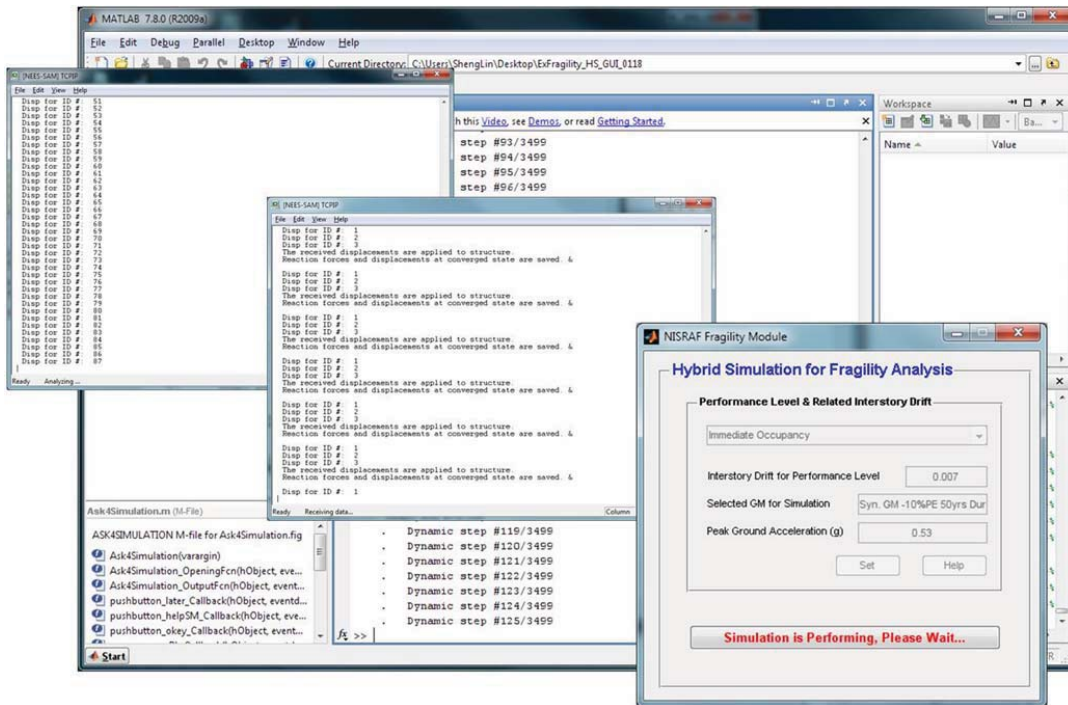
Figure 5-29 Hybrid simulation for fragility analysis (turn off UI-SIMCOR GUIs)
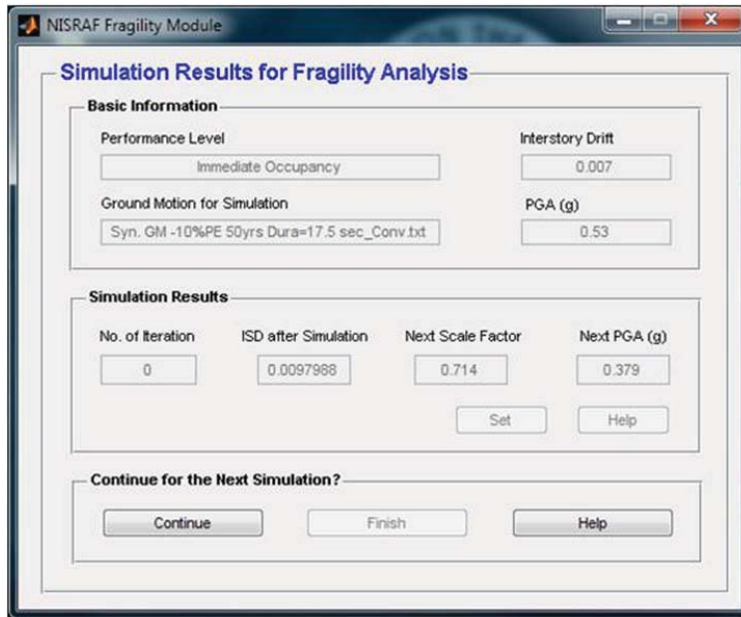
Figure 5-30 GUI to calculate ISDA, scale factor and ask for testing
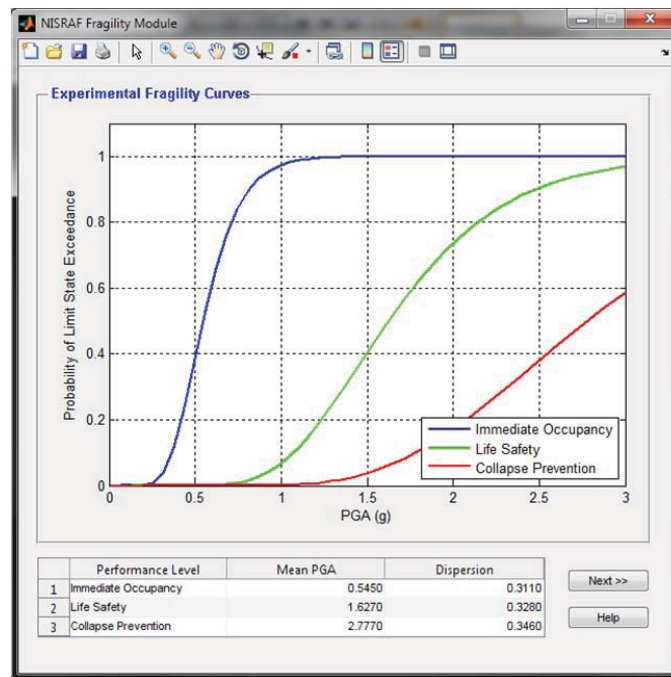
Figure 5-31 Hybrid fragility curves in NISRAF

5.2.8 Impact Assessment Menu

Finally, fragility curves from *Fragility Analysis* and the hazard map from *Hazard Characterization* are fed into earthquake impact assessment packages (MAEviz, for example) to evaluate the seismic loss (Figure 5-33).
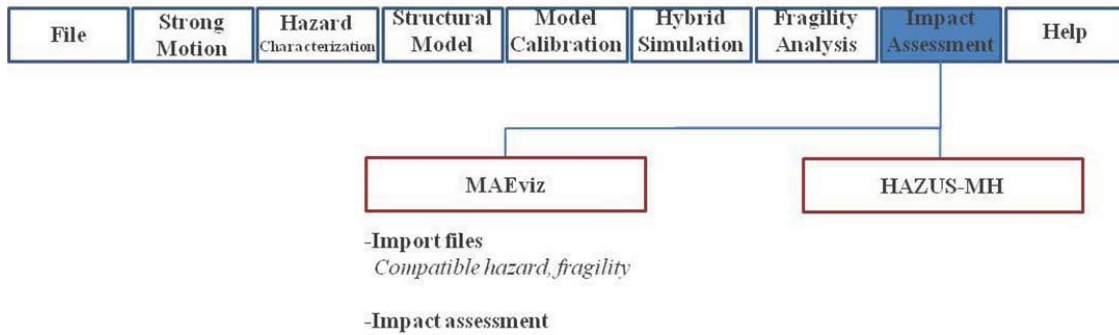
Figure 5-32 Impact Assessment submenus in NISRAF
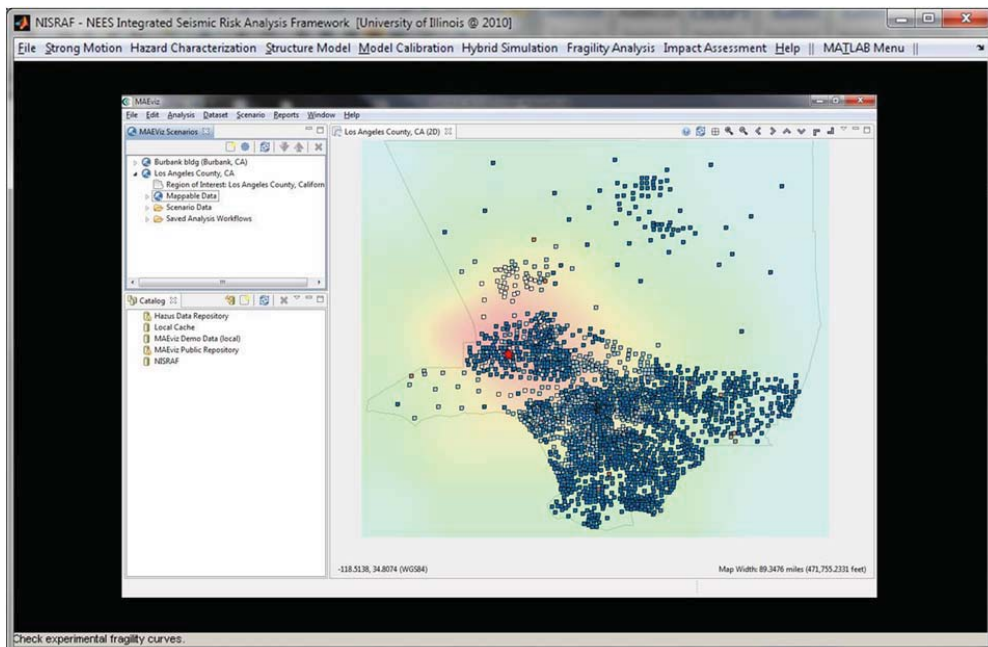
Figure 5-33 Impact assessment (MAEviz) in NISRAF

5.2.9 Help Menu

Manuals of NISRAF, UI-SIMCOR and SimBuild are available. In addition, help information is also available in each GUI with a button embedded. Moreover, *About NISRAF* states the copyright as well as version information.
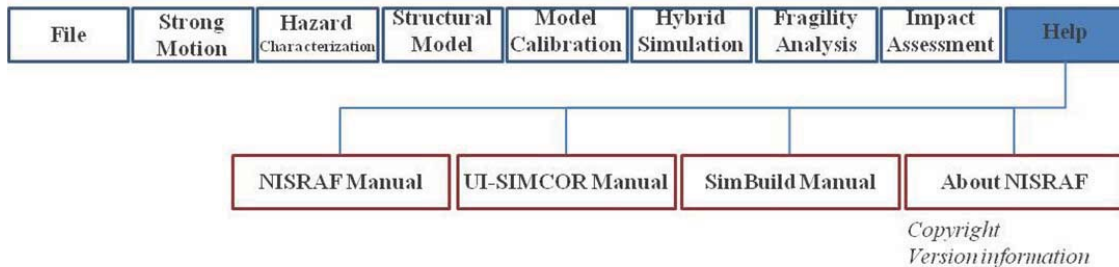
Figure 5-34 Help submenus in NISRAF

5.3 Communication Protocols and Analysis Platforms

NISRAF, a complete GUI-driven system, has been successfully developed in the MATLAB environment. The integration from measured data to impact assessment package is the most important feature of NISRAF. Several different analysis platforms, such as UI-SIMCOR, ZEUS-NL, DEEPSOIL, SIMQKE and MAEviz are coordinated by NISRAF to work seamlessly in a single MATLAB platform. No special challenges and limitations for the communication are observed between components. Moreover, a stand-alone version NISRAF will be released later. Users do not even need to have MATLAB installed in their computers to run NISRAF.

5.4 Features of NISRAF

NISRAF, an earthquake impact assessment platform with graphical user interface has been developed for the purpose to make assessment more efficient and more reliable. Several components, including instrumentation, hazard characterization, system identification, model updating, hybrid simulation, hybrid fragility analysis and impact assessment tool, have been implemented and tailored with novel methods to build the seamless, transparent and extensible framework. Figure 5-35 shows some GUI components developed and implemented in NISRAF.
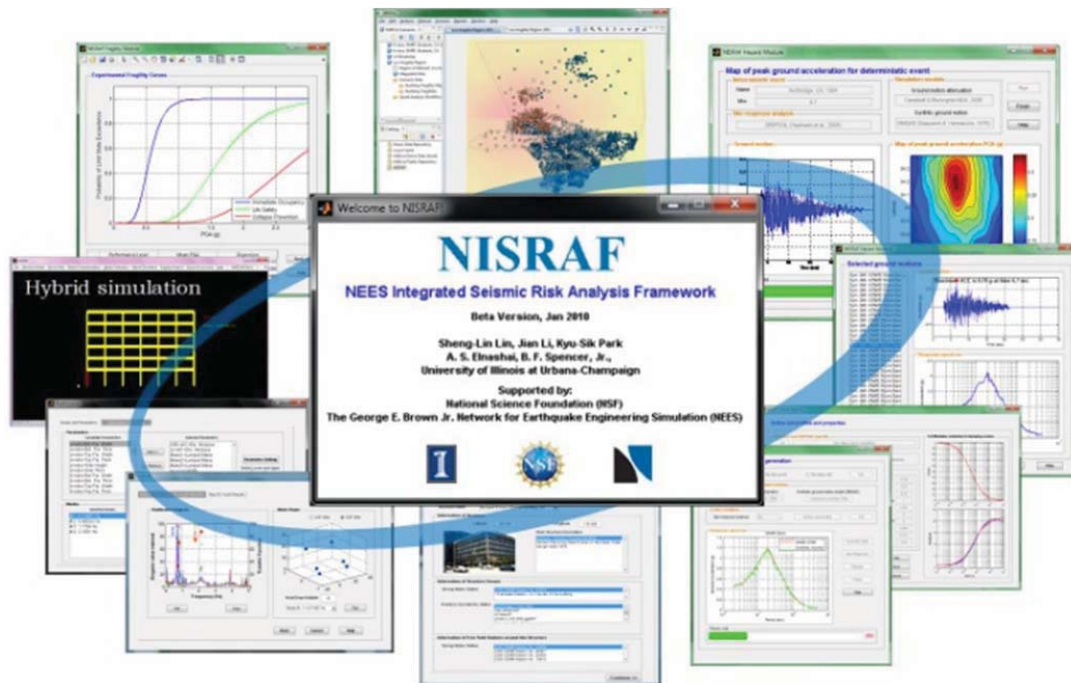
Figure 5-35 Components with GUI in NISRAF

There are several advanced features contained in this integrated framework. Among those features are:

- *Open source software with friendly graphic user interface*:

In NISRAF, each component is developed separately (modularized) before being incorporated into the framework. Consequently, it is easy to understand and maintain. This software, as well as the source code, will be open to the public. The open source feature will allow NISRAF to be utilized efficiently, as well as improve its integrity and robustness.

- *Extensible and accessible*:

As mentioned previously, each component is developed and verified separately. Hence, it is extensible and accessible to any latest research findings and program techniques.

- *Efficient and reliable impact assessment*:

This is the first time that all the components for impact assessment are integrated and work seamlessly in just one software platform. Concurrently, the integrated feature brings the most advanced tools of earthquake hazard and structural reliability analyses into the context for accurate evaluation of impact assessment. Surely, with these seamlessly integrated advanced techniques, which provide a more accurate hazard and structural model and hence generate superb fragility curves, the assessment of earthquake impact will be more efficient and more reliable.

5.5 Potentials, Limitations and Challenges

As mentioned previously, this is the first time to integrate all components of earthquake impact assessment in one analysis platform. Through NISRAF, uncertainties from hazard and fragility can be reduced or managed efficiently; therefore the results from impact assessment can be more realistic and reliable. Meanwhile, NISRAF provides a chance for seismologists, geotechnical and structural earthquake engineers, structural control and impact assessment experts to ameliorate algorithms in order to bring out more confident assessment results. Through its extensible and accessible feature, the new or improved algorithm can be easily incorporated into NISRAF.

Despite the above merits, limitations and challenges remain for the current version NISRAF. First of all, a representative FE structural model is prerequisite and essential for model calibration. Currently, it is allowed to build the model in NISRAF (with limited elements, sections and material); and only ZEUS-NL file is compatible when importing an existing model. However, the model is sometimes too complicated to be built in NISRAF, or it has already been built in other programs, such as OpenSees and SAP2000. Furthermore, several analysis platforms have already been implemented in NISRAF; and it should be expanded in the future. Some of them are operated only by their own GUIs (such as Java, C++ and others). It is therefore an obstacle when incorporating into NISRAF. A current alternative method is to prepare the required files and execute programs in the console modes. To be more robust, and more user-friendly, the above limitations and challenge should be resolved in the future.

CHAPTER 6

CASE STUDIES

6.1 Introduction

NISRAF has been successfully developed, as discussed in *Chapter 5*. Several components (modules) in NISRAF have also been verified already, as illustrated in *Chapter 3* and *Chapter 4*. In this chapter, a verification study of NISRAF is conducted through an actual test bed in the Los Angeles area. Two applications are presented in this chapter. In application 1, a heavily instrumented building along with high-quality strong-motion records was used to demonstrate the methodology and analysis procedure of NISRAF from instrumentation, testing, to loss assessment. Comparison was made between the seismic loss through NISRAF and the field reports of the 1994 Northridge earthquake. Moreover, in application 2, seismic assessment for the Los Angeles area during the Northridge earthquake was performed using a hazard map and fragility curves generated by NISRAF; comparison was also presented.

6.2 Application 1: A 6-Story Steel Building in Burbank, California

An instrumented building was selected to verify NISRAF in this application. In the following sections, background information about this building and site conditions are presented first. Thereafter, step by step analysis in NISRAF is performed. Comparison is made and presented in the end.

6.2.1 Introduction

6.2.1.1 Building Information

A six-story commercial building in Burbank, California (latitude = 34.185°, longitude = -118.308°), was selected for this study (Figure 6-1). This is a steel moment resisting frame building, in which the perimeter frames are the primary lateral load resisting system, and the internal frames are only resisting gravity load, as shown in Figure 6-2. Reference is made to Anderson and Bertero (1991) for detailed information about this building. This building is instrumented by the California Strong Motion Instrumentation Program (CGS - CSMIP Station No. 24370) in 1980 with 13 sensor channels as shown in Figure 6-3. Several significant earthquakes were captured, such as Whittier (1987), Sierra Madre (1991) and Northridge (1994). Data are available in the Center for Engineering Strong Motion Data (CESMD, www.strongmotioncenter.org).

Figure 6-1 Photo of 6-story steel moment frame building in Burbank, California
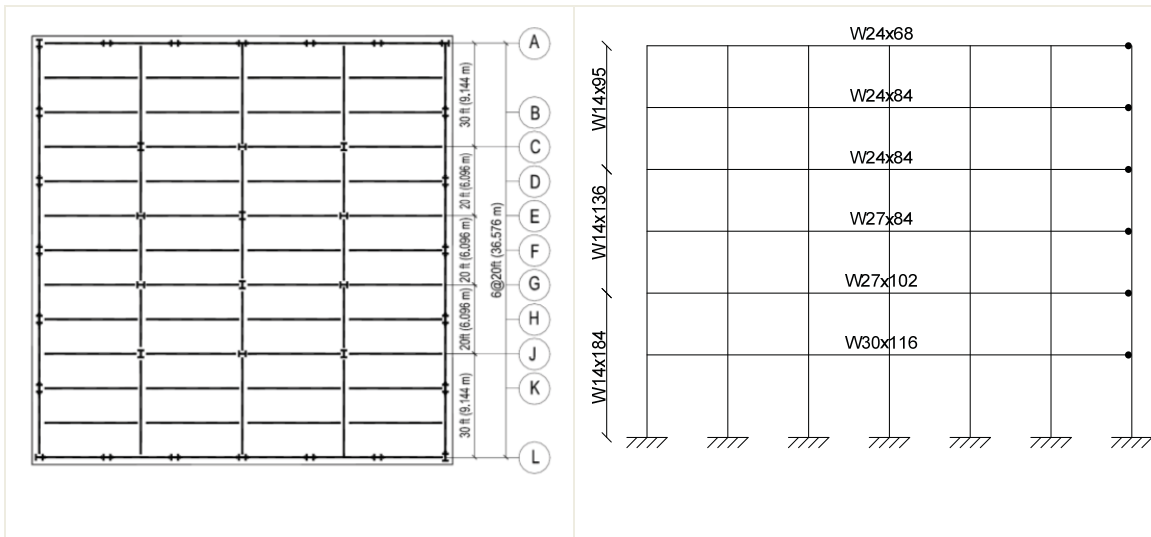
Figure 6-2 Elevation and plan view of Burbank building
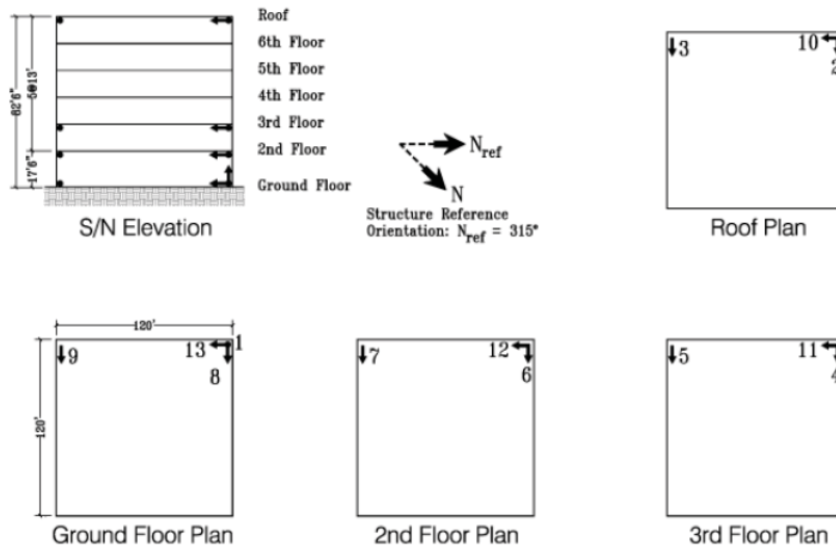
Figure 6-3 Sensor location of Burbank building (CESMD)

6.2.1.2 Site Condition

Site condition of the Burbank Fire Station (latitude = 34.185°, longitude = -118.308°), the same site utilized in *Chapter 3*, was selected to represent the site condition at the Burbank building site due to the absence of geotechnical report at this building site. This substitution is acceptable since the distance between these two sites is only 0.6 kilometers. Site condition of Burbank Fire Station site has been discussed and detained in *Chapter 3*.

6.2.2 Strong Motion

Either *Strong Motion* or *Structural Model* must be the first step in NISRAF. *Strong Motion* was selected as the first step in this application. Through the linkage to web-database, free-field station records around the Burbank building site and structural sensor histories during the past earthquakes were downloaded and deposited in NISRAF. After that, an interactive window with already-downloaded information allows user to add some information (background, description and image), as shown in Figure 6-4.
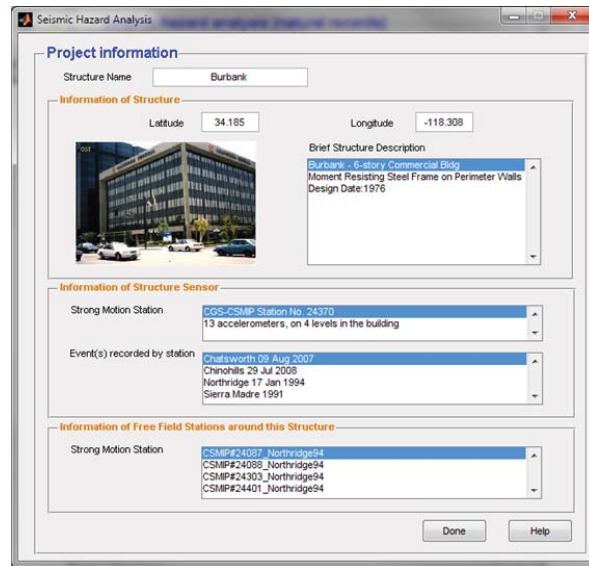
Figure 6-4 GUI to manage project and downloaded records

6.2.3 Hazard Characterization

With instrumented strong-motion records from *Strong Motion*, the hazard characterization analysis was undertaken. Synthetic ground motions with various hazard levels were generated for further use in *Hybrid Simulation* and *Fragility Analysis*. The hazard map for the Northridge earthquake in the Los Angeles area was generated for further use in *Impact Assessment*. Both of them have already been presented in *Chapter 3* and *Chapter 4*. Figure 6-5 shows the generated synthetic ground motions and hazard map in NISRAF.
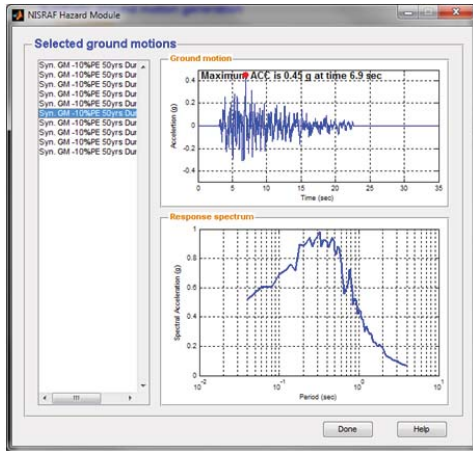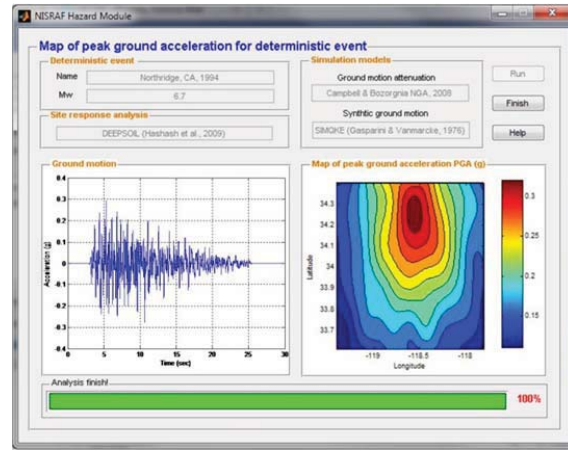
(a) Synthetic ground motions   (b) Hazard map

Figure 6-5 Synthetic ground motions and hazard map in NISRAF

6.2.4 Structural Model

A finite element model was created in NISRAF, as shown in Figure 6-6. Due to the fact that only the perimeter frames are used for the lateral load resisting system, a 2-D model of the exterior frame was modeled to represent the whole structure. Section dimensions and material properties for each beam and column were based on design documents. Lumped mass was used and applied at every beam-column connection. Concrete slabs were modeled and connected to steel girders using rigid elements, to account for their contribution of stiffness. The width of slab was calculated based on the effective width defined in ANSI/AISC 360-05 specification (AISC, 2005) and distances to steel girders were based on design drawings.

138
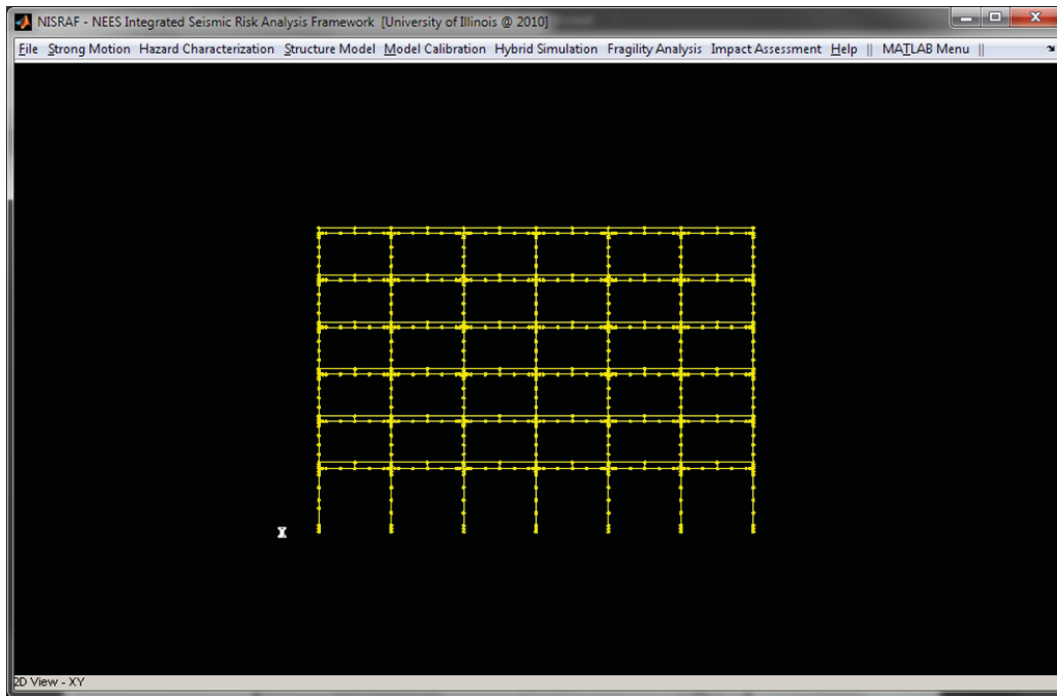
Figure 6-6 2-D FE model of Burbank building in NISRAF

6.2.5 Model Calibration

With FE model created in *Structural Model*, *Model Calibration* is performed to tune the FE model. Two procedures, namely, system identification and model updating, were executed in this step.

6.2.5.1 System Identification

Input channels and output channels were defined first in order to form impulse response functions which were assembled for the Hankel matrix. Based on the design drawings, exterior and interior columns are firstly supported on steel girders and reinforced concrete girders, respectively, and both of them are in turn supported on a pair of 32 feet long and 30 inches diameter reinforced concrete piles. Therefore, it is

reasonable to consider that all columns are fixed. Hence, the records from the ground floor were treated as the input motions, while other records were considered as the responses of the structure. Consequently, channel 8 and 9 were defined as input, while channels 2 to 7 were output channels, and, hence, the dimension of impulse function matrices was 2 by 6. Note that channels 4 and 5 were not working properly during the Northridge earthquake of 1994. Therefore, data from these two channels were not available and only four output channels were available. The dimension of impulse response function matrices was 2 by 4 for the Northridge earthquake.

The ERA method was then performed for the Northridge earthquake record. The stabilization diagrams and the identified mode shapes were shown in Figure 6-7. The first and second bending modes were then identified as 0.72 Hz and 2.14 Hz, respectively. The associated damping ratios were 3.37% and 6.71% (Table 6-1).

Table 6-1 Frequency and δ of identified with ERA method

Mode	f (Hz)	δ(%)
1	0.719	3.373
2	2.144	6.715
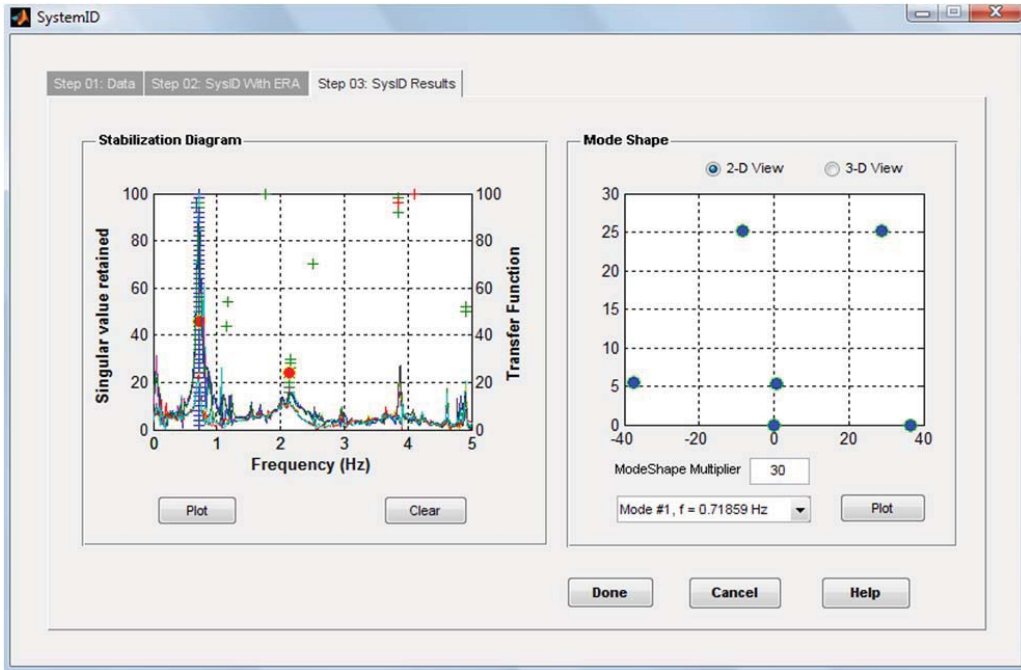
(a) System identification results of Burbank building in NISRAF
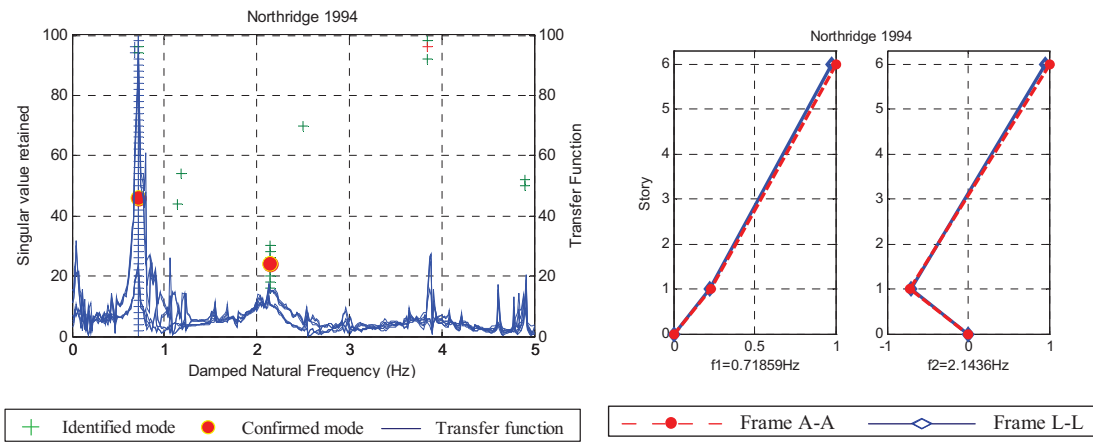
(b) Stabilization diagrams

(b) Identified mode shapes

Figure 6-7 Stabilization diagrams and identified mode shapes for the Northridge earthquake

6.2.5.2 Model Updating

With the identified natural frequencies and mode shapes, dynamic FE model updating was then performed to improve the FE model of the Burbank building. Selection of candidate parameters to be updated was the first step in model updating. The selected parameters for the Burbank building were shown in Table 6-2. The sensitivities of each parameter to the first two natural frequencies were shown in Figure 6-8. To keep the physical meaning of each parameter, lower and upper bounds were applied based on the degree of uncertainties. For example, the effective widths were calculated based on AISC specification, which was likely to be very conservative. In addition, the deflection of the slab defined the contribution of the slab to the composite beam, thus affecting the effective width. Therefore, the effective width of slab had large uncertainty, thus a relatively larger range of variation ($\pm50\%$) was applied.

Table 6-2 Selected parameters for model updating and updated results

Selected Parameters	Description	Initial Value	Bound (%)	Updated Value	Change (%)
Es (N/mm^2)	Young's modulus of steel	2.10E+05	±5	2.21 E+05	5.00
Mass1 (1000kg)	Lumped mass at 2nd floor	45.65	±5	43.37	-4.99
Mass2 (1000kg)	Lumped mass at 3rd-5th floor	36.53	±5	38.36	5.01
Mass3 (1000kg)	Lumped mass at top floor	54.84	±5	52.1	-5.00
WS1 (mm)	Effective width of concrete slab at 2nd-5th floor	762	±50	1143	50.00
WS2 (mm)	Effective width of concrete slab at top floor	914.4	±50	1371	49.93

142
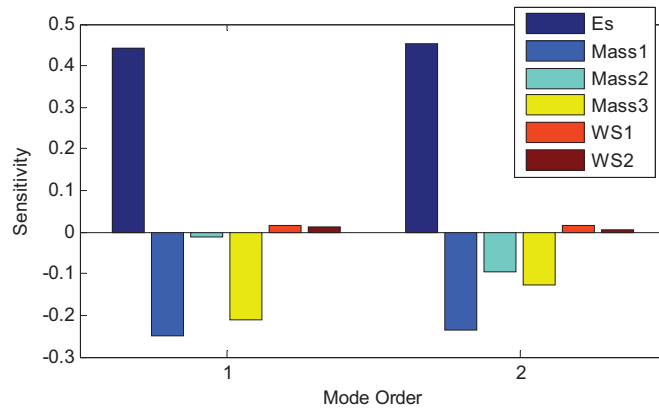
Figure 6-8 Sensitivities of each parameter to the first two identified natural frequencies

The optimization problem defined previously was solved by the Nelder-Mead method. The results listed in Table 6-3 show that the errors between the identified and updated model reduced to 1% and 5.78% for the first and second natural frequency, respectively. Meanwhile, the second mode shape was improved, which gave a value of 0.981 for the *MAC*. With this refined finite element model, hybrid simulation was conducted to yield a seismic response prediction with higher accuracy.

Table 6-3 Comparison of frequency and mode shape between the original and updated

Mode	Original FE model			Updated FE model		
	frequency (Hz)		*MAC*	frequency (Hz)		*MAC*
	value	error (%)		value	error (%)	
1	0.688	-4.312	0.999	0.712	-1.001	0.999
2	1.956	-8.769	0.975	2.020	-5.784	0.981

6.2.6 Hybrid Simulation & Fragility Analysis

The calibrated Burbank building model after *Model Calibration* and ground motions from *Hazard Characterization* were used to perform the hybrid simulation and to derive fragility curves in NISRAF. Both hybrid simulation and hybrid fragility analysis have already been presented in *Chapter 4*.
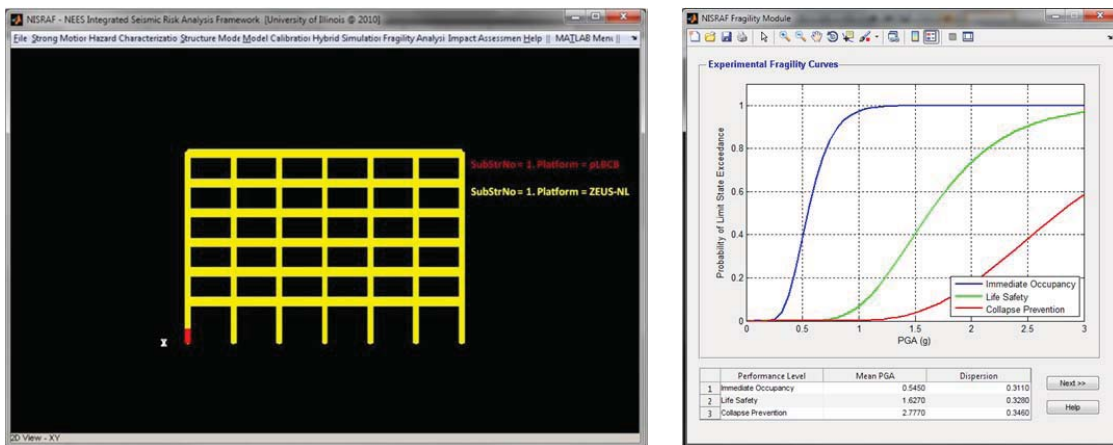
(a) Hybrid simulation model	(b) Hybrid fragility curves

Figure 6-9 Hybrid simulation model of Burbank building and the generated fragility curves

6.2.7 Impact Assessment

Finally, with the generated compatible hazard map and fragility curves, MAEviz under NISRAF was conducted to perform earthquake impact assessment (Figure 6-10). Table 6-4 lists the probabilities of exceeding limit states. Only 15% probability for damage occurred in the immediate occupancy limit state. The results met with the post-earthquake report made by Applied Technology Council (ATC, 2001), which reported slight damage observed to this building from the Northridge earthquake of (Table 6-5).
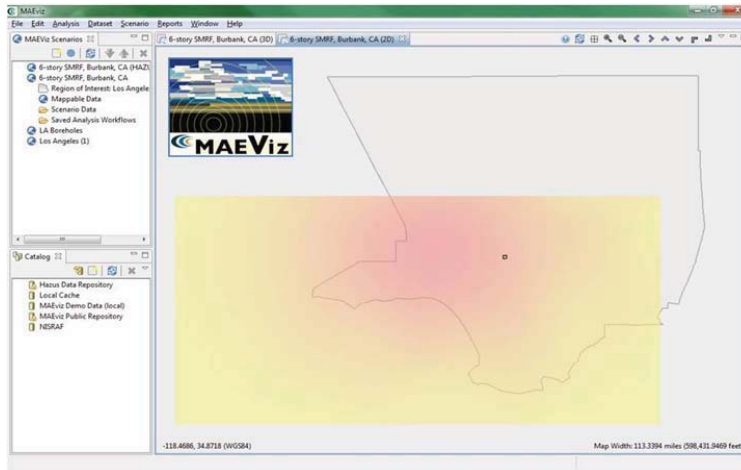
Figure 6-10 Impact assessment for Burbank building in MAEviz

Table 6-4 Comparison between impact assessment results

	Probability of exceeding limit state		
	Immediate Occupancy	Life Safety	Collapse Prevention
NISRAF	0.15	0.00	0.00
MAEviz default	0.37	0.04	0.00

Table 6-5 ATC-38 post-earthquake report for the Northridge earthquake of 1994

Building ID Number	Model Building Type	Number of Stories	Design Date	General Damage State	Structural Damage State	Nonstructural Damage State
…	...	…	…	…	…	…
CDMG370-MF-09	S1	6	1975	I	1	2
…	…	…	…	…	…	…

*I=Insignificant, M=Moderate

*1=None(0% damage), 2=Slight(0-1%damage), 3=Light (1-10% damage)

*ATC-38, Table A-6 Building Damage Summary for Station CDMG 24370

Another comparison of the assessment results was made between NISRAF and MAEviz default. In MAEviz default, the deterministic hazard and default fragility curves in MAEviz were used to evaluate seismic loss. Table 6-6 lists the comparison between these two cases. A comparison of fragility curves between NISRAF and MAEviz default has also been detailed in *Chapter 4*, which shows more vulnerability in MAEviz default fragility relationships (Figure 4-17).

As shown in Table 6-4, assessment results through NISRAF portray less damage than the results from MAEviz default. Unlike for NISRAF, in which only slight damage occurs in the immediate occupancy limit state, damage occurs both in immediate occupancy and life safety limit states for MAEviz default. When comparing with the ATC-38 report, it is concluded that the assessment result through NISRAF is more realistic, while the MAEviz default is more conservative.

Table 6-6 Comparison between NISRAF and MAEviz default

	NISRAF	MAEviz default
Hazard	*Deterministic hazard* • Northridge earthquake mechanism • Campbell and Bozorgnia NGA • 1-D site response analysis	*Deterministic hazard* • Northridge earthquake mechanism • Campbell and Bozorgnia NGA • F_a and F_v site coefficients
Fragility	*Hybrid fragility relationship* • Calibrated FE model • Hybrid simulation • Synthetic motions for LA	*Analytical fragility relationship* • SDOF time history analysis • Synthetic motions for CEUS

6.3 Application 2: the Los Angeles area earthquake impact assessment

Earthquake impact assessment on single building provides the possible damage and loss under scenario or historical earthquake events for this specific building. It indeed provides valuable information to reduce and mitigate loss in particular for the essential buildings (hospitals and schools, for example). However, regional impact assessment—seismic loss for a region, especially urban area—is more valuable for stakeholders to develop emergency response and recovery planning. In this application, impact assessment in the Los Angeles area was carried out; comparison was also presented.

6.3.1 Introduction

The Los Angeles area—a high seismic urban region—was selected to demonstrate the regional impact assessment. Near one million inventory data exported from HAZUS-MH was used as inventory input. The hazard map of PGA for the Northridge earthquake in the Los Angeles area and fragility relationships for all building types and code levels were fed into MAEviz to perform earthquake impact assessment. Both of them have been generated and fully illustrated in *section 3.7.3 Application Examples* and *section 4.5 Fragility Relationships for Other Building Types*, respectively. Therefore, impact assessment for Los Angeles area under the Northridge earthquake of 1994 was executed; assessment results were presented with illustrations in the next section.

6.3.2 Assessment Results and Comparison

The MAEviz interface depicted in Figure 6-11 presents the direct economic building loss for the Los Angeles area in the 1994 Northridge earthquake, using hazard

map and fragility curves generated by NISRAF. The mean total loss was 20.7 billion dollars. In addition, impact assessment using MAEviz deterministic hazard and default fragility relationships was also carried out. Table 6-7 provides a summary comparison of the direct economic building loss of the study area between these two approaches. Meanwhile, an observed loss was also listed in this table for comparison. In this table, Lower_B. and Upper_B. stand for Lower Bound and Upper Bound, respectively. In general, results of Lower_B. and Mean NISRAF loss provide bounding values of the observed loss. While results of Mean and Upper_B. MAEviz default loss provide bounding values of the observed loss. Predicted loss by NISRAF is closer to the observed loss, although both of them are acceptable. The difference between these two approaches results from different hazard input and fragility relationships. Higher hazard input and more vulnerable fragility relationships in NISRAF approach result in the higher structural damage, and then higher economic loss. It is therefore concluded that NISRAF provides more reasonable accurate and modestly conservative assessment results for the Los Angeles area in the 1994 Northridge earthquake.

Table 6-7 Direct economic building loss

(Los Angeles county under the 1994 Northridge earthquake)

	Observed*	NISRAF			MAEviz (Default)		
		Lower_B.	Mean	Upper_B.	Lower_B.	Mean	Upper_B.
Dollar in Millions	18,500	17,938	20,706	23,474	12,055	15,359	18,664
Difference (%)	0.00	-3.13	10.65	26.89	-34.84	-16.98	0.88

Comerio et al., 1996

148
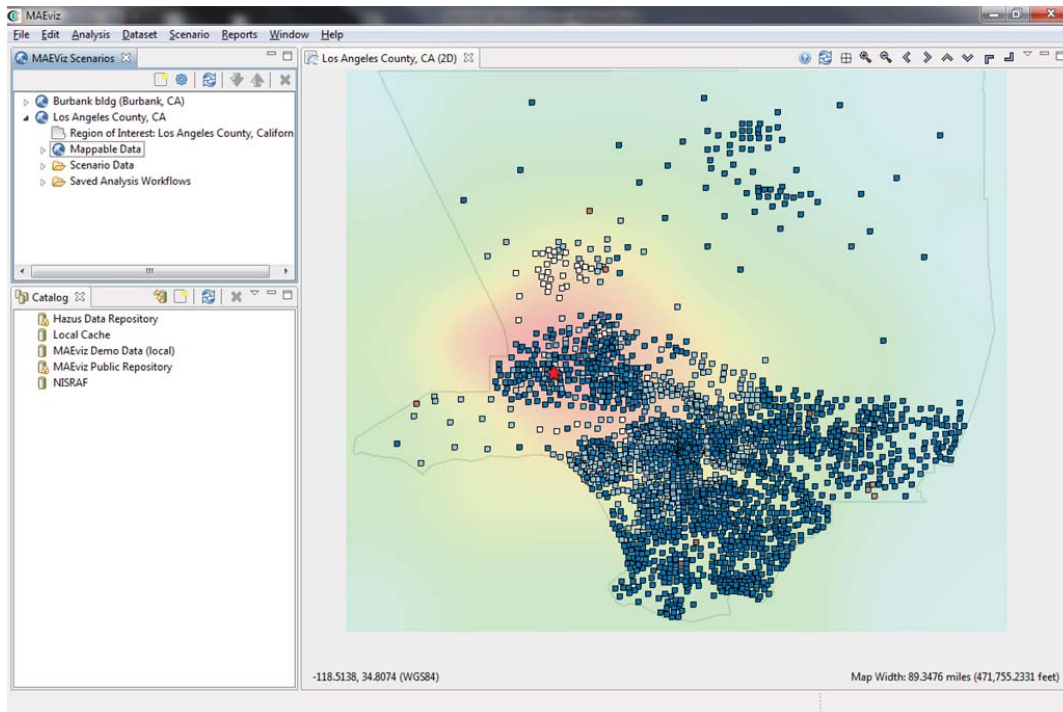
Figure 6-11 Earthquake impact assessment in Los Angeles area

6.4 Uncertainty Analysis in NISRAF

6.4.1 Introduction

Earthquake impact assessment is essential for disaster planning as well as developing risk reduction policies and emergency responses. As mentioned previously, an impact assessment package is composed of seismic hazard, fragility function, inventory data, and integration and visualization capacities. Mathematically, the loss estimation can be described by the following equation (Ellingwood and Wen, 2005):

$$P[Loss] = \sum_{s} \sum_{LS} \sum_{d} P[Loss|D = d] \cdot P[D = d|LS] \cdot P[LS|IM = s] \cdot P[IM = s] \quad (6.1)$$

where $P[\blacksquare]$ is the probability of loss (direct or indirect loss from the earthquake events), IM is the intensity measure of the seismic hazard (PGA or S_a), and s is the realization of the intensity measure. $P[LS|IM = s]$ is the conditional probability of reaching or exceeding structural limit states, and $P[D = d|LS]$ is the conditional probability of reaching damage. Here the term $P[LS|IM = s]$ refers to fragility or vulnerability discussed in previous section.

Due to the random nature and limited knowledge in earthquake engineering, numerous assumptions are made and many approximated methods are applied when performing impact assessment. Therefore, various types (aleatory and epistemic) of uncertainties exist in earthquake impact assessment, for example, the prediction of seismic intensity, the generation of fragility functions, the assumption of distribution of damage ratio, the inventory uncertainties and others.

With additional investigation and knowledge, it is definitely possible to reduce the epistemic uncertainties, such as by providing more realistic seismic hazard characterization, more reliable fragility relationships, and more accurate inventory data. Nevertheless, uncertainties are unavoidable, particularly in the case of aleatory uncertainties (randomness). Many approaches (Grossi, 2000; Chang and Song, 2006; Baker and Cornell, 2008; Elnashai et al., 2009; Choun and Elnashai, 2010) are proposed to quantify the uncertainties in regional impact assessment, in order to provide emergency managers and decision makers more confidence when reviewing the assessment results. Among these proposed approaches, some of them are probabilistic

estimations (Baker and Cornell, 2008); while others are approximated approaches (Chang and Song, 2006; Elnashai et al., 2009; Choun and Elnashai, 2010). In general, the probabilistic method may need more time and effort for its large computation requirements. Therefore, the approximated method is relatively more powerful and more practical for its simple and cost-effective features, in particular for regional impact assessment.

One advanced feature of MAEviz that distinguishes it from HAZUS-MH is its uncertainty quantification analysis, which not only provides users with the mean value of the predicted losses, but also supplies the uncertainty information (the standard deviation value). With this contribution of uncertainty analysis in MAEviz, NISRAF—to be consistent with its user-friendly feature—presents the uncertainties through an intuitive and friendly interface. In the following sections, the methodology of uncertainty quantification analysis implemented in MAEviz is reviewed briefly, followed by the demonstration using Los Angeles area earthquake impact assessment results presented through the developed intuitive interface.

6.4.2 Methodology of uncertainty analysis in MAEviz

The methodology of uncertainty analysis utilized in this study is first proposed by Chang and Song (2006), which has already been implemented in MAEviz. However, only mean and standard deviation values are available. Therefore, a program with user-friendly, intuitive interface is developed and implemented in NISRAF, which allows users to quantify uncertainties by selecting different confidence intervals. In the

following sections, this uncertainty analysis methodology is briefly introduced, followed by an application to impact assessment results for Los Angeles area under the 1994 Northridge earthquake. More details about this method are referring to the related reference (Chang and Song, 2006).

6.4.2.1 Uncertainty in hazard

Due to many uncertainties, including those related to the site conditions, earthquake magnitude, and distance to the seismic source, it is difficult to predict the seismic hazard characterization accurately. To this end, tools for seismic hazard analysis have been developed in the past decades. Deterministic Seismic Hazard Analysis (DSHA - Reiter, 1990) and Probabilistic Seismic Hazard Analysis (PSHA - Cornell, 1968) are the most commonly used methods. For the probabilistic properties and uncertainties from source, path, and site, uncertainties propagate in the procedure and outcome. To account for the uncertainties in seismic characterization, an uncertainty term β_{Sa} is introduced and incorporated into the calculation of the fragility curves as shown below:

$$P_f = \Phi\left(\frac{\lambda}{\sqrt{\beta^2 + \beta_{Sa}^2}}\right) \tag{6.2}$$

where λ and β are mean and dispersion terms, respectively, when defining fragility relationships. β_{Sa} can be computed using the uncertainty term in NGA model (Campbell and Bozorgnia, 2008, for example), based on users' judgment, or from previous studies (Hays, 1980; Cramer, 2001). Therefore, the generated fragility functions will be modified before they are ingested into MAEviz to conduct the impact assessment.

6.4.2.2 Uncertainty in structural damage ratio

In MAEviz, three limit states (i.e. immediate occupancy, life safety and collapse prevention) are utilized, therefore, four structural damage states can be defined (insignificant (I), moderate (M), heavy (H), and complete (C)). Figure 6-12 shows the relationship between the limit states and damage ratio; Equation (6.3) lists the probability calculation for each damage state.

$$
\begin{aligned}
P(I) &= 1 - P(LS_{IO}) \\
P(M) &= P(LS_{IO}) - P(LS_{LS}) \\
P(H) &= P(LS_{LS}) - P(LS_{CP}) \\
P(C) &= P(LS_{CP})
\end{aligned}
\tag{6.3}
$$
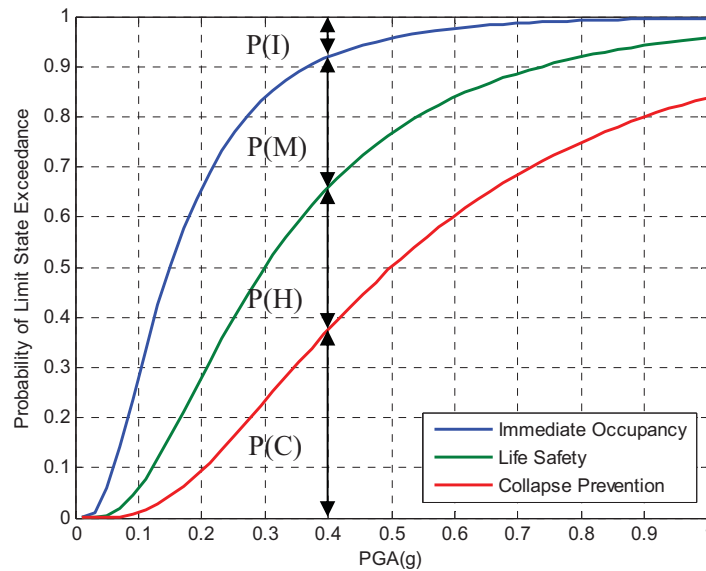
Figure 6-12 Definition and calculation of damage state probability

153

With the probability of each damage state, the total damage of structures after seismic events is calculated using the probabilities multiplied by the ratio for each damage state. In MAEviz, the damage ratio proposed by Bai et al. (2009) is utilized to calculate damage of structures. Table 6-8 lists the mean and standard deviation of the damage ratio for each damage state.

Table 6-8 Probability model for structural damage ratio (Bai et al., 2009)

Damage states DS_i	Range of Beta distribution (%)	Mean of damage ratio $\mu_{D|DS_i}$ (%)	Std. of damage ratio $\sigma_{D|DS_i}$ (%)
Insignificant	[0, 1]	0.5	0.333
Moderate	[1, 30]	15.5	9.67
Heavy	[30, 80]	55	16.7
Complete	[80, 100]	90	6.67

With the above information, the mean and variance of damage ratio (D) are computed using Equation (6.4).

$$
\begin{aligned}
\mu_D &= \sum_{i=1}^{4} [P(DS_i) \cdot \mu_{D|DS_i}] \\
\sigma_D^2 &= E[D^2] - \mu_D^2 \\
&= \sum_{i=1}^{4} [P(DS_i) \cdot (\sigma_{D|DS_i}^2 + \mu_{D|DS_i}^2)] - \mu_D^2
\end{aligned}
\tag{6.4}
$$

where $P(DS_i)$, $i=1,\ldots,4$, denotes the combined probabilities of the i-th damage state.

6.4.2.3 Uncertainty in nonstructural and content damage ratio

Similar procedures and related probabilistic assumptions are applied to nonstructural and content damage. Finally, both mean and variance of nonstructural and content damage ratios can be computed. For more details refer to Chang and Song (2006).

6.4.2.4 Loss estimation

With the damage ratio for structural, nonstructural and contents, the damage loss can be computed by Equation (6.5). Equation (6.5) is the loss for one single inventory only; therefore, the regional seismic loss is calculated by summing up all the inventory losses in the interested region. Moreover, this approach allows users to include inventory uncertainty when performing uncertainty analysis, which is detained in Chang and Song (2006).

$$Loss = M \cdot (\alpha^{SD} \cdot \widetilde{D}^{SD} + \alpha^{NS} \cdot \widetilde{D}^{NS} + \alpha^{CL} \cdot \widetilde{D}^{CL}) \tag{6.5}$$

where M is the total cost of the structure; α^{SD} and α^{NS} are the fractions of the total cost of the structure; α^{CL} is the ratio of the contents value to the structural value. $\widetilde{D}^{SD}$, $\widetilde{D}^{NS}$, and $\widetilde{D}^{CL}$ are the damage ratio of structural, nonstructural components, and contents, respectively. Based on Equation (6.5), mean and variance of seismic loss are estimated by:

$$\begin{aligned} \mu_{Loss} &= \sum M \cdot (\alpha^{SD} \cdot \mu_{\widetilde{D}^{SD}} + \alpha^{NS} \cdot \mu_{\widetilde{D}^{NS}} + \alpha^{CL} \cdot \mu_{\widetilde{D}^{CL}}) \\ \sigma^2_{Loss} &= \sum M^2 \big[(\alpha^{SD})^2 \sigma^2_{\widetilde{D}^{SD}} + (\alpha^{NS})^2 \sigma^2_{\widetilde{D}^{NS}} + (\alpha^{CL})^2 \sigma^2_{\widetilde{D}^{CL}} \big] \end{aligned} \tag{6.6}$$

6.4.2.5 Uncertainty representation

To be more intuitive, the loss uncertainty is quantified using confidence interval presentation, as shown in Equation (6.7), with $(1 - \alpha)\%$ confidence interval. Log-normal distribution assumption is made for the seismic loss.

$$
\begin{aligned}
CI &= \left[e^{(\lambda + k_{\alpha/2} \cdot \beta)}, e^{(\lambda - k_{\alpha/2} \cdot \beta)} \right] \\
&\quad where \; \lambda = ln\mu - 0.5\beta^2 \\
&\quad \beta = \sqrt{ln[1 + (\sigma/\mu)^2]}
\end{aligned}
\tag{6.7}
$$

where λ and β are the logarithmic mean μ and standard deviation σ of the loss, respectively. $k_{\alpha/2}$ is calculated by $k_{\alpha/2} = \Phi^{-1}\left(1 - \alpha/2\right)$.

6.4.3 Uncertainty analysis in NISRAF

Since the uncertainty analysis method mentioned above has been implemented in MAEviz, the impact assessment results of MAEviz (only mean and standard deviation values of structural, nonstructural and contents damage) will be used to quantify the uncertainty effects by showing different confidence intervals of the assessment results. A program with an intuitive and user-friendly interface is developed and implemented in NISRAF to represent the uncertainty quantification analysis. Through this interface, a pie-chart of different losses (i.e. structural, nonstructural and contents) is presented. Losses with upper-bound and lower-bound vary with the selection of the confidence level by the user (Figure 6-13).
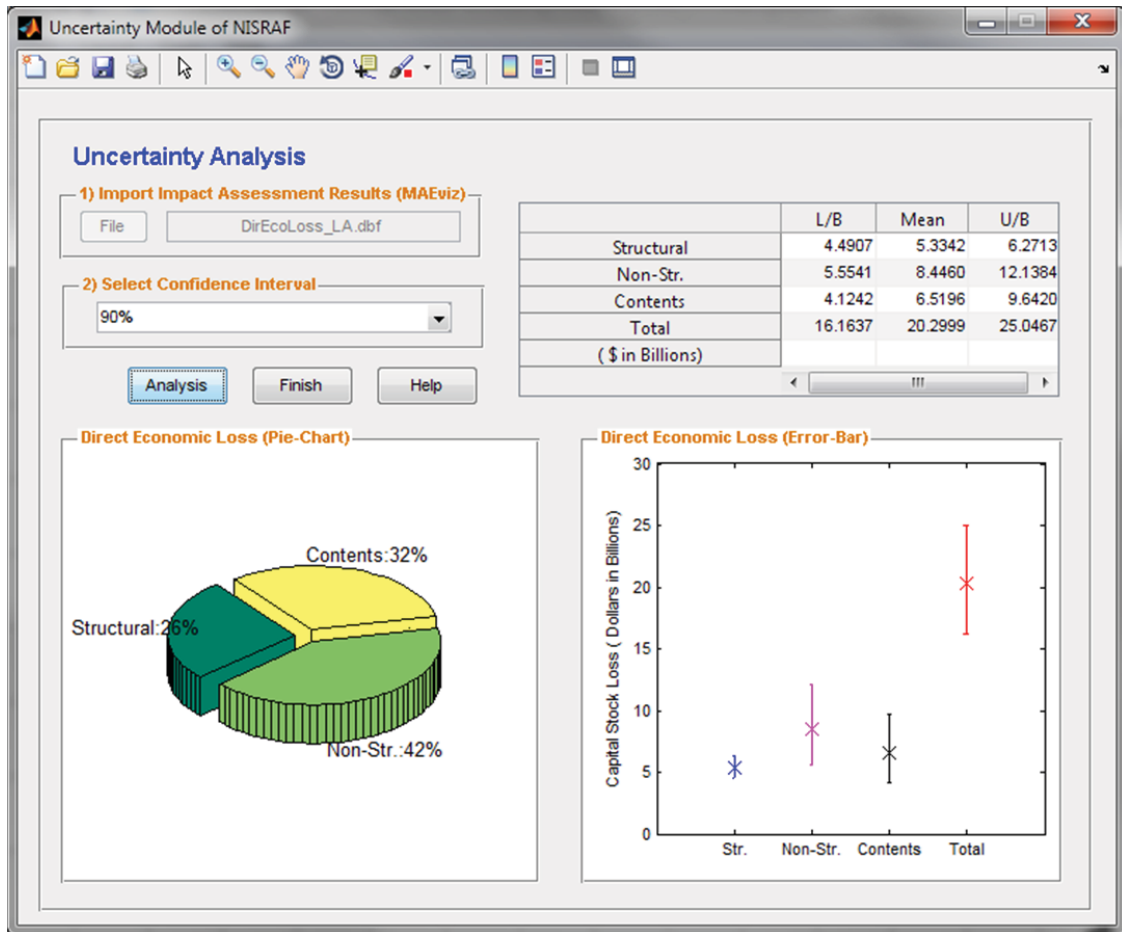
Figure 6-13 GUI in NISRAF with user-friendly interface for uncertainty quantification

6.4.4 Discussion of Uncertainty Analysis

Due to the random nature of seismic hazard and the limited knowledge and data, various types of uncertainties are inherent in earthquake loss estimation, from hazard model, inventory collection, and fragility derivation, to economic loss calculation. These unquantified uncertainties will result in significant under- or over-estimation of the assessment results. With the implemented approximate uncertainty quantification analysis presented through an intuitive way, decision-makers are able to judge the losses

easily and quickly, which will help to make more suitable and more confident recovery plans and emergency responses.

Even though the development and implementation of the proposed uncertainty quantification analysis method were successful, there are some limitations. Many investigations are still needed to improve the uncertainty results. For example, the uncertainty quantification approach is mainly based on many probabilistic assumptions, for example, the Beta distribution for the damage ratio. More studies are required to verify this distribution assumption. Also, more research is required to improve our understanding in earthquake source model, wave propagation, site effect, structural response, and also more accurate and comprehensive inventory data. With this additional information, which reduces the uncertainty effects in loss estimation, decision-makers will surely be more confident with their decisions.

6.5 Summary and Conclusion

The actual test bed in California, the 6-story steel building was carried out to demonstrate the integrated framework as well as its components. This building example demonstrated not only the seamlessly-integrated, extensible and transparent framework, but also that all the elements required for impact assessment can be performed under just one software platform. Consequently, the impact assessment result, which correlated with the post-earthquake reports, confirmed one of the advanced features of NISRAF—more efficient and more reliable impact assessment. Meanwhile, it also proved that the

proposed advanced methods—the hazard characterization analysis, the model calibration and the hybrid fragility analysis—were reliable. As a result of the demonstration of this impact assessment on one individual building, the same procedures can be extended to other different building types, seismic code levels and construction materials, to perform regional impact assessment. In regional impact assessment example, seismic loss through NISRAF for the Los Angeles area in the Northridge earthquake showed reasonable accurate, although conservative. Also, the implemented approximate uncertainty quantification analysis helps decision-makers to judge the losses easily and quickly, which will help to make more suitable and more confident recovery plans and emergency responses.

CHAPTER 7

CONCLUSIONS AND RECOMMENDATIONS

7.1 Summary of Findings

In this study, a reliable and integrated methodology for earthquake impact assessment using sensor data, site response analysis, model updating and hybrid simulation-based fragility analysis is proposed. The methodology is presented through a software framework, referred to as NISRAF, which supports integrated earthquake impact assessment for mitigation, emergency response and recovery planning. The software package is developed and verified in the dissertation. The methodology of NISRAF is described and its applicability and significance are demonstrated in part through an application example. In this integrated approach, the hazard characterization is generated from the measured data, and the structural fragility curves are developed from the hybrid simulation (with the calibrated numerical model, subjected to the derived strong-motion records), along with dispersions from the literature. The integration feature makes use of existing tools in a new approach towards a more efficient and reliable earthquake impact assessment.

Provided herein is a summary of the major findings stemming from not only the integrated framework, but also from the component verification studies carried out as part of the investigation. Also included is the discussion of the contributions and impacts which NISRAF has made upon the NEES and earthquake engineering communities.

The first component verification study, the advanced hazard characterization analysis module, demonstrates the procedure through which ground motion records are generated using SIMQKE along with NGA models and the predicted duration. By utilizing the measured instrumentation along with NGA models and the predicted duration, and by suitably adjusting SIMQKE, the proposed approach provides engineers with improved seismic hazard characterization for regional impact assessment. For example, with the utilization of the measured free-field records to calibrate the hazard characterization, and attenuation models along with site response analysis to generate synthetic ground motions, the proposed method surely provides more realistic hazard characterization than one that is based on mathematical formulations without calibration with the natural records. Meanwhile, with few seismic parameters being specified, the proposed approach calculates all required information automatically and produces the synthetic motions and hazard map efficiently and as accurately as possible.

The second component verification study validates the proposed advanced hybrid method for fragility curves generation. Hybrid simulation results under different synthetic ground motions (10%, 5% and 2% probability of exceedance in 50 years for immediate occupancy, life safety and collapse prevention performance levels, respectively) are used to derive the mean PGA value for each performance level. Using these mean values, along with dispersions from previous studies with similar structures, fragility curves are generated based on the lognormal distribution assumption. This hybrid fragility approach provides a straightforward and efficient way to derive fragility curves. Hence, this

approach is recommended to derive more reliable fragility relationships for other building types, although it requires time and effort.

Finally, the actual test bed in the Los Angeles area, the 6-story steel building and the Los Angeles area impact assessment were carried out to verify the integrated framework as well as its components. The reasonable, although conservative, impact assessment results not only demonstrated one of the advanced features of NISRAF, that is making impact assessment more efficient and more reliable, but also highlighted the high degree of reliability for the new hazard characterization and hybrid fragility methods.

7.2 Ideas for Future Research

The study presented in this dissertation validated the proposed integrated framework as well as the advanced analysis methods in hazard and fragility. In addition, the study demonstrated that all the elements required for an accurate impact assessment can be performed through one software platform. As previously mentioned, the proposed advanced methods—the hazard characterization analysis, the model calibration and the hybrid fragility analysis—has proven to be reliable. Nevertheless, due to its inherently complicated but extensible features, several studies are required to further improve the accuracy and robustness of NISRAF. Provided below are some suggestions for future studies:

- To corroborate the concept of the integration of hybrid simulation in NISRAF, small-scale specimens were used in this study. Additional large-scale hybrid

simulation testing is warranted to capture some inherent limitations in small-scale testing (localized behavior, for example).

- To account for the probabilistic characteristics and uncertainties in hazard analysis, 'Logical Tree' computation scheme is recommended after implementing additional attenuation models in NISRAF.

- Linear model updating algorithm based on the instrumented data is used to improve the numerical model in this study. Additional research on nonlinear model updating algorithms and techniques (such as model updating based on hybrid simulation results) is essential to improve the structural model and hence improve fragility curves.

- NISRAF, a versatile and integrated software tool, provides a platform for earthquake impact assessment and has been developed successfully. Many analysis algorithms and simulation techniques have also been implemented and are currently working seamlessly. To increase flexibility and robustness, research findings and techniques need to be continuously integrated with NISRAF as they appear in the literature. For example, OpenFresco, the University of California at Berkeley hybrid simulation software, can be another coordinator for hybrid simulation; SHAKE91 can be a choice for site response analysis; and HAZUS-MH can also be used to perform the impact assessment under NISRAF.

- Good agreement was achieved between the estimated and field-observed loss for the test bed in the Los Angeles area. However, test bed verifications in different areas for different structural types (highway bridge in Japan and high-technology

industry building in Taiwan, for example) are needed. These future verifications can further validate the methodologies of NISRAF as well as introduce this tool to research communities worldwide.

- The development of a Web-NISRAF, a Web-based NEES Integrated Seismic Risk Assessment Framework, is recommended for its potential impact on collaborative research in earthquake impact assessment. The Web-based feature could enable users to access NISRAF and perform analysis anytime and at any place around the world; therefore, it has no limitations in computational capacity. Moreover, within a unified database, where all simulation data is deposited, users can access previous data and share their own results efficiently.

7.3 Closure

NISRAF serves as a user-friendly software platform through which impact assessment can be efficiently and reliably performed by combining hazard (exposure) and fragility (sensitivity), to provide assessment of impact on the built environment at the regional scale. Concurrently, it extends the state-of-the-art hybrid simulation approach to fragility analysis, and proposes novel methods for hazard characterization. The successful completion of the development of the framework and verification of each component as well as communication between them, not only demonstrate that these objectives are achieved, but they also showcase the power and advantages offered by the George E. Brown, Jr. Network for Earthquake Engineering Simulation (NEES). For example, hybrid simulation enables NISRAF to integrate testing capabilities at multiple NEES sites. The

assessment thereby employs the strength of existing computation models and the expertise of individual research groups to explore previously unapproachable problems. Finally, the application of NISRAF will be a stimulus not only to geotechnical and structural earthquake engineers and impact assessment experts, but also for seismologists and structural control researchers improving their algorithms in order to pursue the ultimate goal of NEES under NEHRP: the assessment and mitigation of earthquake losses.

REFERENCES

Abrahamson, N. and Silva, W. (2008). "Summary of the NGA Ground-Motion Relations," *Earthquake Spectra*, 24(1): 67-98.

AISC (2005). *Specification for structural steel buildings*, ANSI/AISC 360-05, American Institute of Steel Construction, Inc., Chicago.

Allemang, R. J. and Brown, D. L. (1982). "A Correction Coefficient for Modal Vector Analysis," *Proceedings, International Modal Analysis Conference*, Orlando, Florida, 110~116.

Ambraseys, N. N. and Douglas, J. (2003). "Near-field horizontal and vertical earthquake ground motions," *Soil Dynamics and Earthquake Engineering*, 23(1): 1-18.

Ambraseys, N. N. and Bommer, J. J. (1991). "The attenuation of ground accelerations in Europe," *Earthquake Engineering and Structural Dynamics*, 20(12): 1179-1202

Anderson, J. C., Bertero, V. V. (1991). *Seismic performance of an instrumented six-story steel building*, Report UCB/EERC-91/11, University of California, Berkeley, U.S.A.

Applied Technology Council (2001). *Database on the performance of structures near strong-motion recordings: 1994 Northridge, California, earthquake,* Report No. ATC-38, Redwood City, CA.

Bai, J. W., Hueste, M. B. D., and Gardoni, P., (2009), "Probabilistic Assessment of Structural Damage due to Earthquakes for Buildings in Mid-America", *Journal of Structural Engineering*, Accepted, May 2009.

Baker, J. W. and Cornell, C. A., (2008), "Uncertainty propagation and feature selection for loss estimation", *Structural Safety*, 30(3): 236-252.

Bommer, J. J. and Martinez-Pereira, A. (1999). "The effective duration of earthquake strong-motion," *Journal of Earthquake Engineering*, 3(2): 127-172.

Boore, D. M. and Atkinson, G. M. (2008). "Ground-Motion Prediction Equations for the Average Horizontal Component of PGA, PGV, and 5%-Damped PSA at Spectral Period between 0.01 s and 10.0 s," *Earthquake Spectra*, 24(1): 99-138.

Boore, D. M., Joyner, W. B., and Fumal, T. E. (1997). "Equations for estimating horizontal response spectra and peak acceleration from western North American earthquakes: A summary of recent work," *Seismological Research Letters*, 68(1): 128-153.

Calvi, G. M., Magenes, G., Bommer, J. J. Restrepo-Velez, L. F. and Crowley, H. (2006). "Development of Seismic Vulnerability Assessment Methodologies over the Past 30 Years," *ISET Journal of Earthquake Technology*, 43(2): 75-104.

Campbell, K. W. (1997). "Empirical near-source attenuation relationships for horizontal and vertical components of peak ground acceleration, peak ground velocity, and pseudo-absolute acceleration response spectra," *Seismological Research Letters*, 68(1): 154-179.

Campbell, K. W. and Bozorgnia, Y. (2008). "NGA Ground Motion Model for the Geometric Mean Horizontal Component of PGA, PGV, PGD and 5% Damped Linear Elastic Response Spectra for Periods Ranging from 0.01 to 10 s," *Earthquake Spectra*, 24(1): 139-172.

Campbell, K. W. and Bozorgnia, Y. (2007). "Campbell-Bozorgnia NGA Ground Motion Relations for the Geometric Mean Horizontal Component of Peak and Spectral Ground Motion Parameters," UCB/PEER 2007/02, Pacific Earthquake Engineering Research Center.

Campbell, K. W. and Bozorgnia, Y. (2003). "Updated near-source ground-motion (attenuation) relationships for the horizontal and vertical components of peak ground acceleration and acceleration response spectra," *Bulletin of the Seismological Society of America*, 93(1): 314-331.

Chang, F. K. and Krinitzsky, E. L. (1977). "Duration, spectral content and predominant period of strong motion earthquake records from western United States," Miscellaneous Paper 5-73-1, US Army Corps of Engineers Waterways Experiment Station, Vicksburg, Mississippi.

Chang, L. and Song, J., (2006) "Systematic Treatment of Uncertainty in Consequence-Based Management of Seismic Regional Losses," Mid-America Earthquake Center, University of Illinois at Urbana-Champaign.

Chen, C. H., Lai, W. C., Cordova, P., Deirelein, G. G., and Tsai, K. C. (2003). "Pseudo-Dynamic Test of Full-Scale Rcs Frame: Part I – Design, Construction and Testing," *Proceedings of International Workshop on Steel and Concrete Composite Constructions*, Taipei, Taiwan, 107-118.

Chiou, B. and Youngs, R. (2008). "An NGA Model for the Average Horizontal Component of Peak Ground Motion and Response Spectra," *Earthquake Spectra*, 24(1): 173-216.

Choun, Y. -S. and Elnashai, A. S., (2010), "A simplified framework for probabilistic earthquake loss estimation", *Probabilistic Engineering Mechanics*, 25(2010): 355-364.

Cmerio, M. C., Landis, J. D., Firpo, C. J. And Monzon, J. P. (1996). "Residential Earthquake Recovery'' *California Policy Seminar,* University of California, Berkeley, CA.

Cornell, C. A. (1968). "Engineering seismic risk analysis," *Bulletin of the Seismological Society of America*, 58(4): 1583-1606.

Cornell, C. A., Jalayer, F., Hamburger, R. O., and Foutch, D. A. (2002). "Probabilistic Basis for 2000 SAC Federal Emergency Management Agency Steel Moment Frame Guidelines,'' *Journal of Structural Engineering*, 128(4): 526-533.

Cramer, C. H., (2001), "A seismic hazard uncertainty analysis for the New Madrid seismic zone", *Engineering Geology*, 62(1-3): 251-266.

Department of Conservation, Division of Mines and Geology (1998). *Seismic hazard zone report for the Burbank 7.5-minute quadrangle, Los Angeles County, California*, Seismic Hazard Zone Report 016.

Ellingwood, B. R. and Wen, K. Y., (2005), "Risk-benefit-based design decisions for low-probability/high consequence earthquake events in Mid-America," Progress in Structural Engineering and Material, 7:56-70.

Elnashai, A. S., Cleveland, L. J., Jefferson T., and Harrald, J., (2009) "Impact of New Madrid Seismic Zone Earthquakes on the Central USA," Mid-America Earthquake Center Report 09-03, University of Illinois at Urbana-Champaign.

Elnashai, A. S., Elghazouli, A. Y. and Dowling, P. J. (1990). "Verification of Pseudo-Dynamic Testing of Steel Members," *Journal of Constructional Steel Research,* Vol. 16, pp. 153-161.

Elnashai, A. S., Papanikolaou V., and Lee, D. (2002). *Zeus NL – a system for inelastic analysis of structures,* Mid-America Earthquake Center, University of Illinois at Urbana-Champaign, Program Release January 2004.

Federal Emergency Management Agency (2000a). *Recommended Seismic Design Criteria for New Steel Moment-Frame Buildings,* Report No. FEMA-350, Washington D.C.

Federal Emergency Management Agency (2000b). *Prestandard and Commentary for the Seismic Rehabilitation of Building,* Report No. FEMA-356, Washington D.C.

Federal Emergency Management Agency (2006). *HAZUS-MH technical manual*, FEMA, Washington, D.C.

Federal Emergency Management Agency (2009). *NEHRP (National Earthquake Hazard Reduction Program) Recommended Seismic Provisions for New Buildings and Other Structures,* Report No. FEMA-P-750, Washington D.C.

Filippou, F. C. and Constantinides, M. (2004). *FEDEASLab Getting Started Guide and Simulation Examples*, Technical Report NEESgrid-2004-22.

Frankie, T. M. (2010). *Simulation-Based Fragility Relationships for Unreinforced Masonry Buildings*, MS thesis, Department of Civil and Environmental Engineering, University of Illinois at Urbana-Champaign, Urbana, Illinois.

Friswell, M. I. and Mottershead, J. E. (1995). "Finite Element Model Updating in Structural Dynamics," Kluwer Academic Publishers, Dordrecht.

Fumal, T. E., Gibbs, J. F., and Roth, E. F. (1979). *In-situ measurements of seismic velocity at 19 locations in the Los Angeles, California region*, SMIP geotechnical report No. 131, U.S. Geological Survey.

Gasparini, D. A. and Vanmarcke, E. H. (1976). *Simulated Earthquake Motions Compatible with Prescribed Response Spectra*, Evaluation of Seismic Safety of Buildings Report No.2, Massachusetts Institute of Technology.

Gencturk, B. E. (2007). *Fragility Relationships for Populations of Building Based on Inelastic Response*, MS thesis, Department of Civil and Environmental Engineering, University of Illinois at Urbana-Champaign, Urbana, Illinois.

Gencturk, B. E. and Elnashai, A. S. (2008). "Development and application of an advanced capacity spectrum method," *Engineering Structures*, 30:3345–3354.

Grossi, P., (2000), "Quantifying the Uncertainty in Seismic Risk and Loss Estimation," University of Pennsylvania-Electronic Dissertations, Paper AAI9976429, University of Pennsylvania, Philadelphia, Pennsylvania.

Harris, H. G. and Sabnis, G. M. (1999). "Structural Modeling and Experimental Techniques," CRC Press, Florida.

Hartzell, S., Leeds, A., Frankel, A. and Michael J. (1996). "Site Response for Urban Los Angeles Using Aftershocks of the Northridge Earthquake," *Bulletin of the Seismological Society of America*, 86(1B):S168–S192.

Hashash, Y., Groholski, D.R., Phillips, C.A., Park, D. (2009). *DEEPSOIL V3.5beta, User Manual and Tutorial.*

Hays, W. W., (1980), "Procedures for estimating earthquake ground motions," US geological survey professional paper 1114. Washington DC.

Hibbit, H. D., Karlsson, B. I., and Sorensen (2001). *ABAQUS theory manual. Version 6.2.*

Holub, C. J. (2009). *Interaction of Variable Axial Load and Shear Effects in RC Bridges,* Ph.D. thesis, Department of Civil and Environmental Engineering, University of Illinois at Urbana-Champaign, Urbana, Illinois.

Idriss, I. M. (2008). "An NGA Empirical Model for Estimating the Horizontal Spectral Values Generated By Shallow Crustal Earthquakes," *Earthquake Spectra*, 24(1): 217-242.

Idriss, I. M. and Sun, J. I. (1992). *User's Manual for SHAKE91, A Computer Program for Conducting Equivalent Linear Seismic Response Analyses of Horizontally Layered Soil Deposits.*

Jeong, S. H. and Elnashai, A. S. (2004). "Analytical and Experimental Seismic Assessment of Irregular RC Buildings," *Proceedings of 13th World Conference on Earthquake Engineering*, Vancouver, B.C., Canada.

Jeong, S. H. and Elnashai, A. S. (2006). "Probabilistic fragility analysis parameterized by fundamental response quantities," *Engineering Structures.*, 29:1238-1251.

Juang, J. N. and Pappa, R. S. (1985). "An eigensystem realization algorithm for modal parameter identification and model reduction," *Journal of Guidance, Control, and Dynamics*, 8(5): 620-627.

Kawashima, K. and Aizawa, K. (1989). "Bracketed and normalized durations of earthquake ground accelerations," *Earthquake Engineering and Structural Dynamics*, 18, 1041-1051.

Kempton, J. J. and Stewart, J. P. (2006). "Prediction Equations for Significant Duration of Earthquake Ground Motions Considering Site and Near-Source Effects," *Earthquake Spectra*, 22(4), 985-1013.

Kramer, S. L. (1996). *Geotechnical earthquake engineering*, Prentice Hall, Upper Saddle River, NJ.

Kunnath, S. K., Nghiem, Q., and El-Tawil, S. (2004). "Modeling and Response Prediction in Performance-Based Seismic Evaluation: Case Studies of Instrumented Steel Moment-Frame Buildings," *Earthquake Spectra*, 20(3): 883-915.

Kwon, O. S. and Elnashai, A. S. (2006). "The effect of material and ground motion uncertainty on the seismic vulnerability curves of RC structure," *Engineering Structures*, 28(2):289-303.

Kwon, O. S. and Kim, E. S. (2010). "Evaluation of building period formulas for seismic design," *Earthquake Engineering and Structural Dynamics*, n/a. doi: 10.1002/eqe.998.

Kwon, O. S., Nakata, N., Park, K. S., Elnashai, A. S., and Spencer, B. J. (2007). *User Manual and Examples for UI-SIMCOR v2.6*, Department of Civil and Environmental Engineering, University of Illinois at Urbana-Champaign, Urbana, Illinois.

Li, J., Lin, S. L., Zong, X., Spencer, B. F., Elnashai, A. S. and Agrawal, A. K. (2009). "An Integrated Earthquake Impact Assessment Framework," *ANCER Annual Meeting,* August 13-14, Urbana, Illinois.

Lin, B. Z., Hsu, F. W., Chuang, M. C., Wang, K. J. and Tsai, K. C. (2006). "Development of an object-oriented platform and graphical user interface for nonlinear structural analysis," *Proceedings of the 8th U.S. National Conference on Earthquake Engineering (8NCEE)*, San Francisco, California.

Mahin, S. A. and Shing, P. B. (1985). "Pseudodynamic Method for Seismic Testing," *Journal of Structural Engineering*, ASCE, 111(7): 1482-1503.

McKenna, F. and Fenves, G. L. (2001). *The OpenSees command language manual, version 1.2.,* Pacific Earthquake Engineering Research Center, University of California at Berkeley.

Mid-America Earthquake Center (2007). *Mid-America Earthquake Center Seismic Loss Assessment System, MAEviz v3.1.1*, University of Illinois at Urbana-Champaign, Urbana, Illinois.

Minas and Inman, D. J. (1990). "Matching Finite Element Models to Modal Data, Transactions of the ASME," *Journal of Vibration and Acoustics,* 112 (1): 84–92.

Naeim, F. (2005). "Instrumented Buildings Response Analysis and 3D Visualization System," CGS CSMIP contract no. 1002-776, CD ROM.

Nakashima, M. and Kato, H. (1987). *Experimental Error Growth Behavior and Error Growth Controlling Online Computer Test Control Method*, Building Research Institute, BRI-Report No. 123, Ministry of Construction, Tsukuba, Japan.

Nelder, J. A. and Mead, R., (1965). "A simplex method for function minimization," *Computer Journal*, 7: 308-313.

Pappa, R. S., Elliott, K. B., (1993). "Consistent-mode indicator for the eigensystem realization algorithm," *Journal of Guidance, Control, and Dynamics*, 16(5): 852-858.

Park, K. S., Kwon, O. S., Spencer, B. F., Elnashai, A. S., (2007). *Tutorial for Beta version of SimBuild, Pre- and Post-processor for UI-SimCor*, Department of Civil and Environmental Engineering, University of Illinois at Urbana-Champaign, Urbana, Illinois.

Power, M., Chiou, B., Abrahamson, N., Bozorgnia, Y., Shantz, T., and Roblee, C. (2008). "An Overview of the NGA Project," *Earthquake Spectra*, 24(1): 3-22.

Reiter, L. (1990). "Earthquake hazard analysis – issues and insights," Columbia University Press, New York.

Rinaldis, D., Berardi, R., Theodulidis, N., and Margaris, B. (1998). "Empirical predictive models based on a joint Italian & Greek strong-motion database: I. Peak ground acceleration and velocity," *Proceedings of the 11th European Conference on Earthquake Engineering*, Balkema, Rotterdam.

Rossetto, T. and Elnashai, A. (2003). "Derivation of Vulnerability Functions for European-type RC Structures Based on Observational Data," *Engineering Structures*, 25(10):1241-1263.

Seed, H. B., Ugas, C. and Lysmer, J. (1976). "Site-dependent spectra for earthquake-resistant design," *Bulletin of the Seismological Society of America*, 66 (4):221-243.

Seed, H. B., Dickenson, S. E., Reimer, M. F., Bray, J. D., Sitar, N., Mitchell, J. K., Idriss, I. M., Kayen, R. E., Kropp, A., Harder, L. F., and Power, M. S. (1990). *Preliminary report on the principal geotechnical aspects of the October 17, 1989 Loma Prieta earthquake*, Report UCB/EERC90/05, Earthquake Engineering Research Center, University of California, Berkeley.

Schnabel, P. B., Lysmer, J. and Seed, H. B. (1972). *SHAKE: A computer program for earthquake response analysis of horizontally layered sites,* Report No EERC 72-12, Earthquake Engineering Research Center, University of California, Berkeley, California.

Spencer Jr., B. F., Elnashai, A. S., Kuchma, D., Kim, S. J., Holub, C. and Nakata, N. (2007). *Multi-Site Soil-Structure-Foundation Interaction Test (MISST)*, *Final report to NESS project,* University of Illinois at Urbana-Champaign, Illinois.

Spencer Jr., B. F., Elnashai, A. S., Park, K., and Kwon, O. (2006). *Hybrid Test Using UI-SimCor, Three-Site Experiment*, *Final report to NEESit for Phase I project of hybrid simulation framework development*, University of Illinois at Urbana-Champaign, Illinois.

Stone, W. C., Yokel, F. Y., Celebi, M., Hanks, T., and Leyendecker, E. V. (1987). "Engineering aspects of the September 19, 1985 Mexico earthquake," NBS Building Science Series 165, National Bureau of Standards, Washington, DC.

Takahashi, T., Kobayashi, S., Fukushima, Y., Zhao, J. X., Nakamura, H., and Somerville, P. G. (2000). "A spectral attenuation model for Japan using strong motion data base," *Proceedings of the 6th International Conference on Seismic Zonation: Managing Earthquake Risk in the 21th Century*, Earthquake Engineering Research Institute, Oakland, CA.

Takanashi, K., Udagawa, K., Seki, M., Okada, T. and Tanaka, H. (1975). "Nonlinear Earthquake Response Analysis of Structures by a Computer-Actuator On-Line System," *Bull. of Earthquake Resistant,* Structure Research Centre, No.8, Inst. of Industrial Science, University of Tokyo, Japan.

Tong, H. and Katayama, T. (1998). "Peak acceleration attenuation by eliminating the ill-effect of the correlation between magnitude and epicentral distance," *Proceedings of the 9th World Conference on Earthquake Engineering*, II: 349-354.

Trifunac, M. D., and Brady, A. G. (1975). "A study of the duration of strong earthquake ground motion," *Bulletin of the Seismological Society of America*, 65(3): 581-626.

U. S. Geological Survey (1999). *Requirement for an Advanced National Seismic System*, U. S. Geological Survey Circular 1188 Report.

U. S. Geological Survey (1996). *USGS Response to an Urbana Earthquake: Northridge '94*, Open-File Report 96-263.

Vahdani, S. and Wikstrom, S. (2002). "Response of the Tarzana strong motions site during the 1994 Northridge earthquake," *Soil Dynamics and Earthquake Engineering*, 22: 837-848.

Vanmarcke, E. H., and Lai, S. S. (1980). "Strong motion duration and RMS amplitude of earthquake records," *Bulletin Seismological Society of America*, 70(4): 1293-1307.

Vecchio, F. J. and Wong, P. (2003). *VecTor2 and FormWorks Manual,* University of Toronto, Toronto, Canada.

Wen, Y. K., and Ellingwood, B. R. (2004), "Vulnerability Function Framework for Consequence-Based Engineering," Mid-America Earthquake Center, University of Illinois at Urbana-Champaign, Illinois.

Wu, J. R., and Li, Q. S. (2004). "Finite Element Model Updating for a High-Rise Structure Based on Ambient Vibration Measurements," *Engineering Structures*, 26(7):979-990.

Yeh, C. H., Loh, C. H., and Tsai, K. C. (2006). "Overview of Taiwan Earthquake Loss Estimation System," *Natural Hazards*, 37: 23-37.

Youngs, R. R., Chiou, S. J., Silva, W. J., and Humphrey, J. R. (1997). "Strong ground motion attenuation relationships for subduction zone earthquakes," *Seismological Research Letters*, 68(1): 58-73.

Yun, S. Y., and Foutch D. A. (2000). *Performance prediction and evaluation of low ductility steel moment frames for seismic loads*, SAC Background Document SAC/BD-00/26, Richmond, CA: SAC Joint Venture.

APPENDIX A

SYNTHETIC GROUND MOTIONS AT BURBANK SITE

In this section, synthetic ground motions with various hazard levels at Burbank, California were generated through the proposed advanced hazard characterization analysis method. First of all, the USGS 2008 Interactive Deaggregations online analysis tool (http://eqint.cr.usgs.gov/deaggint/2008/index.php) was performed to derive seismic parameters for different hazard levels (i.e. 10%, 5% and 2% probability of exceedance in 50 years). Figure A-1, Table 3-7 and Table 3-8 show the deaggregation results at the Burbank site.

Moreover, geotechnical report at Burbank Fire Station site (Table 3-1 and Figure 3-8) was used to create soil column in order to perform site response analysis. With the above information and following the steps illustrated in *section 3.4: Synthetic Ground Motion Generation*, 27 synthetic ground motions varying with duration and hazard levels were generated automatically. Figure A-2 to Figure A-7 lists the 27 generated synthetic ground motions. Rather, Figure A-2, Figure A-4 and Figure A-6 also show the response spectra in different hazard levels. These motions were then used as seismic inputs to evaluate structural response in hybrid simulation testing (Appendix B) as well as to derive fragility curves (Appendix C).
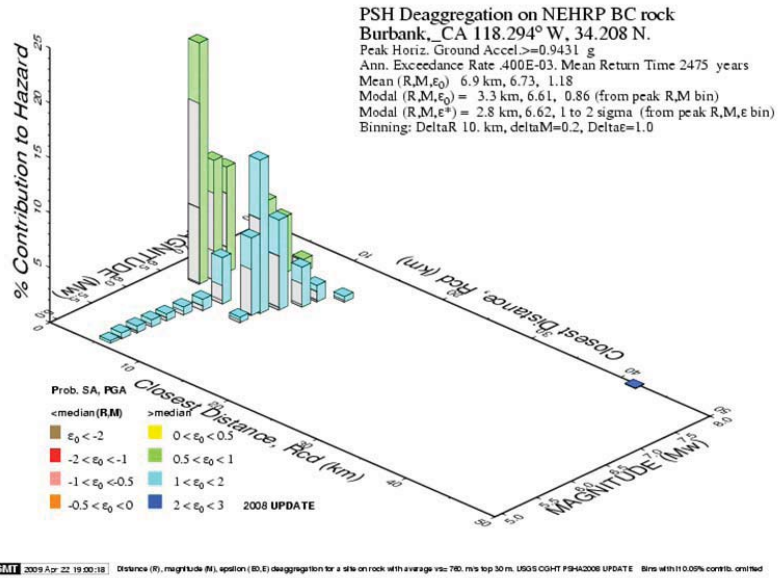
Figure A-1(a) Deaggregation results (2% PE/50yrs) at Burbank site
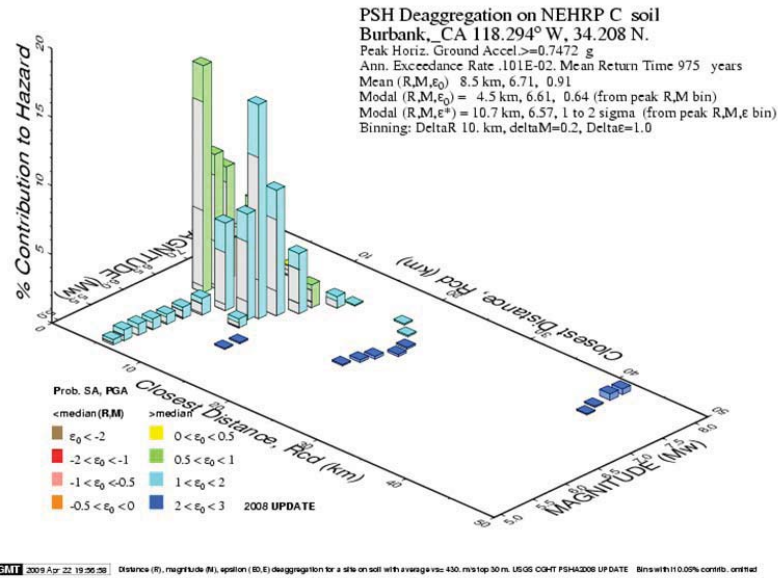
Figure A-1(b) Deaggregation results (5% PE/50yrs) at Burbank site
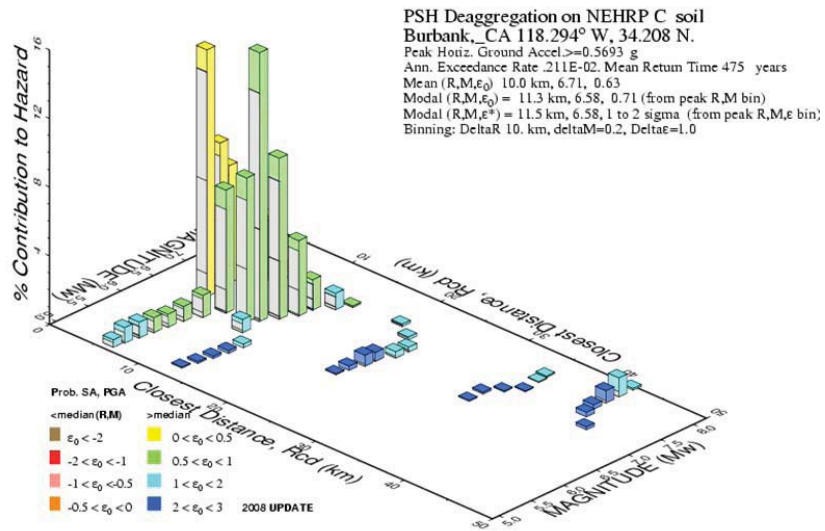
Figure A-1(c) Deaggregation results (10% PE/50 yrs) at Burbank site
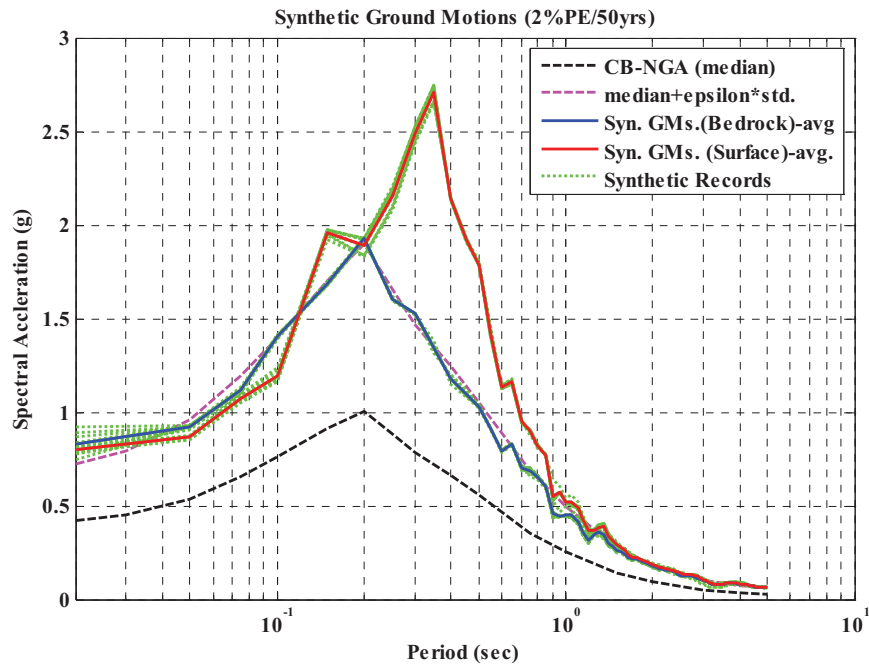
(a) Response spectrum
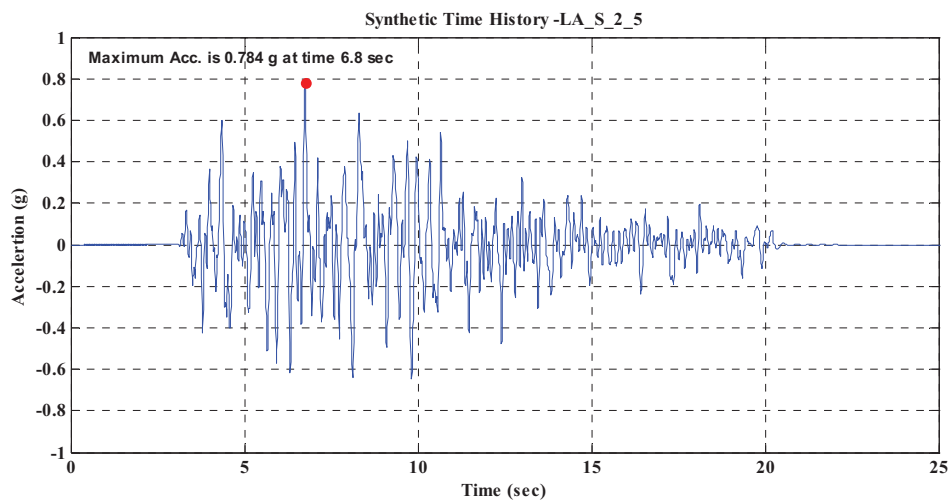
(b) Synthetic ground motion

Figure A-2 Response spectrum and synthetic ground motion for 2% PE/50 yrs hazard level
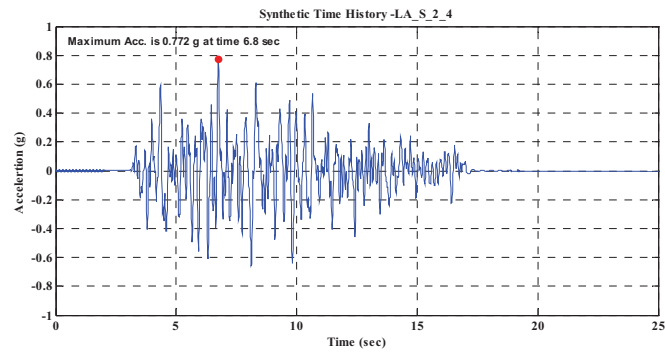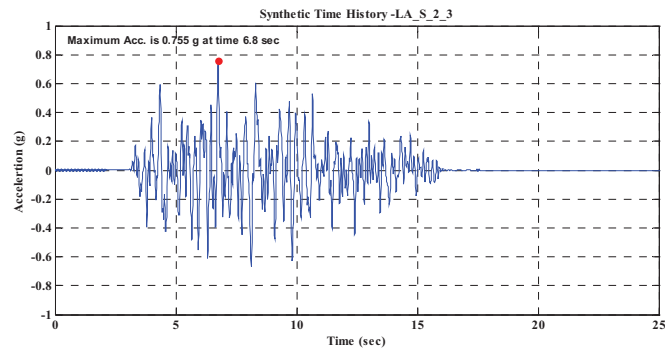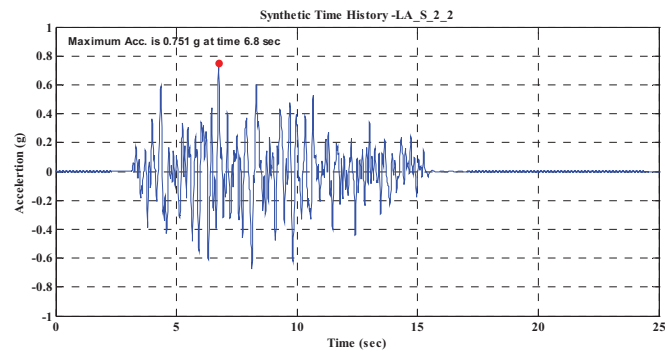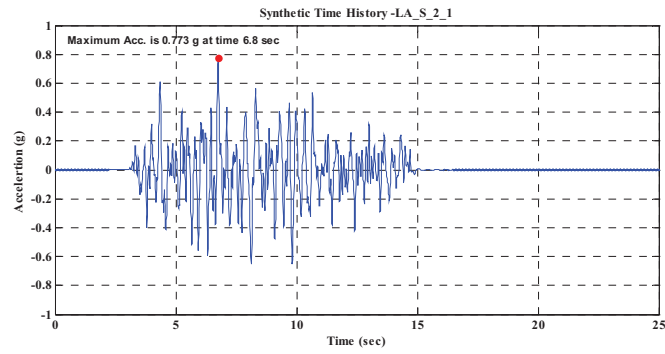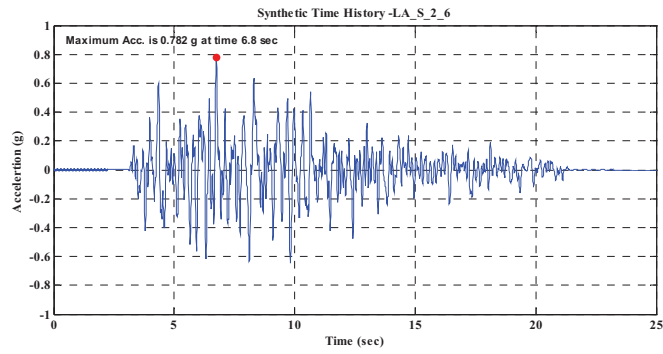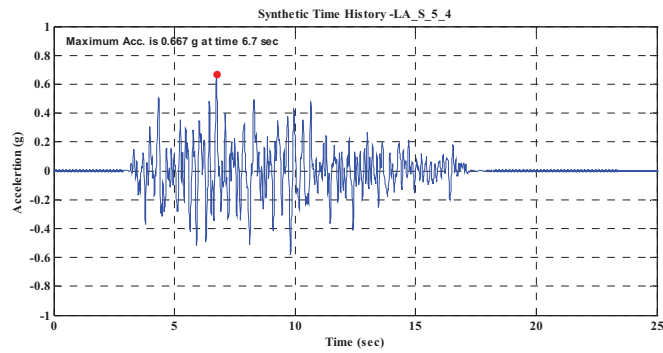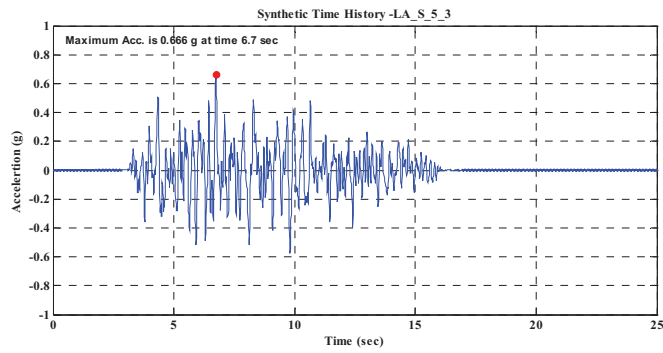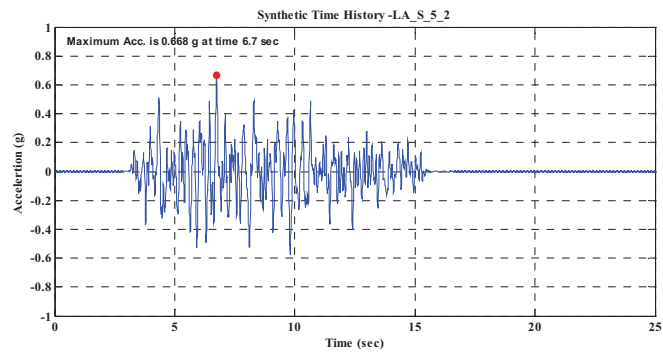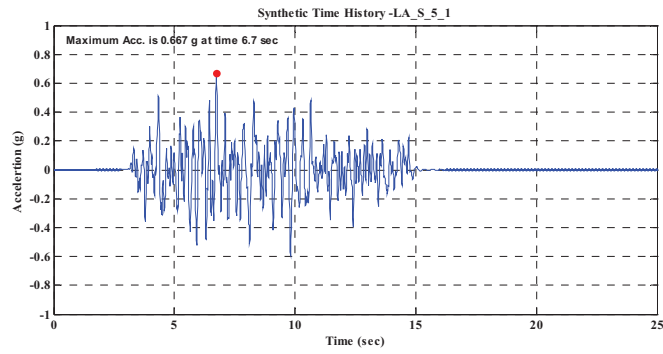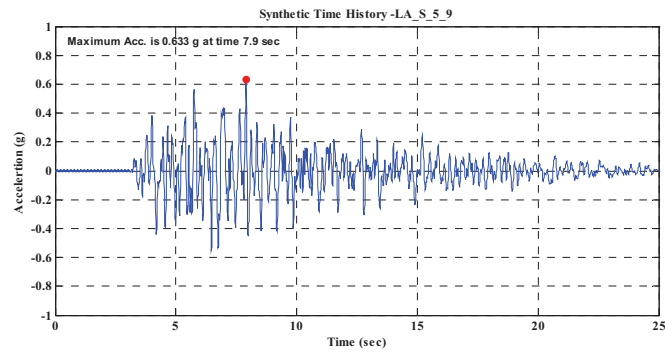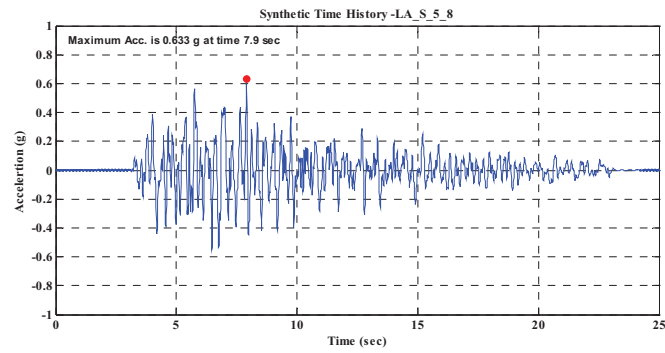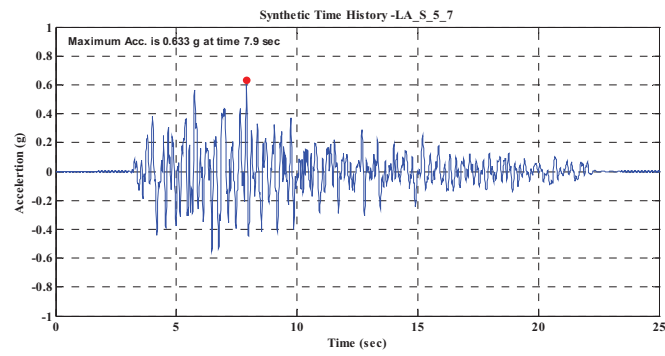
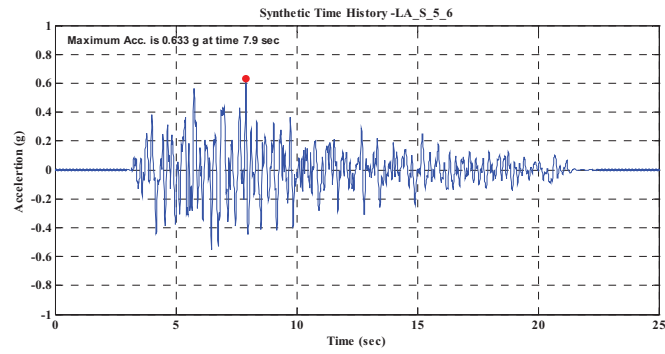**Figure A-3** Synthetic ground motions (2% PE/50yrs)
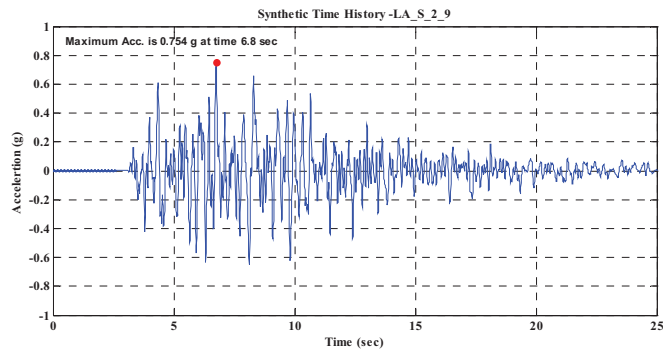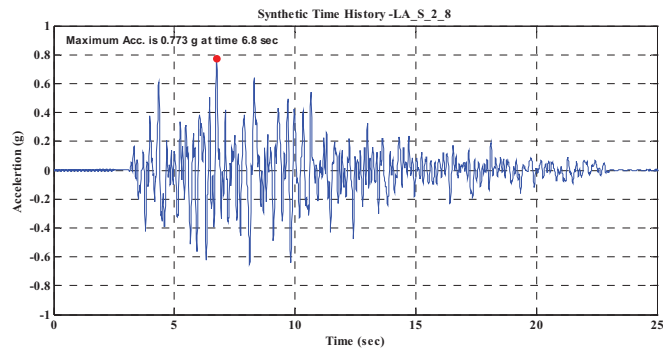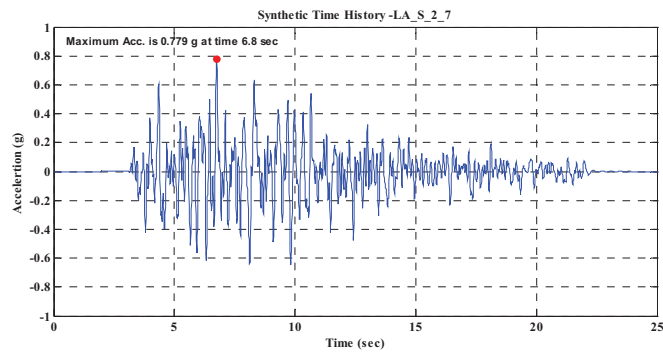
Figure A-3 Synthetic ground motions (2% PE/50yrs)
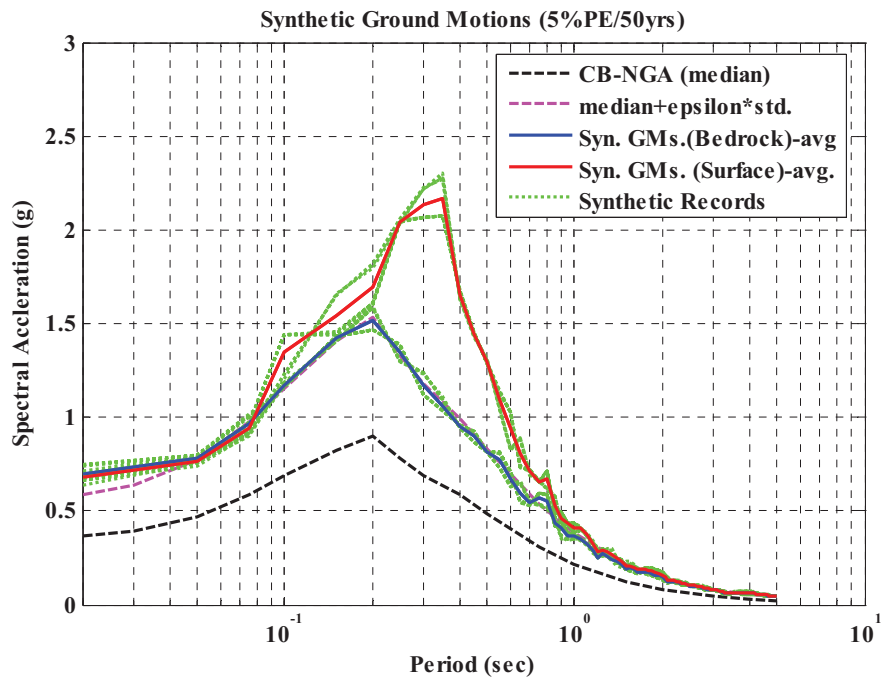
(a) Response spectrum
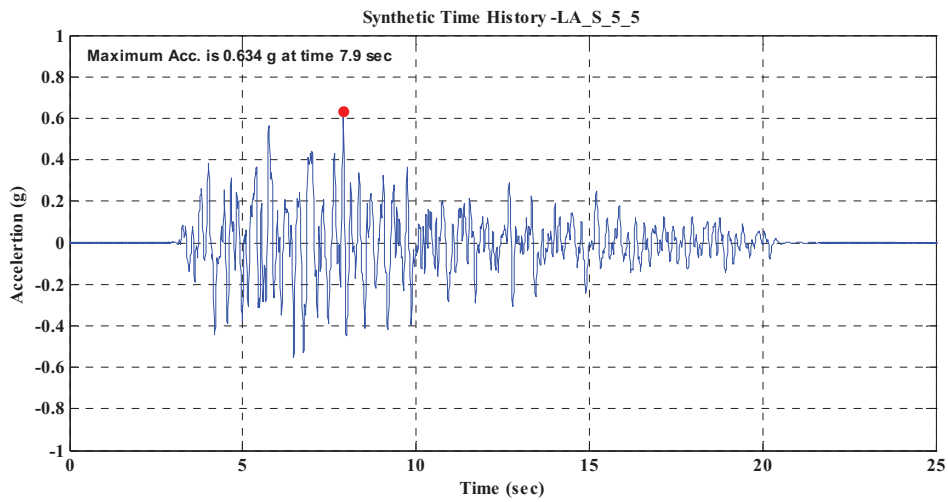
(b) Synthetic ground motion

Figure A-4 Response spectrum and synthetic ground motion for 5% PE/50 yrs hazard level

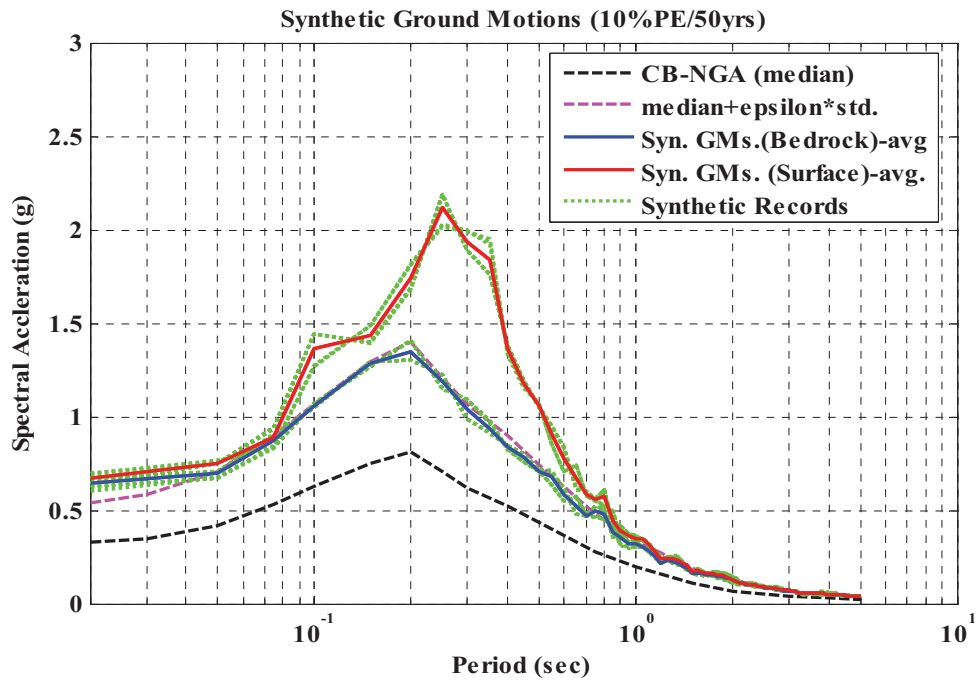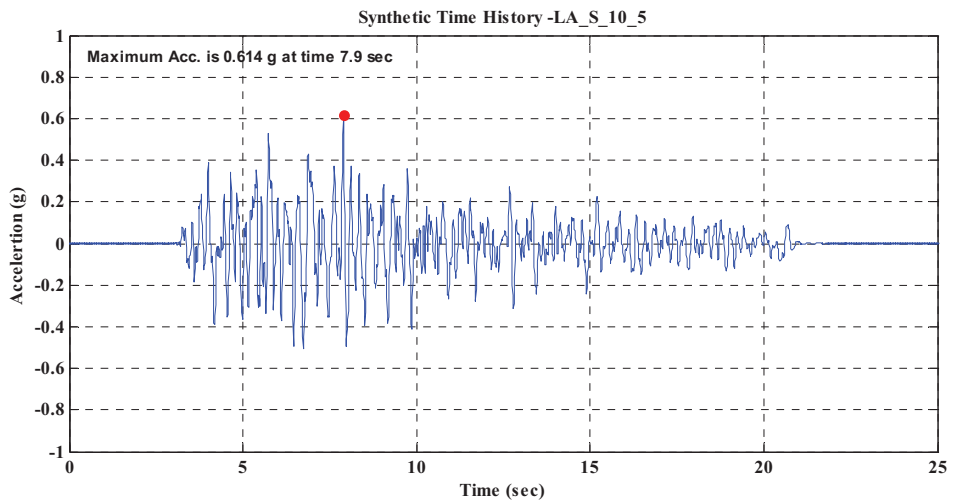**Figure A-5** Synthetic ground motions (5% PE/50yrs)

Figure A-5 Synthetic ground motions (5% PE/50yrs)

(a) Response spectrum

(b) Synthetic ground motion

Figure A-6 Response spectrum and synthetic ground motion for 10% PE/50 yrs hazard level
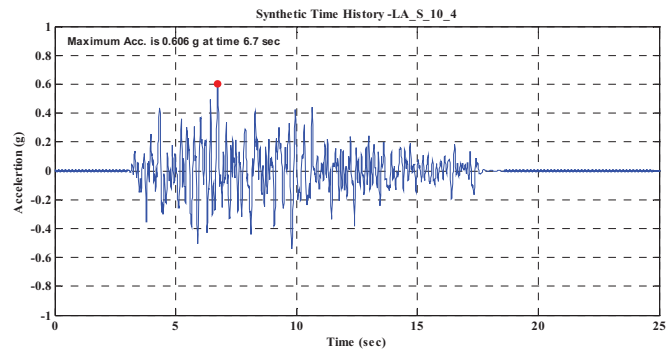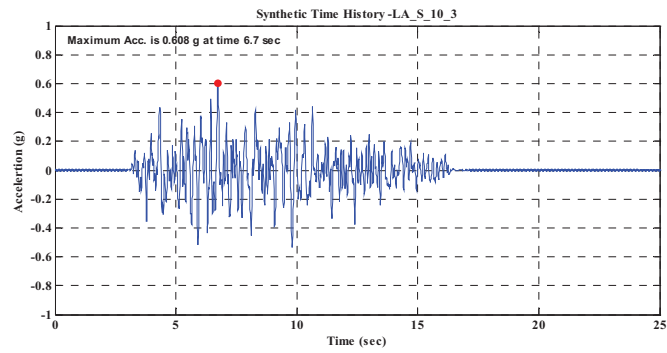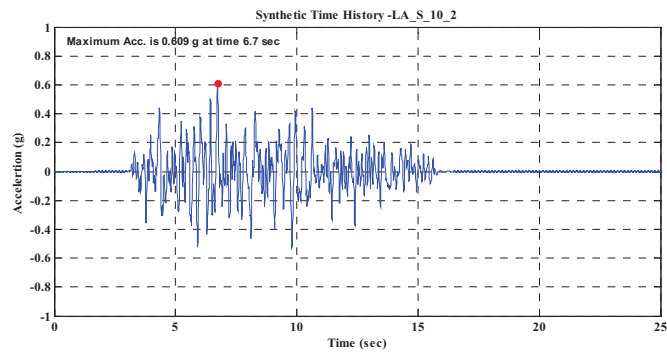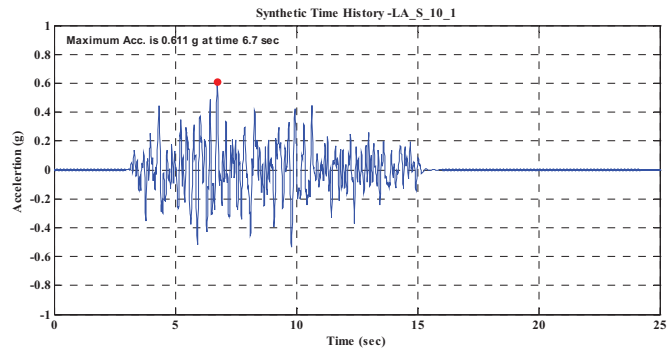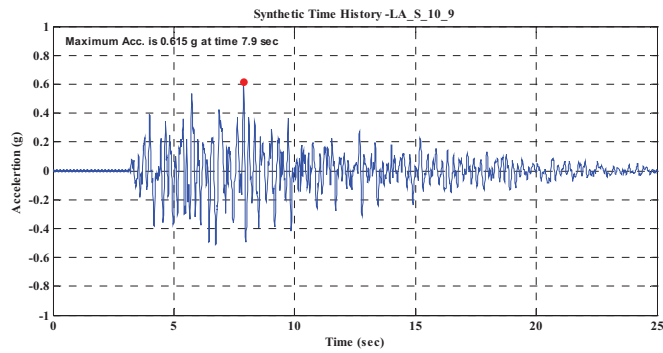
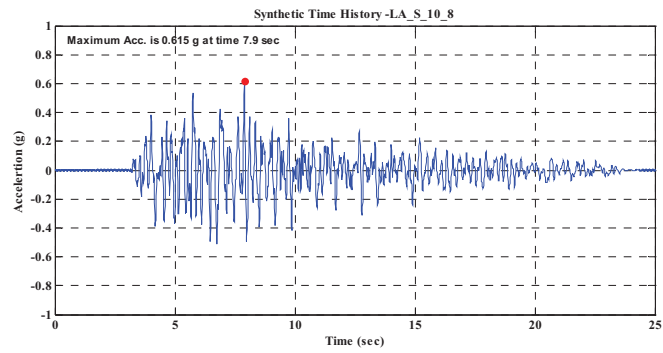**Figure A-7** Synthetic ground motions (10% PE/50yrs)

184
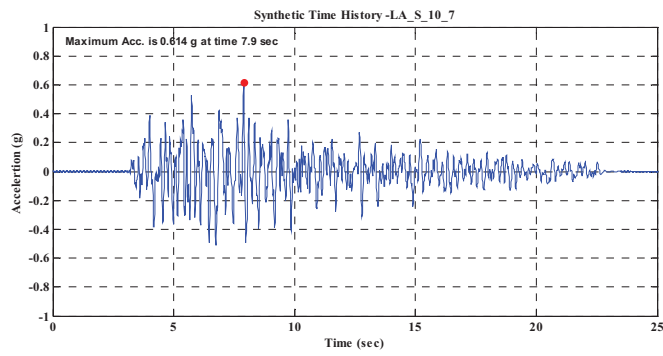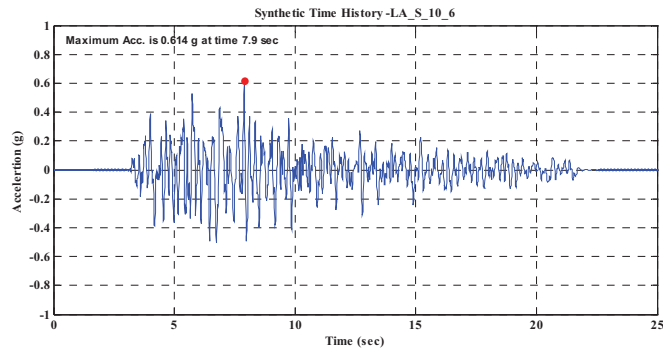
Figure A-7 Synthetic ground motions (10% PE/50yrs)

APPENDIX B

HYBRID SIMULATION TESTING DATA

In this section, instrumented data collected during the hybrid simulation testing were included in the following pages. Tests were grouped in the following categories:

- Proof test

  (Ground motion: the 1994 Northridge earthquake record)

- Mean PGA value for immediate occupancy limit state

  (Ground motion: 10% probability of exceedance in 50 years)

- Mean PGA value for life safety limit state

  (Ground motion: 5% probability of exceedance in 50 years)

- Mean PGA value for collapse prevention limit state

  (Ground motion: 2% probability of exceedance in 50 years)

Meanwhile, multiplatform simulation testing was also conducted. Comparison between hybrid and multiplatform simulation were made. Included for each testing are the following:

- Testing description

- Applied ground motion

- Comparison of interstory drift angle (ISDA) between the target and the one calculated based on hybrid simulation result.

- Relationship between lateral force and displacement on top of specimen column.

- Displacement (lateral displacement, axial displacement and rotation) history on the top of specimen column.

- Force (lateral force, axial force and moment) history on the top of specimen column.

Test No. 1

Description: This was a proof test to evaluate the hybrid model and experimental setting. The 1994 Northridge earthquake record was used as seismic input, roof drift history was compared with the measured response.

Test No. 1

Lateral Displacement of the Top of Cloumn

Hybrid Simulation
Multiplatform Simulation

Axial Displacement of the Top of Cloumn

Rotation of the Top of Clolumn

Time (sec)

Lateral Force of the Top of Clolumn

Hybrid Simulation
Multiplatform Simulation

Axial Force of the Top of Clolumn

Moment of the Top of Clolumn

Time (sec)
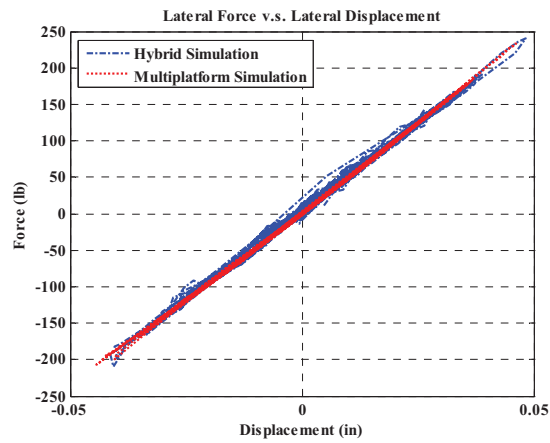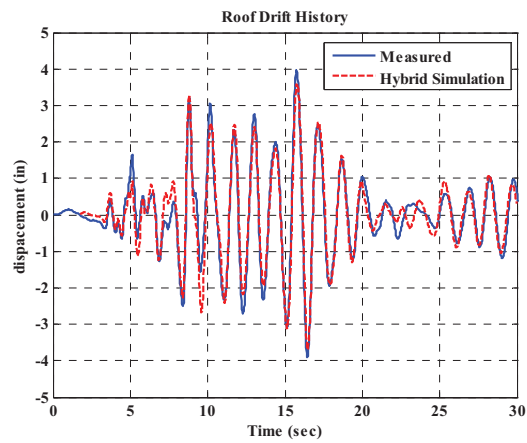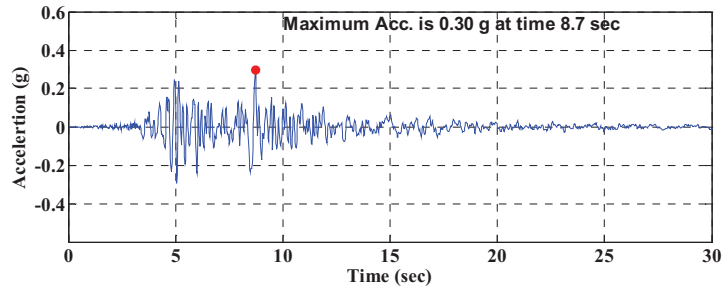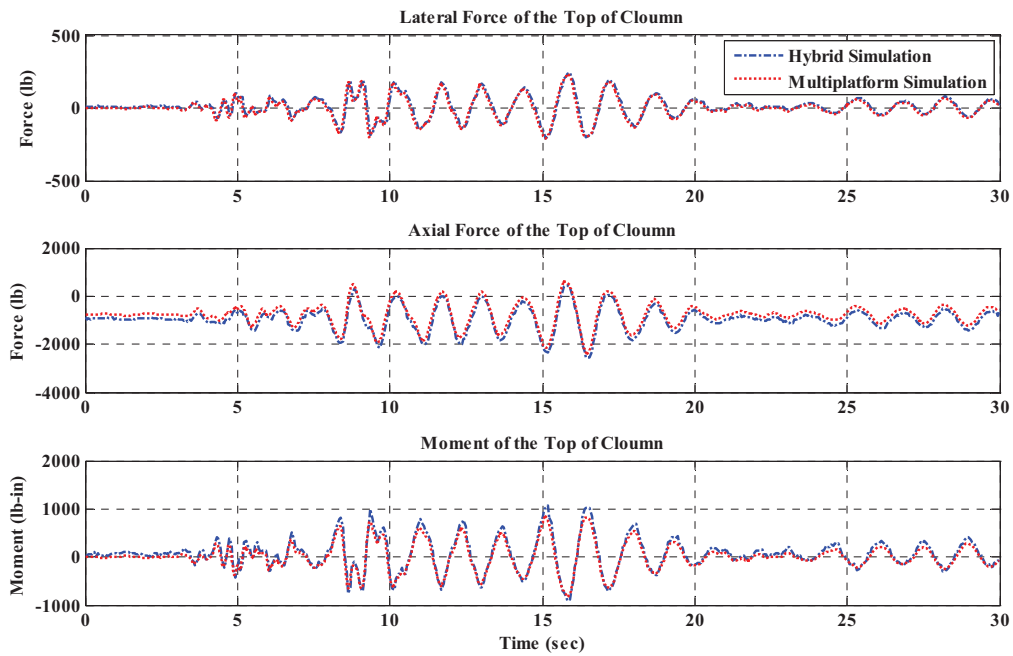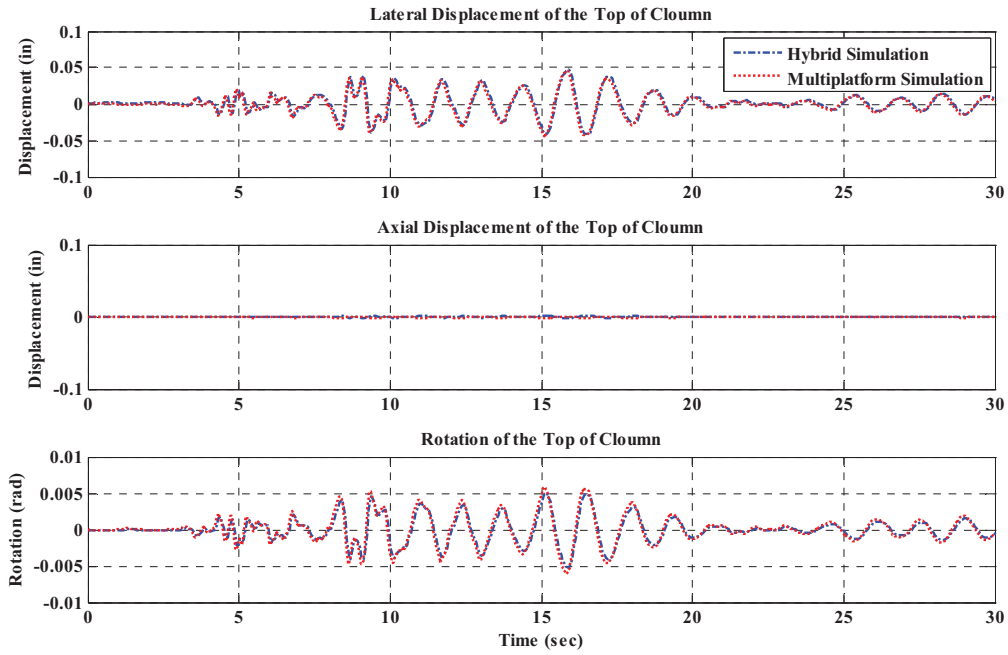
Test No. 2

Description: This was the first test conducted to derive the mean PGA value for the immediate occupancy limit state. 10% PE/50 yrs ground motion was selected as seismic input.

Maximum Acc. is 0.614 g at time 7.9 sec

ISDA = 0.008

Scale factor for next testing = 0.89

Lateral Force v.s. Lateral Displacement

Test No. 2

191
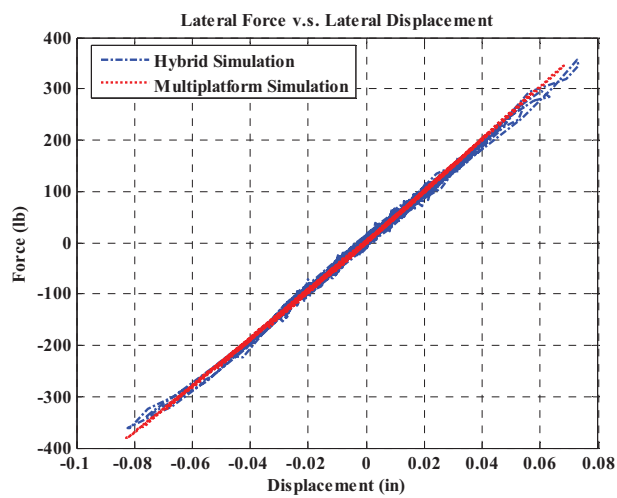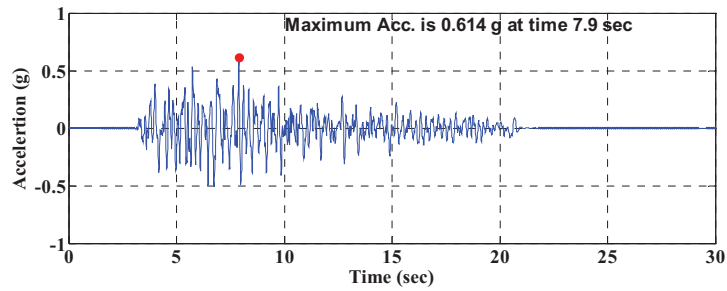
Test No. 3

Description: This was the second test conducted to derive the mean PGA value for the
immediate occupancy limit state. 10% PE/50 yrs ground motion with scale factor
equal to 0.89 was selected as seismic input.

Test No. 3

Lateral Displacement of the Top of Cloumn

Axial Displacement of the Top of Cloumn

Rotation of the Top of Cloumn

Lateral Force of the Top of Cloumn

Axial Force of the Top of Cloumn

Moment of the Top of Cloumn
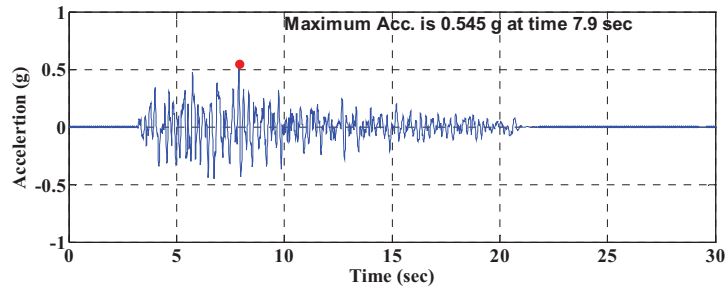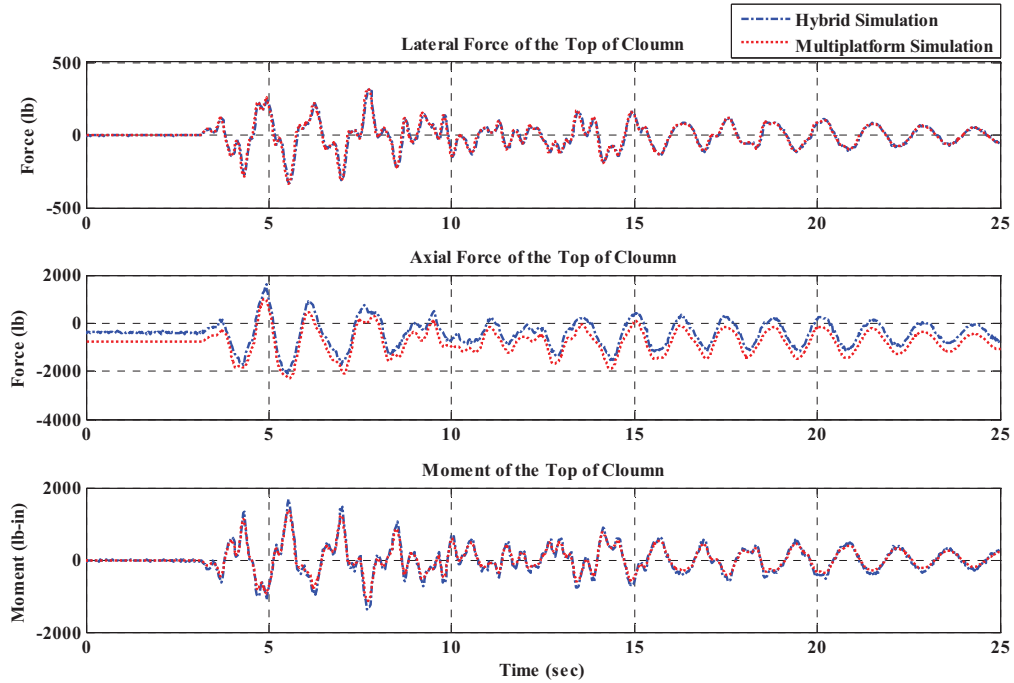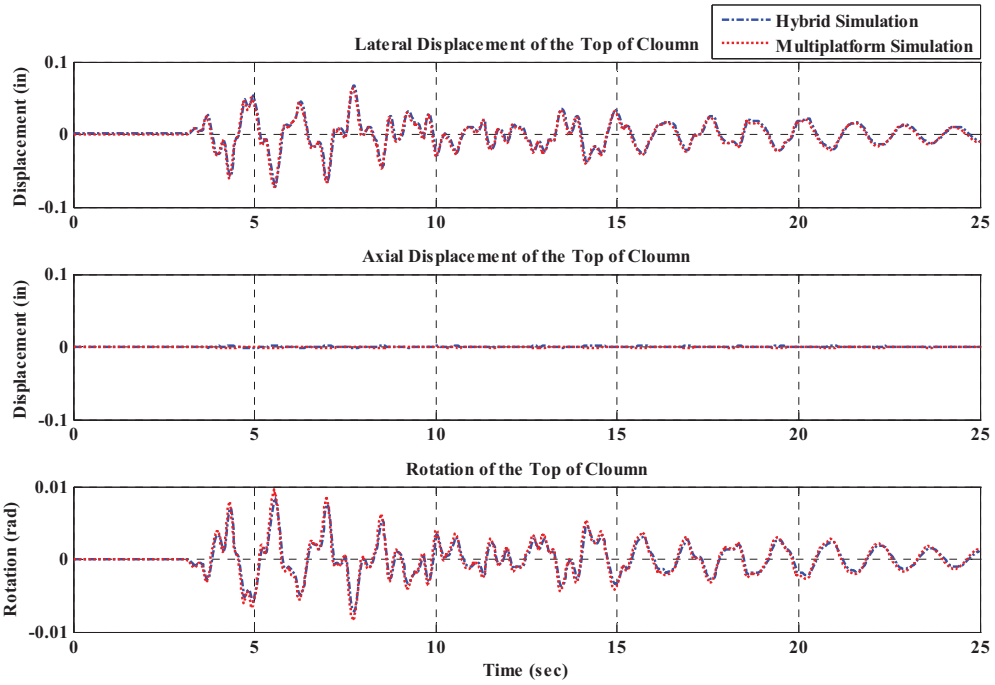
Test No. 4

Description: This was the first test conducted to derive the mean PGA value for the life safety limit state. 5% PE/50 yrs ground motion was selected as seismic input.

Test No. 4

Lateral Displacement of the Top of Cloumn

Hybrid Simulation
Multiplatform Simulation

Axial Displacement of the Top of Cloumn

Rotation of the Top of Cloumn

Lateral Force of the Top of Cloumn

Hybrid Simulation
Multiplatform Simulation

Axial Force of the Top of Cloumn

Moment of the Top of Cloumn
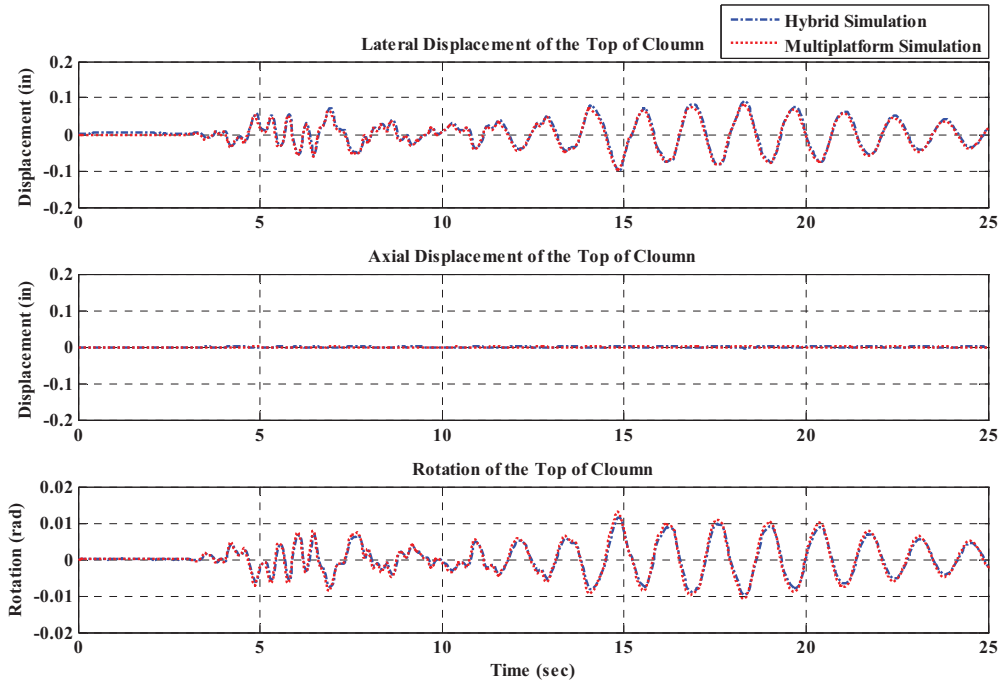
Test No. 5

Description: This was the second test conducted to derive the mean PGA value for the life safety limit state. 5% PE/50 yrs ground motion with scale factor equal to 2.57 was selected as seismic input.

Maximum Acc. is 1.627 g at time 7.9 sec

ISDA = 0.0247 (Difference = 1.2%)

Mean PGA for LS limit state = 1.627 g

Lateral Force v.s. Lateral Displacement

Test No. 5

Lateral Displacement of the Top of Cloumn

Axial Displacement of the Top of Cloumn

Rotation of the Top of Cloumn

Lateral Force of the Top of Cloumn
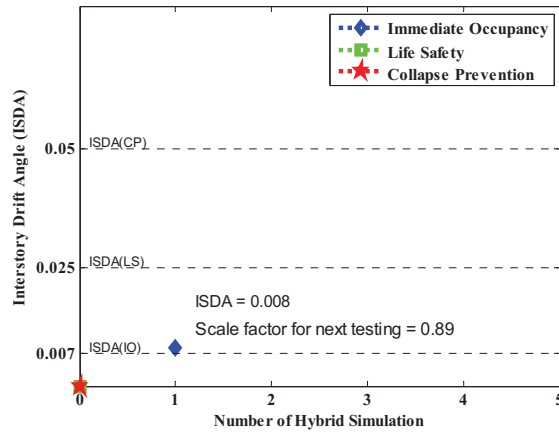
Axial Force of the Top of Cloumn
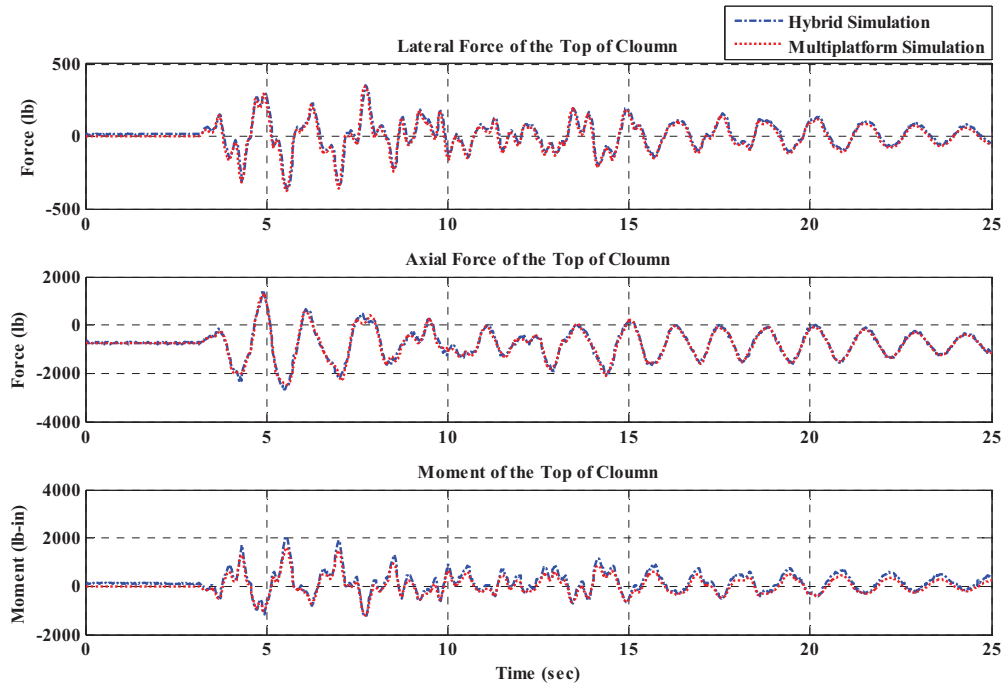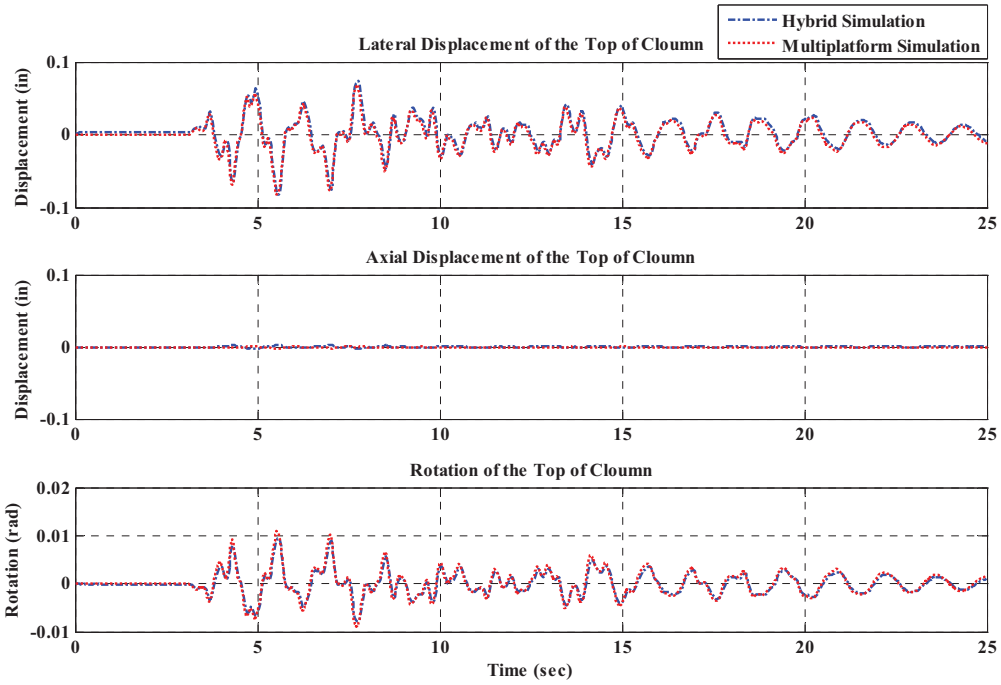
Moment of the Top of Cloumn
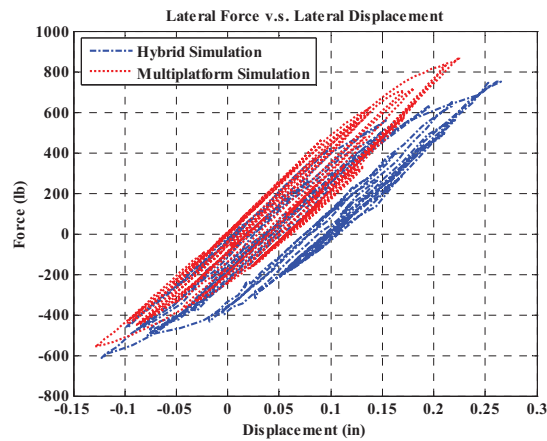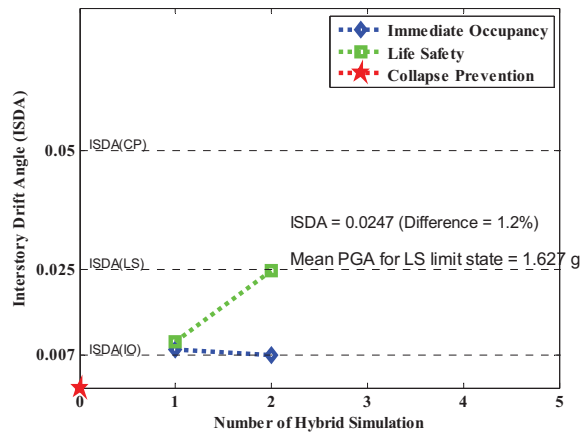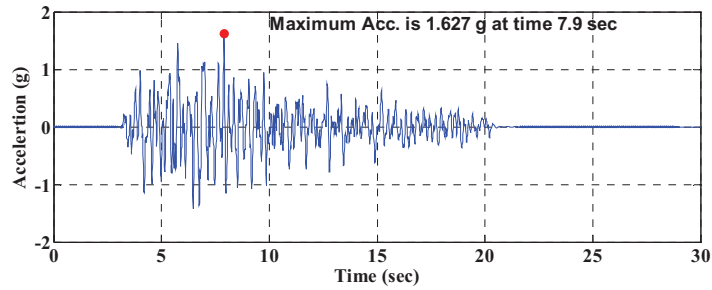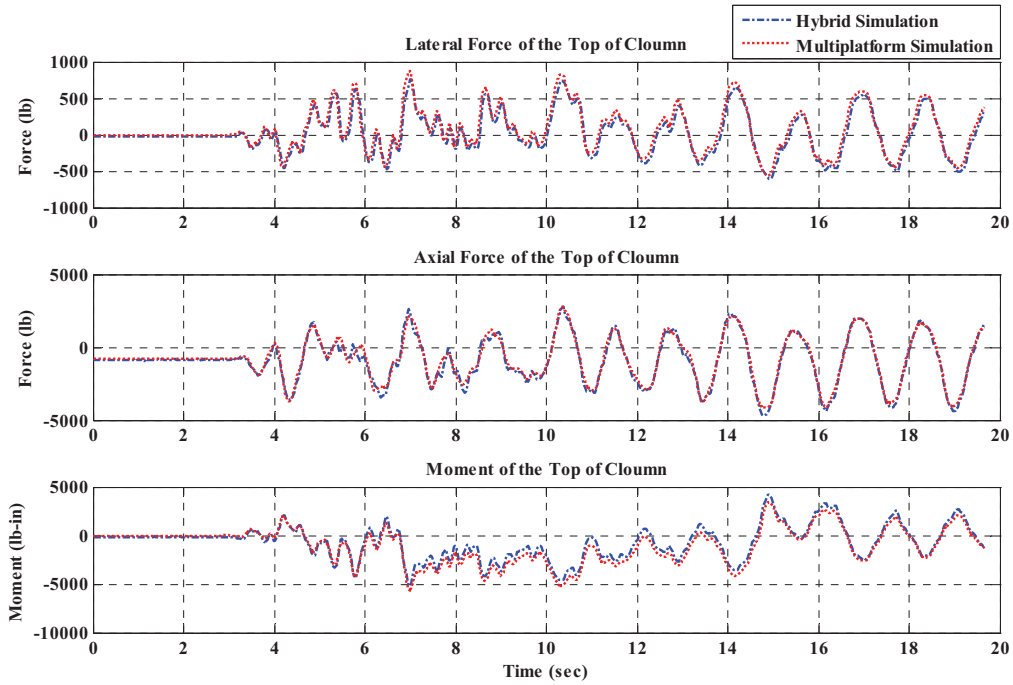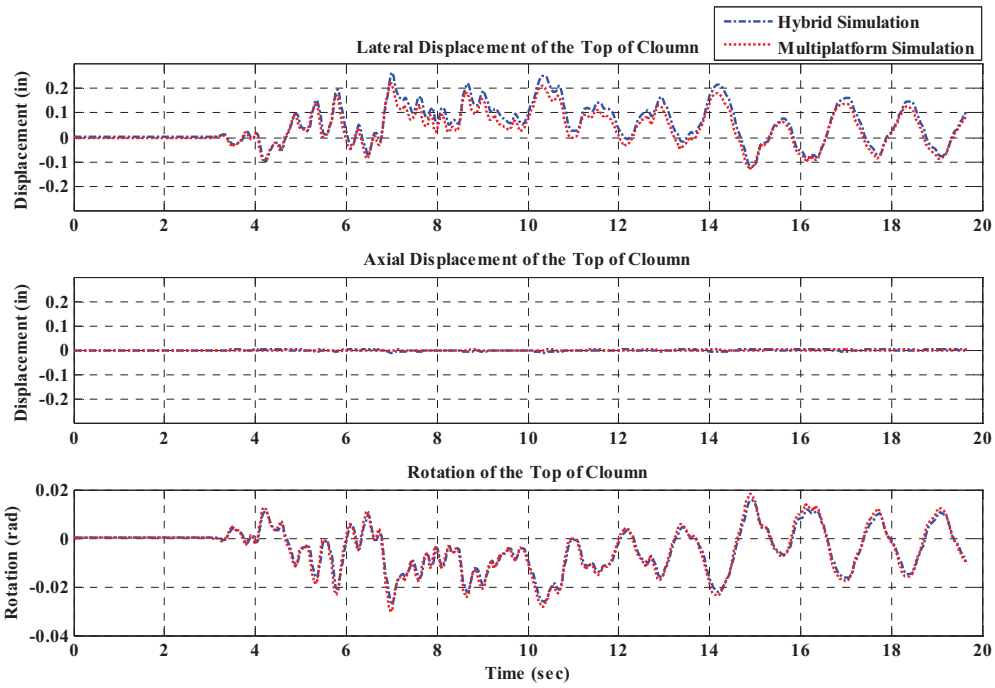
Test No. 6

Description: This was the first test conducted to derive the mean PGA value for the collapse

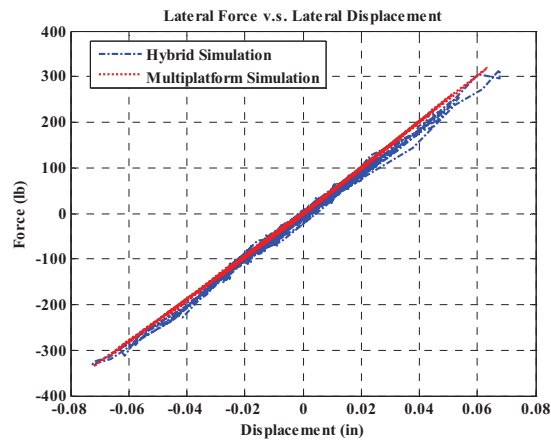prevention limit state. 2% PE/50 yrs ground motion was selected as seismic input.

Test No. 6

Lateral Displacement of the Top of Cloumn

Hybrid Simulation
Multiplatform Simulation

Axial Displacement of the Top of Cloumn

Rotation of the Top of Cloumn

Time (sec)

Lateral Force of the Top of Cloumn

Hybrid Simulation
Multiplatform Simulation

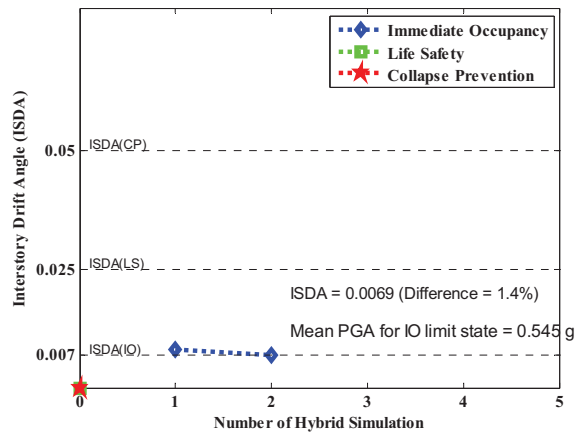**Axial Force of the Top of Cloumn**

Moment of the Top of Cloumn

Time (sec)
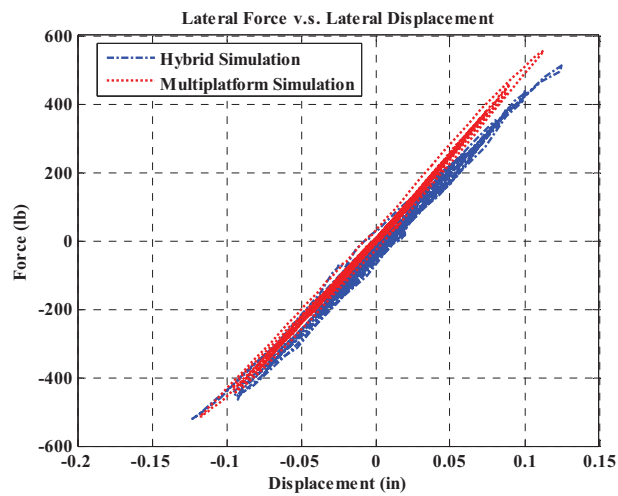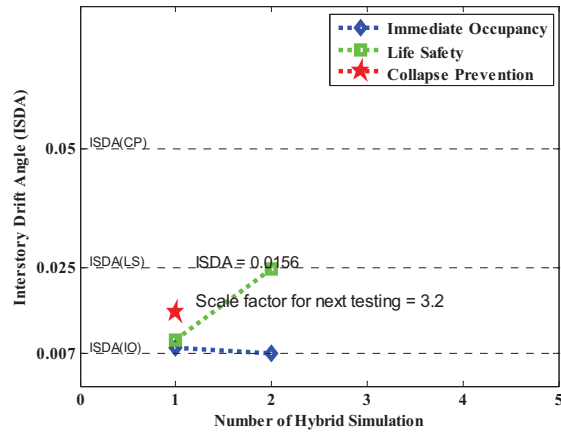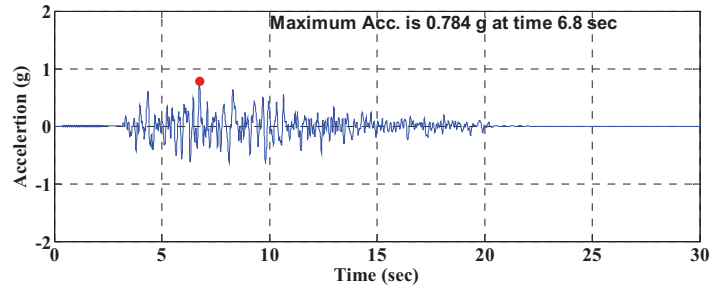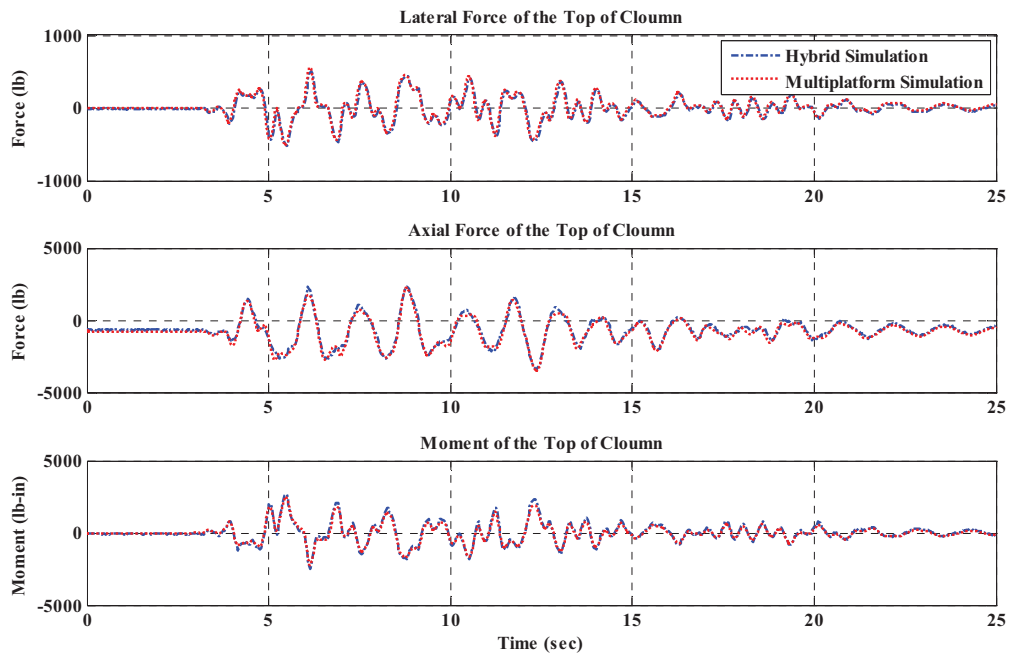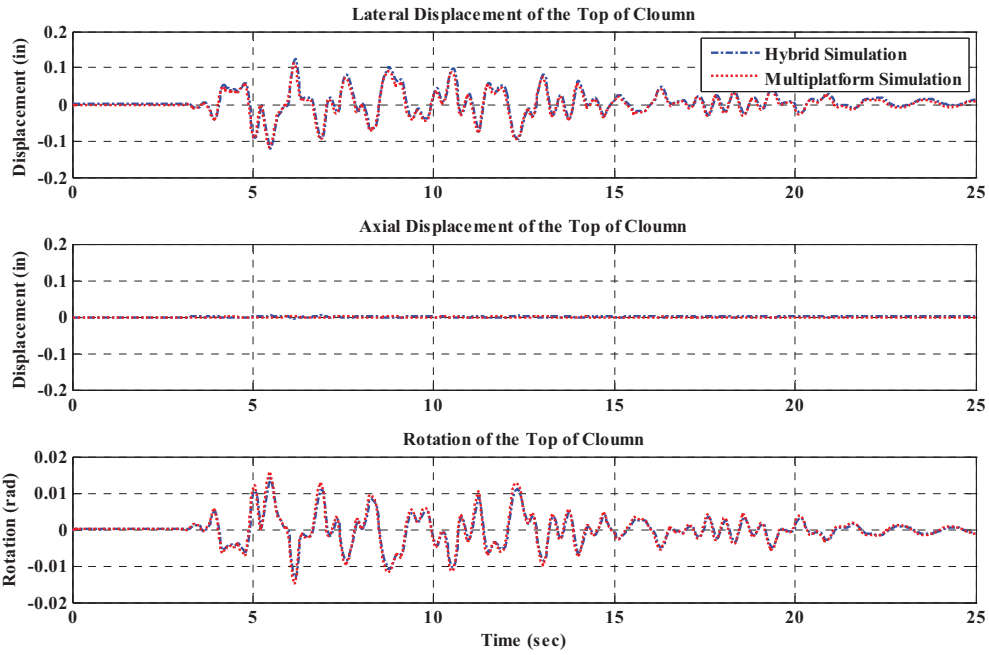
Test No. 7

Description: This was the second test conducted to derive the mean PGA value for the collapse prevention limit state. 2% PE/50 yrs ground motion with scale factor equal to 3.2 was selected as seismic input.

Maximum Acc. is 2.507 g at time 6.8 sec

ISDA = 0.043

Scale factor for next testing = 3.54

Lateral Force v.s. Lateral Displacement

Test No. 7

Lateral Displacement of the Top of Clolumn

Hybrid Simulation
Multiplatform Simulation

Axial Displacement of the Top of Cloumn

Rotation of the Top of Cloumn

Time (sec)

Lateral Force of the Top of Cloumn

Hybrid Simulation
Multiplatform Simulation

Axial Force of the Top of Cloumn

Moment of the Top of Cloumn

Time (sec)

Test No. 8

Description: This was the third test conducted to derive the mean PGA value for the collapse

prevention limit state. 2% PE/50 yrs ground motion with scale factor equal to 3.54
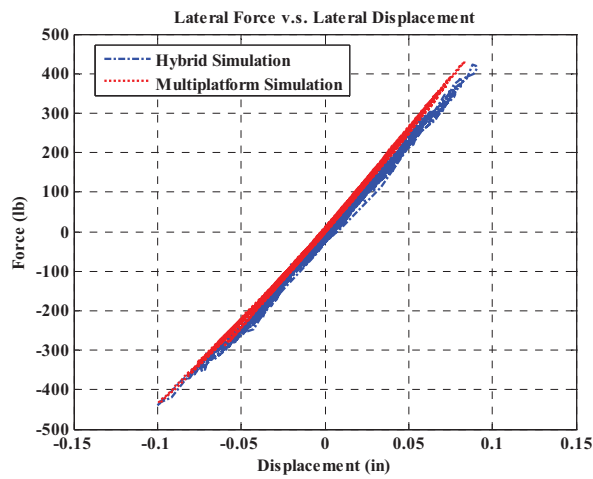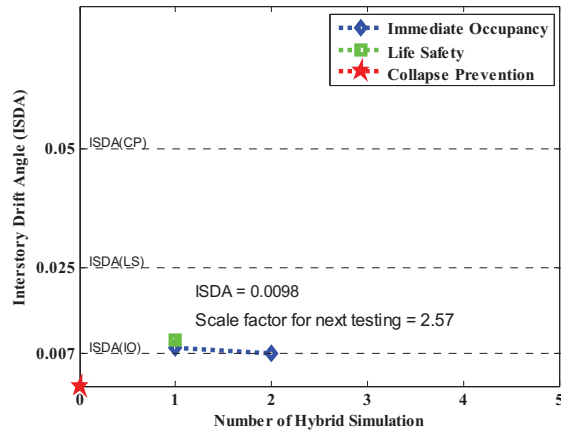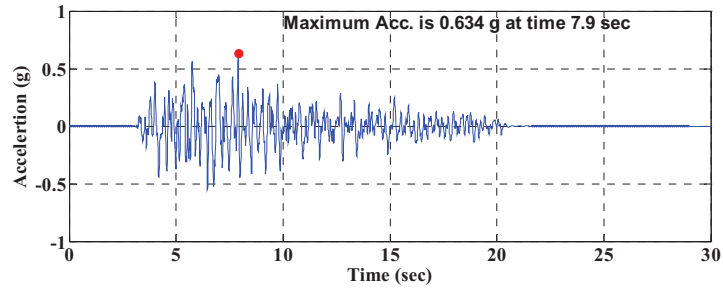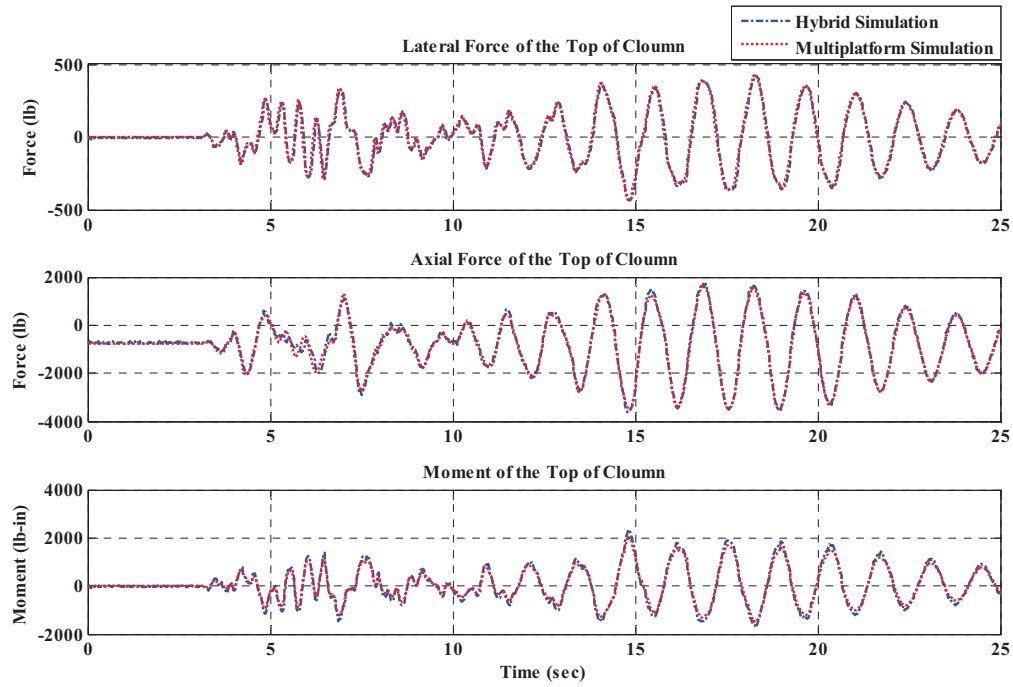
was selected as seismic input.

Test No. 8

Lateral Displacement of the Top of Cloumn

Axial Displacement of the Top of Cloumn

Rotation of the Top of Cloumn

Lateral Force of the Top of Cloumn

Axial Force of the Top of Cloumn

Moment of the Top of Cloumn

203
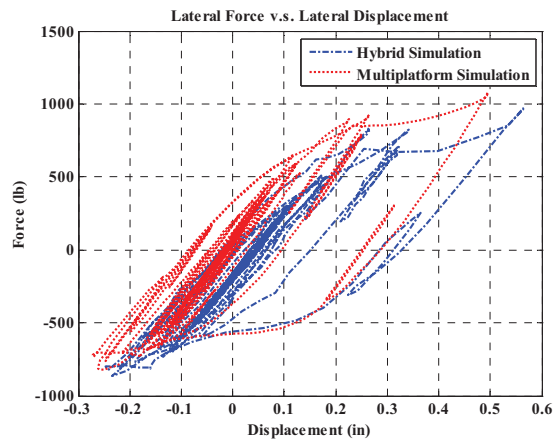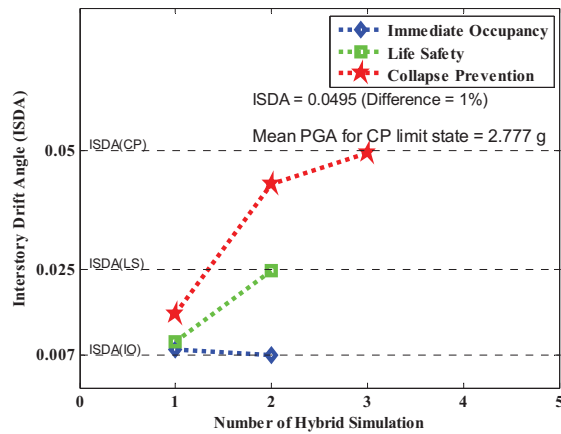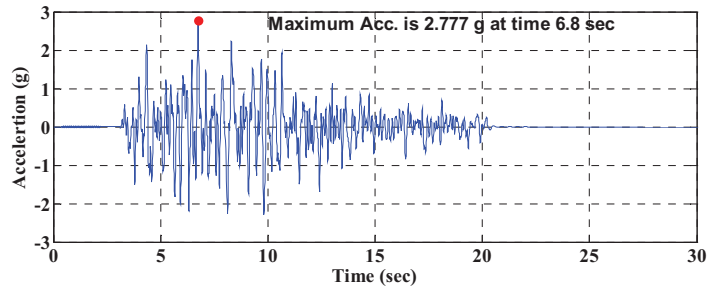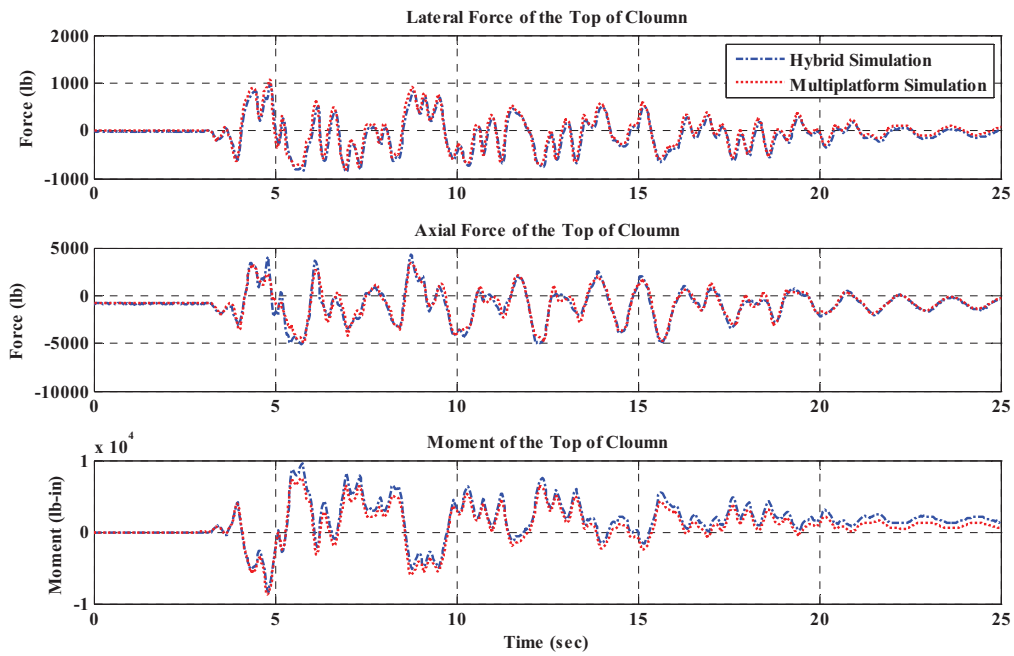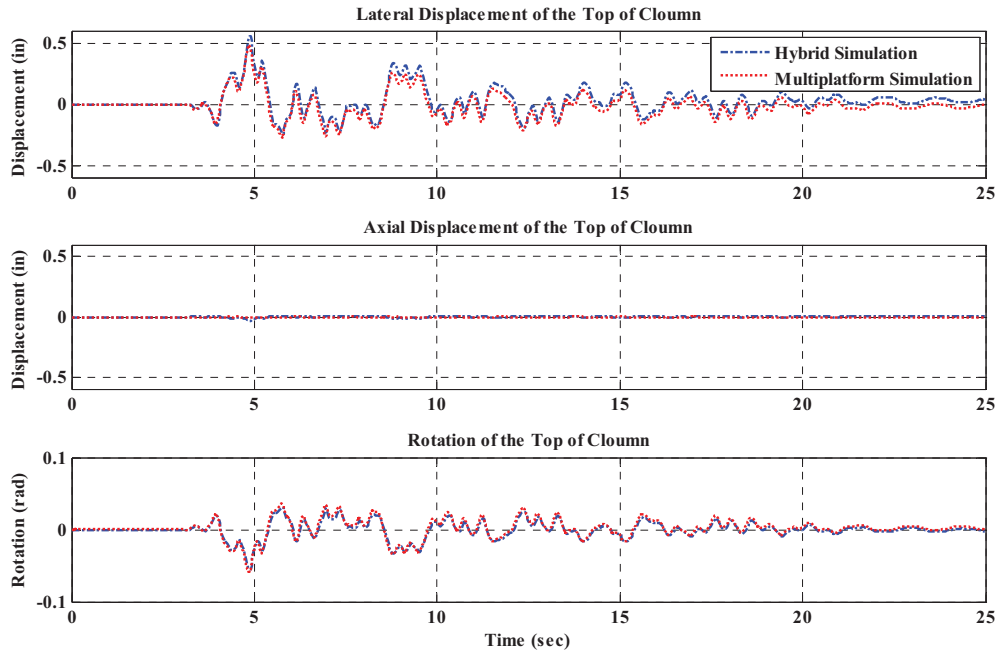
APPENDIX C

FRAGILITY RELATIONSHIPS FOR OTHER BUILDING TYPES

In this section, procedures and results using Parameterized Fragility Method (PFM, Jeong and Elnashai, 2006) to derive fragility relationships for 36 building types under 4 code levels were presented.

C.1 Structural Parameters for PFM

Figure C-1 tabulates the structural parameters which were fed into PFM to derive fragility relationships for 36 building types under 4 code levels. This table is based on the HAZUS-MH Technical Manual but updated with the latest research findings in wood frame (Gencturk and Elnashai, 2008) and unreinforced masonry building (Frankie, 2010).

C.2 Earthquake Demand

Synthetic ground motions generated for the Burbank site (Appendix A) were used as earthquake demand in PFM.

C.3 Fragility Relationships

With the above structural parameters and earthquake demand, PFM was performed. Eventually, fragility relationships for 36 building types under 4 code levels were generated. Figure C-2 tabulated the fragility relationships results.

Figure C-1 Structural parameters for PFM to generate fragility relationships

No.	Label	Description	Height Range Name	Stories	Period	SR-Ultimate strength High-Code	Moderate-Code	Low-Code	Pre-Code
1	W1*	Wood, Light Frame (>= 5,000 sq. ft.)		1-2	0.35	1.15	0.81	0.47	0.23
2	W2*	Wood, Commercial and Industrial (> 5,000 sq. ft.)		All	0.4	0.67	0.41	0.24	0.14
3	S1L	Steel Moment Frame	Low-Rise	1-3	0.5	0.749	0.375	0.187	0.187
4	S1M		Mid-Rise	4-7	1.08	0.468	0.234	0.117	0.117
5	S1H		High-Rise	8+	2.21	0.293	0.147	0.073	0.073
6	S2L	Steel Braced Frame	Low-Rise	1-3	0.4	0.8	0.4	0.2	0.2
7	S2M		Mid-Rise	4-7	0.86	0.667	0.333	0.167	0.167
8	S2H		High-Rise	8+	1.77	0.508	0.254	0.127	0.127
9	S3	Steel Light Frame		All	0.4	0.8	0.4	0.2	0.2
10	S4L	Steel Frame with Cast-in-Place Concrete Shear Walls	Low-Rise	1-3	0.35	0.72	0.36	0.18	0.18
11	S4M		Mid-Rise	4-7	0.65	0.6	0.3	0.15	0.15
12	S4H		High-Rise	8+	1.32	0.457	0.228	0.114	0.114
13	S5L	Steel Frame with Unreinforced Masonry Infill Walls	Low-Rise	1-3	0.35			0.2	0.2
14	S5M		Mid-Rise	4-7	0.65			0.167	0.167
15	S5H		High-Rise	8+	1.32			0.127	0.127
16	C1L	Concrete Moment Frame	Low-Rise	1-3	0.4	0.749	0.375	0.187	0.187
17	C1M		Mid-Rise	4-7	0.75	0.624	0.312	0.156	0.156
18	C1H		High-Rise	8+	1.45	0.293	0.147	0.073	0.073
19	C2L	Concrete Shear Walls	Low-Rise	1-3	0.35	1	0.5	0.25	0.25
20	C2M		Mid-Rise	4-7	0.56	0.833	0.417	0.208	0.208
21	C2H		High-Rise	8+	1.09	0.635	0.317	0.159	0.159
22	C3L	Concrete Frame with Unreinforced Masonry Infill Walls	Low-Rise	1-3	0.35			0.225	0.225
23	C3M		Mid-Rise	4-7	0.56			0.188	0.188
24	C3H		High-Rise	8+	1.09			0.143	0.143
25	PC1	Precast Concrete Tilt-Up Walls		All	0.35	1.2	0.6	0.3	0.3
26	PC2L	Precast Concrete Frames with Concrete Shear Walls	Low-Rise	1-3	0.35	0.8	0.4	0.2	0.2
27	PC2M		Mid-Rise	4-7	0.56	0.667	0.333	0.167	0.167
28	PC2H		High-Rise	8+	1.09	0.508	0.254	0.127	0.127
29	RM1L	Reinforced Masonry Bearing Walls with Wood or Metal Deck Diaphragms	Low-Rise	1-3	0.35	1.066	0.533	0.267	0.267
30	RM1M		Mid-Rise	4+	0.56	0.889	0.444	0.222	0.222
31	RM2L	Reinforced Masonry Bearing Walls with Precast Concrete Diaphragms	Low-Rise	1-3	0.35	1.066	0.533	0.267	0.267
32	RM2M		Mid-Rise	4-7	0.56	0.889	0.444	0.222	0.222
33	RM2H		High-Rise	8+	1.09	0.677	0.338	0.169	0.169
34	URML**	Unreinforced Masonry Bearing Walls	Low-Rise	1-2	0.35			0.3	0.3
35	URMM**		Mid-Rise	3+	0.5			0.222	0.222
36	MH	Mobile Homes		All	0.35	0.3	0.3	0.3	0.3

*Gencturk and Elnashai, 2008
**Frankie, 2010

205

Building Types	High-Code Seismic Design Level PGA (g)						Moderate-Code Seismic Design Level PGA (g)						Low-Code Seismic Design Level PGA (g)						Pre-Code Seismic Design Level PGA (g)					
	IO λ	IO β	LS λ	LS β	CP λ	CP β	IO λ	IO β	LS λ	LS β	CP λ	CP β	IO λ	IO β	LS λ	LS β	CP λ	CP β	IO λ	IO β	LS λ	LS β	CP λ	CP β
W1	-1.259	0.635	0.148	0.618	1.302	0.617	-1.425	0.624	0.070	0.613	0.991	0.611	-1.367	0.477	-0.025	0.465	0.681	0.522	-1.713	0.490	-0.110	0.486	0.292	0.515
W2	-0.517	0.421	0.193	0.436	1.358	0.494	-0.689	0.422	0.125	0.438	1.061	0.492	-0.924	0.344	0.015	0.362	0.596	0.403	-1.383	0.341	-0.122	0.351	0.101	0.393
S1L	-0.678	0.520	0.189	0.541	0.997	0.535	-0.804	0.535	-0.029	0.547	0.822	0.562	-0.908	0.496	-0.308	0.504	0.357	0.490	-1.204	0.492	-0.633	0.497	0.055	0.495
S1M*	**-0.607**	**0.311**	**0.487**	**0.328**	**1.021**	**0.346**	-0.744	0.473	-0.024	0.481	0.792	0.489	-0.815	0.495	-0.139	0.498	0.644	0.498	-1.087	0.504	-0.450	0.502	0.256	0.494
S1H	-0.404	0.473	0.424	0.474	1.277	0.474	-0.558	0.470	0.161	0.469	0.946	0.467	-0.673	0.463	-0.024	0.468	0.767	0.477	-0.909	0.483	-0.280	0.487	0.423	0.481
S2L	-0.550	0.553	0.611	0.569	1.560	0.555	-0.677	0.547	0.336	0.571	1.182	0.559	-0.947	0.471	-0.137	0.486	0.615	0.478	-1.345	0.456	-0.659	0.474	0.031	0.466
S2M	-0.561	0.492	0.507	0.506	1.539	0.534	-0.620	0.523	0.404	0.545	1.362	0.551	-0.786	0.486	0.019	0.488	0.799	0.488	-1.136	0.483	-0.418	0.477	0.276	0.472
S2H	-0.515	0.496	0.500	0.518	1.370	0.522	-0.644	0.500	0.289	0.522	1.149	0.525	-0.688	0.511	0.193	0.527	0.981	0.515	-0.972	0.523	-0.139	0.542	0.573	0.525
S3	-1.411	0.490	-0.457	0.501	0.445	0.492	-1.577	0.478	-0.732	0.487	0.158	0.502	-1.663	0.494	-0.876	0.498	-0.102	0.478	-1.903	0.498	-1.157	0.496	-0.409	0.478
S4L	-0.477	0.540	0.618	0.540	1.506	0.496	-0.655	0.516	0.267	0.527	1.111	0.505	-0.855	0.459	-0.076	0.478	0.763	0.475	-1.203	0.465	-0.520	0.463	0.187	0.448
S4M	-0.433	0.502	0.640	0.511	1.706	0.523	-0.422	0.555	0.576	0.554	1.590	0.556	-0.647	0.488	0.174	0.493	1.043	0.496	-1.035	0.471	-0.319	0.471	0.433	0.463
S4H	-0.369	0.472	0.641	0.477	1.597	0.480	-0.497	0.477	0.424	0.482	1.391	0.491	-0.557	0.490	0.294	0.490	1.135	0.481	-0.880	0.484	-0.104	0.482	0.668	0.474
S5L													-0.951	0.504	-0.117	0.510	0.537	0.492	-1.278	0.500	-0.485	0.517	0.187	0.503
S5M													-0.689	0.515	0.174	0.520	0.838	0.510	-1.019	0.518	-0.217	0.524	0.477	0.523
S5H													-0.721	0.459	0.003	0.443	0.640	0.438	-0.971	0.471	-0.263	0.456	0.338	0.448
C1L	-0.576	0.540	0.548	0.547	1.516	0.538	-0.693	0.546	0.288	0.566	1.152	0.561	-0.883	0.477	-0.067	0.500	0.765	0.509	-1.273	0.465	-0.507	0.491	0.178	0.480
C1M	-0.483	0.479	0.559	0.495	1.544	0.522	-0.479	0.545	0.517	0.552	1.467	0.560	-0.687	0.482	0.109	0.487	0.908	0.488	-1.051	0.463	-0.330	0.469	0.354	0.465
C1H	-0.502	0.476	0.504	0.472	1.373	0.475	-0.595	0.502	0.373	0.508	1.326	0.522	-0.757	0.472	-0.026	0.459	0.587	0.449	-1.041	0.468	-0.351	0.453	0.223	0.440
C2L	-0.475	0.530	0.621	0.528	1.472	0.489	-0.672	0.511	0.275	0.521	1.080	0.506	-0.831	0.490	-0.009	0.495	0.755	0.486	-1.172	0.475	-0.438	0.476	0.251	0.466
C2M	-0.343	0.505	0.752	0.531	1.807	0.552	-0.369	0.554	0.659	0.561	1.637	0.573	-0.572	0.505	0.325	0.523	1.205	0.520	-0.944	0.490	-0.148	0.511	0.611	0.504
C2H	-0.404	0.473	0.588	0.472	1.417	0.475	-0.553	0.487	0.395	0.497	1.303	0.517	-0.601	0.503	0.327	0.514	1.236	0.528	-0.925	0.494	-0.115	0.496	0.686	0.511
C3L													-1.149	0.488	-0.326	0.505	0.335	0.484	-1.458	0.483	-0.677	0.510	-0.007	0.493
C3M													-0.845	0.509	0.028	0.527	0.764	0.522	-1.156	0.511	-0.338	0.528	0.413	0.536
C3H													-0.857	0.510	-0.023	0.514	0.638	0.506	-1.153	0.499	-0.385	0.497	0.242	0.488
PC1	-1.083	0.501	-0.013	0.508	0.976	0.480	-1.183	0.511	-0.265	0.514	0.666	0.501	-1.263	0.499	-0.473	0.505	0.355	0.483	-1.594	0.489	-0.868	0.479	-0.119	0.460
PC2L	-0.698	0.537	0.397	0.535	1.319	0.494	-0.857	0.516	0.067	0.528	0.936	0.506	-1.020	0.471	-0.242	0.485	0.608	0.479	-1.363	0.467	-0.656	0.470	0.077	0.457
PC2M	-0.521	0.528	0.580	0.539	1.686	0.549	-0.563	0.555	0.456	0.565	1.512	0.571	-0.757	0.498	0.080	0.508	0.987	0.510	-1.118	0.484	-0.393	0.491	0.372	0.488
PC2H	-0.626	0.473	0.361	0.472	1.270	0.473	-0.718	0.504	0.272	0.525	1.335	0.549	-0.761	0.512	0.137	0.520	1.086	0.522	-1.111	0.491	-0.301	0.500	0.511	0.497
RM1L	-0.740	0.522	0.358	0.525	1.331	0.489	-0.875	0.511	0.045	0.519	0.947	0.504	-1.000	0.495	-0.208	0.498	0.643	0.492	-1.340	0.488	-0.624	0.482	0.141	0.465
RM1M	-0.597	0.492	0.471	0.521	1.609	0.545	-0.605	0.551	0.392	0.555	1.444	0.566	-0.757	0.504	0.098	0.521	1.063	0.526	-1.094	0.493	-0.339	0.506	0.506	0.513
RM2L	-0.740	0.522	0.358	0.525	1.331	0.489	-0.875	0.511	0.045	0.519	0.947	0.504	-1.000	0.495	-0.208	0.498	0.643	0.492	-1.340	0.488	-0.624	0.482	0.141	0.465
RM2M	-0.597	0.492	0.471	0.521	1.609	0.545	-0.605	0.551	0.392	0.555	1.444	0.566	-0.757	0.504	0.098	0.521	1.063	0.526	-1.094	0.493	-0.339	0.506	0.506	0.513
RM2H	-0.626	0.473	0.365	0.472	1.285	0.475	-0.755	0.483	0.151	0.489	1.112	0.506	-0.793	0.501	0.098	0.514	1.084	0.528	-1.093	0.498	-0.304	0.500	0.562	0.511
URML													-1.441	0.454	-0.678	0.461	-0.036	0.435	-1.683	0.463	-0.971	0.459	-0.339	0.441
URMM													-1.201	0.500	-0.538	0.526	0.105	0.521	-1.479	0.511	-1.020	0.522	-0.346	0.528
MH	-1.516	0.570	-0.428	0.571	0.503	0.518	-1.516	0.570	-0.428	0.571	0.503	0.518	-1.516	0.570	-0.428	0.571	0.503	0.518	-1.864	0.546	-0.862	0.542	0.075	0.529

*Hybrid fragility approach

Figure C-2 Fragility relationships database (PFM along with hybrid fragility approach)

APPENDIX D

AN EFFICIENT MODEL CALIBRATION METHOD

An automatic system identification-based model updating technique was developed and incorporated into NISRAF. Provided below, the methodology, procedures and GUIs of this method are developed by Jian Li at University of Illinois (Li et al., 2009).

D.1 System Identification

Among the state-space based system identification methods, Eigensystem Realization Algorithm (ERA) (Juang and Pappa, 1985) is selected to identify the modal parameters of structures, due to its wide application and good performance in multi-input multi-output (MIMO) problems. The basic idea of ERA is to find a minimum realization of system (state-space representation with minimum dimension) using Singular Value Decomposition (SVD) on the Hankel matrix built by Markov parameters (impulse response functions). The modal properties can be extracted from the realized minimum state-space representation. Therefore, to start with ERA, 'generalized Hankel matrices' are constructed, assuming that there are *p* inputs and *q* outputs:

$$\mathbf{H}_{rs}(k) = \begin{bmatrix} \mathbf{Y}(k) & \cdots & \mathbf{Y}(k+s-1) \\ \vdots & \ddots & \vdots \\ \mathbf{Y}(k+r-1) & \cdots & \mathbf{Y}(k+r+s-2) \end{bmatrix} \tag{D.1}$$

where $k = 0, 1$; $\mathbf{Y}(k)$ is the impulse response function at time k, consisting of p rows and q columns; r and s are the number of block rows and block columns. Singular value decomposition is then performed for $\mathbf{H}_{rs}(k)$ which yields:

$$\mathbf{H}_{rs}(0) = \underline{\mathbf{P}}\,\underline{\mathbf{D}}\,\underline{\mathbf{Q}}^{\mathrm{T}} \tag{D.2}$$

where $\underline{\mathbf{P}}$ and $\underline{\mathbf{Q}}$ are unitary matrices, $\underline{\mathbf{D}}$ is an $r \times p$ by $s \times q$ diagonal matrix with singular values on the diagonal. The number of non-zero singular values gives the dimension of the minimum realization of the system if $\mathbf{Y}(k)$ is noise free. In reality this is not the case, therefore $\underline{\mathbf{D}}$ is usually of full rank. The singular values corresponding to noise are usually much smaller compared with those corresponding to real modes. By preserving the first N ordered significant singular values, by which noise modes are eliminated, the minimum realization can be calculated as follows:

$$\begin{aligned}
\mathbf{A} &= \mathbf{D}^{-1/2}\mathbf{P}^T\mathbf{H}_{rs}(1)\mathbf{Q}\mathbf{D}^{-1/2}\\
\mathbf{B} &= \mathbf{D}^{1/2}\mathbf{Q}\mathbf{E}_q\\
\mathbf{C} &= \mathbf{E}_p^T\mathbf{P}\mathbf{D}^{1/2}
\end{aligned} \tag{D.3}$$

In the above equations, $\mathbf{P}$ and $\mathbf{Q}$ contain the first N corresponding columns of $\underline{\mathbf{P}}$ and $\underline{\mathbf{Q}}$, respectively. $\mathbf{E}_p^T = [\mathbf{I}_p \quad \mathbf{0}_p \quad ... \quad \mathbf{0}_p]$ and $\mathbf{E}_q^T = [\mathbf{I}_q \quad \mathbf{0}_q \quad ... \quad \mathbf{0}_q]$. The realization is then transformed to modal coordinates by using the eigenvalues $\mathbf{Z}$ and eigenvector matrix of $\mathbf{A}$, which yields:

$$\mathbf{A}' = \mathbf{\psi}^{-1}\mathbf{A}\mathbf{\psi} = \mathbf{Z}$$
$$\mathbf{B} = \mathbf{\psi}^{-1}\mathbf{B} \qquad \qquad \text{(D.4)}$$
$$\mathbf{C} = \mathbf{C}\mathbf{\psi}$$

Modal participation factors and mode shapes are the corresponding rows of $\mathbf{B}'$ and columns of $\mathbf{C}'$, respectively. The modal damping ratio ξ_i and damped natural frequencies ω_{di} can be calculated from the eigenvalues of $\mathbf{A}$ after transforming back to continuous domain:

$$s_i = -\xi_i\omega_{ni} \pm i\omega_{di} = \ln(z_i)\,/\Delta t \qquad \qquad \text{(D.5)}$$

where $\omega_{ni} = \omega_{di}/\sqrt{1 - \xi_i^2}$ are undamped natural frequencies, and Δt is the sampling interval.

A two-step strategy is applied to filter out computational and noise modes. Since more singular values are retained, more potential genuine modes can be identified. In this study, the dimension of realized system N is increased in a range until adequate modes are included finally. First, for each particular order of system, three commonly used mode accuracy indicators, namely Modal Amplitude Coherence (MAC) (Juang and Pappa, 1985), Extended Modal Amplitude Coherence (EMAC) and Modal Phase Colinearity (MPC) (Pappa and Elliott, 1993) are used to filter out the computational or noise modes. The retained modes are then deemed trustable and a stabilization diagram is plotted for further confirmation. The stabilization diagram gathers all modes identified from the realized systems with different system order, based on the idea that a genuine mode should always be identified with a different order of realized system, as long as the

system order is adequate for that mode. Among the same order of modes identified and plotted in the stabilization diagram, the one with highest EMAC value is then selected as the final confirmed mode.

D.2 Model Updating

For model updating, to keep the physical meaning, the iterative or parametric method is implemented in NISRAF. Currently, only linear model updating is available. In the linear approach, the objective function represented the modal parameter (natural frequencies and mode shapes) residuals are formed as linear combination of natural frequency residuals and model shape residuals with different weighting factors.

$$F(x) = w_f \sum_{k=1}^{N_f} \left(\frac{f_{ak} - f_{ek}}{f_{ek}} \right)^2 + w_m \sum_{k=1}^{N_m} \frac{\cos^{-1}\left(\sqrt{MAC_k}\right)}{(\pi/2)} \tag{D.6}$$

where f_{ak} and f_{ek} denote analytical and experimental natural frequencies; w_f and w_m are weighting factor applied to frequency residuals and mode shape residuals, respectively. 0.8 and 0.2 are used here considering the factor that natural frequencies usually have higher accuracy than mode shapes in practical system identification. *MAC* (Modal Assurance Criteria) is a measurement of mode shape discrepancy and is defined as Equation (D.7) (Allemang and Brown, 1982).

$$MAC_i = \frac{(\phi_{ai}^T \phi_{ei})^2}{(\phi_{ai}^T \phi_{ai})(\phi_{ei}^T \phi_{ei})} \tag{D.7}$$

where ϕ_{ai} and ϕ_{ei} are analytical and experimental mode shapes. $MAC = 1$ means ϕ_{ai} and

ϕ_{ei} are perfectly matched and $MAC = 0$ means they are orthogonal. It is known that MAC

is rather insensitive to the change of mode shape. Also it is noticed that MAC is actually

the square of the inner product between the two mode shape vectors. Therefore, the

objective function for mode shape residual is formed as the normalized angle between the

two mode shape vectors, which is much more sensitive to the change of mode shape.

Nelder-Mead method (Nelder and Mead, 1965) is applied to solve the

optimization problem defined above. This method is computationally quite simple and

relatively robust. It requires no computation of derivative information; iteration is driven

by the evaluation of the value of objective function only. The algorithm starts by

generating a set of $n+1$ vertices that defines a simplex, where n is the number of

parameters to be updated. Then a set of tie-breaking rules, including reflection, expansion,

contraction and shrinkage, are carried out to update the simplex for the next iteration until

convergence rules are satisfied.